CORE
Metadata, citation and similar papers at core.ac.uk
Provided by Universidad Carlos III de Madrid e-Archivo

Tesis Doctoral

Kinematic and Dynamic Analysis for Biped Robots Design

David Mauricio Alba Lucero

Director: Juan Carlos García Prada

Universidad Carlos III de Madrid

Escuela Politécnica Superior

Departamento de Ingeniería Mecánica

Leganés, 2012

Departamento Ingeniería Mecánica
Escuela Politécnica Superior
Universidad Carlos III de Madrid

Título de la Tesis Kinematic and Dynamic Analysis for Biped Robots Design

Autor David Mauricio Alba Lucero

Titulación Ingeniero Mecánico
Escuela Superior
Politécnica del Litoral

Director Juan Carlos García Prada

Tesis Doctoral

Kinematic and Dynamic Analysis for Biped Robots Design

Autor: David Mauricio Alba Lucero
Director: Juan Carlos García Prada

Firma del tribunal calificador:

Presidente:

Vocal:

Vocal:

Vocal:

Secretario:

Leganés, de de

A mis padres

Acknowledgments

This thesis is the contribution of many people around me. I would like to extend my sincerely gratitude to Professor Juan Carlos García Prada to offer his patience and knowledge to finish this work. My colleges from whom I have gathered important experience like Dr. Cristina Castejon, Dr. Higinio Rubio and Dr. Jesus Meneses. They have helped me to overcome many difficulties during my work. Also I would like to thank all the people who began this adventure at the IAI-CSIC specially Professor Manuel Armada who provide me the first contact with robotics and Dr. Roberto Ponticelli who gave me important advice at the beginning of my studies. Also, I would like to thank Professor Sebastian Dormido who helped me to get into the MAQLAB team and Dr. Alfonso Urquia for all Modelica advices.

To my colleagues Alvaro, Javier, Patri, Nacho, Efren and María Jesus, they have been around to support me in important matters outside academic matters, but I must say, still very important. The human quality they have offered has been a provision to stand the long path covered to reach the completion of this work.

I would like to show all my thankfulness to my family. My parents who have always been very supportive and selfless about all my decisions, they provide me a wiser point of view of trivial and very important matters that helped to continue my way. My brother and sister that no matter the distance are always with me. Veronica, who suffered with me the ups and downs of this thesis. Finally, Jesus and his family who embrace me as another kinfolk.

Resumen

En esta tesis un nuevo método para encontrar sistemas dinámicamente equivalentes es propuesto. El objetivo es el de crear una herramienta para el análisis de robots bípedos. La herramienta consiste en modelos simplificados obtenidos del *principio de equivalencia dinámica*, que dice que si dos sistemas poseen la misma masa, el mismo centro de masa y el mismo momento de inercia entonces son dinámicamente equivalentes. Este concepto no es nuevo y es comúnmente utilizado en el diseño de máquinas alternativas, o para encontrar el *sweet spot* de objetos esbeltos tales como bates o espadas. Con la aplicación del principio de equivalencia dinámica se encuentra el centro de percusión. La aportación en esta tesis es la aplicación de este concepto al análisis de robots bípedos, y la extensión del centro de percusión a cadenas cinemáticas.

La herramienta fundamental para la obtención de resultados de investigación en esta tesis hace uso del lenguaje de simulación Modelica®. Las simulaciones son altamente detalladas gracias a la librería estándar Multibody incluida en las especificaciones del mismo. Como consecuencia de los trabajos desarrollados se crearon nuevas clases para extender la capacidad de la librería y aplicarla a máquinas caminantes.

El desarrollo de esta tesis está centrado en el desarrollo de dos modelos. El primero es un péndulo invertido equivalente, con la característica que posee las mismas propiedades dinámicas del robot que modela. Dichas propiedades son la masas total, el centro de masa y el momento de inercia. Este modelo es luego utilizado para generar el caminar de un bípedo simple. El bípedo es simulado con un volante de inercia como cuerpo, y pies de contacto puntual. Posee rodillas y está totalmente actuado. Los eslabones del robot poseen propiedades de sólido rígido y ninguna simplificación ha sido considerada.

El segundo modelo tiene el objetivo de imitar la topología del bípedo que representa, por lo tanto tiene un grado mayor de complejidad que el anterior. Este modelo es construido al dividir al robot en tres grupos: Las dos piernas, y otro grupo compuesto por la cabeza, los brazos y el torso (Denominado HAT por sus siglas en inglés). Este modelo es denominado modelo de cuatro masas puntuales. Este modelo es posteriormente validado utilizandolo para desacoplar la dinámica del sistema, la única información utilizada para llevar a cabo esta tarea es proporcionada por dicho modelo.

Abstract

In this thesis a method to find dynamically equivalent systems is proposed. The objective is to provide a tool to analyze biped robots by simplifying their dynamics to simpler models. The equivalent models are obtained with the concept of dynamic equivalence that states that if two systems share the same total mass, the same center of mass, and the same moment of inertia then they are considered to be dynamically equivalent. This concept is not new and it is used in the design of alternative machines, or to find the *sweet spot* of long object like swords or bats. The result of the application of the dynamic equivalence principle is the point known as the center of percussion. The novelty in this thesis is to apply this concept to the analysis of biped robots, and the extension of the center of percussion to kinematic chains.

The work in this thesis developed with the help of the simulation language Modelica®. The simulations are very detailed by implementing elaborated rigid body dynamics provided by the multibody standard library included in the language specifications. New classes were created in order to be able to simulate walking machines. Those classes introduce contact objects at ground foot interactions and mechanical stops for knee joints.

The development of this thesis is centered around the proposal of two models. The first model is an equivalent inverted pendulum with the characteristic that it has the same dynamic properties, i.e., total mass, center of mass and moment of inertia, of the biped that models. This model is later used to synthesize gait in a simple, but realistic biped. The biped is simulated with a flywheel body, and point feet. It has knees and it is fully actuated. Also all the links have complete rigid body properties and no simplifications were done.

The second model has the objective to resemble the topology of the biped it represents, therefore it is slightly more complex than the equivalent inverted pendulum. This model is constructed by grouping the components of the robot in three groups: Two legs and the HAT group (HAT stands for head, arms and trunk). This model is denominated four point masses model. The model is later validated by decoupling the dynamics of the system only with the information provided by the four point masses model.

Contents

1 Motivation and objectives **1**

1.1 Motivation 1

1.2 Objectives 2

2 State of the art **5**

2.1 Basic inverted pendulum based models 5

2.1.1 Inverted pendulum model 6

2.1.2 Linear inverted pendulum model 7

2.1.3 Reaction mass and reaction wheel pendulums 9

2.1.4 Parametric pendulum 12

2.2 Ground reference points for biped robots 15

2.2.1 Zero moment point and center of pressure 15

2.2.2 Centroidal moment pivot 17

2.2.3 Capture points 18

2.3 Other models 21

2.3.1 Rimless wheel 21

2.3.2 Complete models 24

2.3.3 Reduced models 28

3 Theoretical Framework and Methods **31**

3.1 Dynamic equivalence 32

3.1.1 Center of percussion 32

3.1.2 What is missing? 35

3.1.3 Center of percussion of a system of particles 37

3.2 Object oriented modeling 42

3.2.1 DAEs and computational causality . . . 43
3.2.2 Modelica . . . 44
3.2.3 Ground-foot interactions . . . 45
3.2.4 Joint simulation . . . 47

4 Center of percussion and gait design of biped robots 49

4.1 Finding the equivalent inverted pendulum of a biped robot . . . 49
4.2 Description of the model . . . 52
4.3 Gait generation . . . 54
4.3.1 Gait parameters . . . 55
4.3.2 Swinging leg control . . . 55
4.3.3 Stance leg control . . . 57
4.3.4 Putting it all together . . . 59
4.4 Simulation results . . . 60
4.5 Conclusions of the chapter . . . 64
4.5.1 Some words about stability . . . 65
4.5.2 Mass distribution of the biped . . . 65
4.6 Improvements of the technique . . . 66
4.6.1 Adding a torso and feet . . . 66
4.6.2 Energy optimization . . . 66

5 Four point masses equivalent model of a biped robot 69

5.1 Modeling a biped with four point masses . . . 69
5.1.1 Selection of a suitable reference . . . 70
5.1.2 Calculating the equivalent model . . . 71
5.2 Some words about impedance control . . . 75
5.3 Fast swinging of one leg . . . 76
5.3.1 Selection of the parameters . . . 76
5.3.2 “Kicking” experiments . . . 78
5.3.3 Results of the “kicking” experiments . . . 80
5.4 Oscillation experiments . . . 85
5.4.1 Parameters used in the simulations . . . 85
5.4.2 Results of the oscillation experiments . . . 87
5.5 Conclusions of the chapter . . . 89

6 Analysis of the models 91

6.1 Four point masses model and torque analysis . . . 92

6.1.1 Components of the control action 92
6.1.2 Analysis of the torque components 93
6.1.3 Varying the proportional gains 96
6.2 Analysis of the equivalent inverted pendulum 100
6.2.1 The inverted pendulum system 100
6.2.2 Description of the experiments 102
6.2.3 Results of the experiments 103

7 Conclusions and future work **107**
7.1 Conclusions 107
7.1.1 Equivalent system of a kinematic chain 108
7.1.2 Equivalent inverted pendulum 108
7.1.3 Four point masses model 109
7.1.4 Summary 110
7.2 Observations and remarks 111
7.3 Future work 112

Bibliography **115**

APPENDIX **125**

A Dynamic equivalence of a rigid body in 2D **127**

B Equations of motion of a mechanism **131**
B.1 Equations of motion of the mechanism 132
B.2 Equations of motion of the equivalent mechanism 134

C Modelica code for point contact objects **139**
C.1 Contact with viscous friction 139
C.2 Contact with sticky friction 141
C.3 Contact with continuous functions 142

D Modelica code for rotational joints with mechanical stops **145**
D.1 Rotational joint with mechanical stops based on events 145
D.2 Joint with mechanical stops and no events 147

List of Figures

2.1 Schematic of an inverted pendulum. 6
2.2 Center of pressure of a human foot 7
2.3 Inverted pendulum of a biped system 8
2.4 Linear inverted pendulum model 9
2.5 Reaction wheel pendulum equivalence 10
2.6 Reaction mass pendulum 11
2.7 Inertia shaping method 12
2.8 Parametric pendulum 13
2.9 Parametric excited robot 13
2.10 Driven pendulum 14
2.11 Extensible pendulum 15
2.12 Center of pressure 16
2.13 ZMP and center of pressure differences 17
2.14 Centroidal moment pivot 18
2.15 Capture point of an inverted pendulum 19
2.16 Capture point of a linear inverted pendulum 20
2.17 The rimless wheel 22
2.18 Centroidal angular and linear velocity of link i 25
2.19 Variable topology system 29
2.20 A three mass model of a robot 30

3.1 Rigid body with its equivalent point masses 33
3.2 Center of percussion of a baseball bat 34
3.3 Comparison of different simplifications of a rigid body 36
3.4 Kinematical chain represented by a system of particles 38

3.5 Center of percussion of a mechanism . . . 40
3.6 Free body diagram of the equivalent mechanism . . . 41
3.7 Causality of a simple circuit . . . 43

4.1 Biped with its equivalent inverted pendulum . . . 50
4.2 Dynamic equivalent systems . . . 52
4.3 Flywheel biped . . . 53
4.4 Angles of the flywheel biped . . . 53
4.5 Some parameters of the gait . . . 54
4.6 Swinging leg . . . 56
4.7 Plot of the hip joint angle . . . 61
4.8 Plot of the angles of the knees plus θ . . . 62
4.9 Plot of angle α for the right leg . . . 63
4.10 Stroboscopic picture of the animated simulation. . . . 64

5.1 Four mass equivalent system . . . 71
5.2 Equivalent system of the HAT group . . . 72
5.3 Equivalent system of the leg . . . 73
5.4 Equivalent system of the leg . . . 74
5.5 Schematic of the equivalent model . . . 74
5.6 Parameters of the model . . . 78
5.7 Stroboscopic animation of the "kicking" experiment . . . 79
5.8 Compensation of the reaction torques . . . 80
5.9 Experiments using no compensated controllers . . . 82
5.10 Experiments using center of mass compensation . . . 83
5.11 Experiments using center of percussion compensation . . . 84
5.12 Oscillation experiments . . . 86
5.13 Parameters of the oscillation experiments . . . 87

6.1 Gravity compensation . . . 93
6.2 Torques at joints using propotional gains of 10N·m/rad. . . . 95
6.3 40N·m/rad gain at the hip joint of the stance leg . . . 97
6.4 40N·m/rad gain at the swinging leg . . . 98
6.5 40N·m/rad gain at the ankle joint . . . 99
6.6 Pendulum system . . . 101
6.7 Schematic of the simulations . . . 103
6.8 Plots of the experiments . . . 105

A.1 Rigid body with two point masses 128

B.1 Center of percussion of a mechanism 131
B.2 Free body diagrams of the bars 132
B.3 Schematic of the equivalent mechanism 135
B.4 Free body diagram of the equivalent mechanism 137

1 Motivation and objectives

The wheel is considered as one of the most relevant inventions in the whole mankind, almost every mobile system that moves on the ground will require at least one. But nature has chosen to avoid this great invention, and yet, successfully develop the most impressive mechanisms of locomotion. Legs have an unmatchable versatility to adapt to a great variety of terrains, and particularly human gait displays a graceful symphony of movements to perform this task. Despite the presence of impacts, alternative cycles, an other undesirable effects, the efficiency is surprisingly high.

How human gait works is still an active research field. Countless algorithms are proposed in order to perform bipedal walking, but a great amount of work still should be done in order to be comparable against nature's work. Improved analysis tools, methods to develop simplified systems that could help a better understanding of the dynamics behind this fascinating phenomenon should be discovered. All this facts are the perfect ingredients to keep the curiosity alive.

In this section the motivation to start this research is exposed, this includes a brief discussion about limitations of the current techniques,it should be noticed that a detailed exposition will be done in Chapter 2 where the state of the art is discussed. After this discussion has been done, the objectives will be presented.

1.1 Motivation

In most control courses the stabilization of an inverted pendulum is used as the perfect introduction to new students into the field. The simplicity and transparency of the equations is a very interesting tool that provides an intuitive point of view to the abstract mathematics behind this science. Humans, being systems having a high center of mass

are perfect candidates to be modeled with inverted pendulums. As mentioned before, with the early experience in pendulum systems the possibilities become intuitive from the mathematical point of view, simple models and ingenious solutions can now be proposed to generate gait to a wide range of walking machines.

But pendulums are not the only option to simplify a biped. Other approaches include rimless wheels, replacing links or group of links by point masses, etc. The simplifications are done depending on particular necessities, depending on how the problem is focused as for example passive dynamics, limit cycle walking, zero moment point control, among others. This simplifications are often extended to simulations where the solution normally works perfectly because only the assumptions are taken into account when the model implemented. The simplifications during simulations can be go even further by introducing changes in the topology of the original system.

Although the just mentioned simplifications have proved effectiveness in different applications, in general there is no criteria to apply them. Most of them are based on the hypothesis that the mass is concentrated at the center of mass of the system or subsystem being studied, but no further analysis is done whether or not this assumption is valid. From this short discussion we can conclude that justified simplifications will be welcomed to improve the present state of the art.

1.2 Objectives

In general, the intuitive simplifications applied when analyzing biped robots have been successfully used in countless applications. Despite the achievements reported in prestigious journals of the field, part of the credit of the attainments belongs to the controllers. Carefully tunned algorithms are implemented in order to compensate the *non-modeled dynamics* and the result is walking machines that work. The problems faced to perform this accomplishments are the proof that more research is necessary in order to provide better analysis tools.

The general objective of this thesis is to provide a justified method to obtain simplified models that can be used to analyze biped robots. The idea is that the proposed method can be used not only to create new models, but to improve the existing ones. In this way the essence of the original ideas is maintained.

A particular objective is the improvement of the inverted pendulum based models, by considering the rotational dynamics of the original model. This improvement is based on the concept of *dynamic equivalence*. Once the equivalence have been proved, the

improved pendulum is used to demonstrate the possibilities of gait generation with a simplified, but not idealized biped[1].

Another problem that is the objective of this thesis is the design of biped robots. The design of the links and joints composing the robot is easily solved with classical mechanical design. Resistance, fatigue or other criteria are well suited tools to produce the required parts. But joints and links are not enough to produce a robot. Actuators are very important elements that should match the existing mechanics. Besides, once the actuators are selected the previous design steps should be reviewed in order to optimize the system.

The methodology proposed in this thesis has the objective to provide alternative models to decouple the dynamics of the controllers in each joint. Once each joint can be treated independently, the frequency response can be analyzed under different conditions. With this information the solicitations of the actuators and the different mechanical parts can be adjusted.

As final words the objectives can be itemized as follows:

- To develop a methodology to provide justified simplifications to model biped robots.
- To demonstrate the usage of the obtained models to generate gait.
- Generate alternative models with the proposed methodology to be used as analysis tools.
- Decoupling of the dynamics of the system in order to perform a guided mechanical design.

[1]This difference is done to specify that the models used in this thesis can be constructed in reality, because all the elements have finite mechanical properties. That means that no massless links, point masses or other idealizations are allowed without formal validation.

2
State of the art

In this chapter different mathematical models used in biped robots will be exposed. The objective of most of these models is to design control strategies. The strategies are focused in different problems that range from reject disturbances until gait design. Their simplicity is the most attractive quality. They successfully reproduce most of the dynamics, and they have probed usefulness in their respective applications.

The idea behind of the majority of the proposed models is to simplify the properties of the biped systems in few parameters that can be handled in a more friendly way. Although there are models of high complexity their objective is to construct simulators to probe other ideas, or to be used in a simplified way to be included in on-line algorithms. In the following lines some of the most popular models will be exposed.

2.1 Basic inverted pendulum based models

The inverted pendulum has been a source of inspiration from the beginning of formal locomotion research. The simplicity of its dynamic equations allows full analytical solutions. The major drawback of these models is how they are made. The mass of the pendulum corresponds to the mass of the robot itself, and its location is the same of the center of mass of the robot. The rod of the pendulum is supported over the center of pressure of the system. Such a simplification has the trade off that not all dynamic effects are modeled. A common improvement is to consider the moment of inertia in order to include additional dynamics, but still simplicity is kept in mind. Despite the simplifications, many experiments have demonstrated that it is a powerful tool. In this section some of the most popular models are exposed.

2.1.1 Inverted pendulum model

A pendulum system is a widely popular model, its study is part of the introduction of any physics course as a simple model of vibrational systems. In order to be used with bipedal system small modifications need to be taken into account, and the result is the inverted pendulum model.

The derivation of the equations of motion starts by writing the angular momentum of the point mass around O shown in Figure 2.1 as follows:

$$L_o = mr^2\dot{\theta} \tag{2.1}$$

The derivative of the angular momentum is:

$$\dot{L}_0 = mr^2\ddot{\theta} \tag{2.2}$$

If other accelerations are dismissed, Newton's second law can be written as:

$$\dot{L}_0 = mgr\sin\theta \tag{2.3}$$

Replacing 2.2 and 2.3 in order to eliminate $\dot{L}_0$:

$$\ddot{\theta} = \frac{g}{r}\sin\theta \tag{2.4}$$

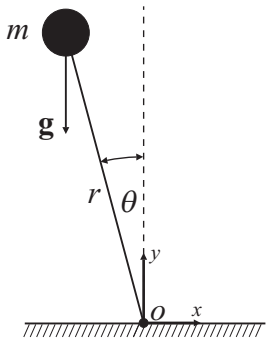

Figure 2.1: Schematic of an inverted pendulum.

By intuition the pendulum has two equilibrium points, when θ equals 0 (unstable equilibrium) and when θ equals $\pi/2$ (stable equilibrium), these equilibrium points extends to Equation 2.4. The application of this model to study locomotion comes by the fact that humans lie on a single leg during most of the walking cycle. In order to apply

this model to a biped system the concept of *Center of Pressure* is introduced, although it is discussed in detail in section 2.2.1.

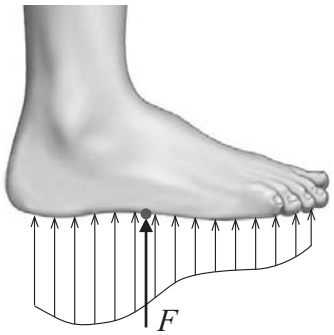

Figure 2.2: Example of the location of the center of pressure on a human foot. A very popular concept in aerodynamics and hydrostatics.

Center of pressure is defined as the point where the pressure field acting over the feet produces no moment and a force, this can be better seen in Figure 2.2. The inverted pendulum of a biped is constructed when the pivot is located over the center of pressure, the point mass has the same value of the total mass of the system and its location has the same position of the center of mass of the biped as shown in Figure 2.3.

The problem of stability of a biped is now reduced to the balancing of an inverted pendulum. This has been widely exploited to design gait algorithms or to study bipedal gait [49, 63, 73, 76, 95, 84, 102, 112]. Their simplicity and the available analytic solutions are some of the reasons of its popularity. Although different equations of motion can be obtained according to the necessities, for example a 3D extension in [21], the ones described in this section give a general view of how this model works.

2.1.2 Linear inverted pendulum model

The linear inverted pendulum model is obtained by restricting the point mass to travel into a straight path. The pendulum used to derive the equations of motion of this section is shown in Figure 2.4. The pendulum is borne over the point O by an extensible support without mass and it can only exert forces on the direction of it, therefore no torque can be applied over its base. Finally, in this derivation the pendulum is restricted to move parallel to the ground.

First, the balance of vertical forces is performed, according to Figure 2.4 it is written as follows:

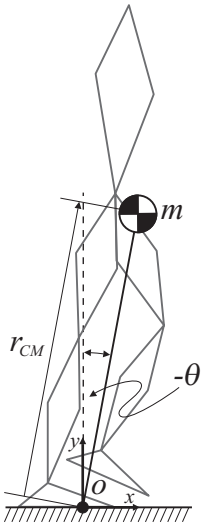

Figure 2.3: Inverted pendulum of a biped system. The location of the point mass of the pendulum and the center of mass of the biped is the same. The same happens with the value of the point mass.

$$F_y = -mg \tag{2.5}$$

F_x can be obtained by the geometric constrains imposed on the movement of the pendulum:

$$\frac{F_x}{F_y} = \frac{x}{y_h} \tag{2.6}$$

Replacing 2.5 into 2.6 to eliminate F_y and solving for F_x:

$$F_x = -mg\frac{x}{y_h} \tag{2.7}$$

The dynamics in x direction is summarized as:

$$F_x = m\ddot{x} \tag{2.8}$$

Finally, F_x is eliminated with equations 2.7 and 2.8:

$$\ddot{x} + x\frac{x}{y_h} = 0 \tag{2.9}$$

The previous equations are a simplification of the work developed in [54, 53, 55]. The simplification is required because this equations will be used in further sections,

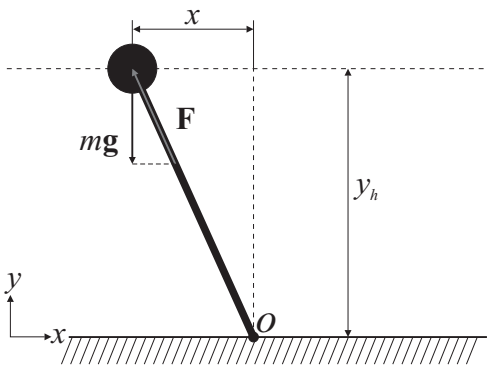

Figure 2.4: Linear inverted pendulum model (LIPM) restricted to move parallel to the ground. A massless and extensible leg is required to perform the restricted motion.

besides in the present form they allow to better understand the method. In the papers previously cited, detailed simulations of gait synthesis and a more general model can be found. The strong assumption of massless legs in both models (the ones in the original papers and the ones developed in this thesis) is an important simplification that should be considered in future improvements. The body dynamics is considered in the original model, although some simplifications are performed.

The form of equation 2.9 has the same form of a linearized simple pendulum, with the difference that the last one can be applied to the whole space state and is not restricted to small values of x. Besides it is important to note that the movement is restricted to be linear but not necessarily parallel to the ground, again more details can be found in the original publications.

2.1.3 Reaction mass and reaction wheel pendulums

The previous pendulum based models have the particularity that they cannot apply torque over its support. This is against the common sense, because humans rely on ankle torques to compensate small perturbations. This can be probed easily by standing still over one foot and feel how the reaction forces of the floor changes when the equilibrium is restored. Important rotational body dynamics is lost in the previous models; as was mentioned, for the sake of simplicity some sacrifices are required.

One of the most attractive qualities in the previous models is the ability to simplify the complex contact forces in one point (the center of pressure). In order to keep the original one point contact, and at the same time, add the capacity to apply torque over its support, in [59, 65, 95, 84] the point mass is replaced by a mass with a moment of

inertia. The mass can turn around its center of mass and it is supported by a massless leg. Depending on the context of work, two models arise, the one used on 2D cases called the reaction wheel pendulum and the 3D case called the reaction mass pendulum.

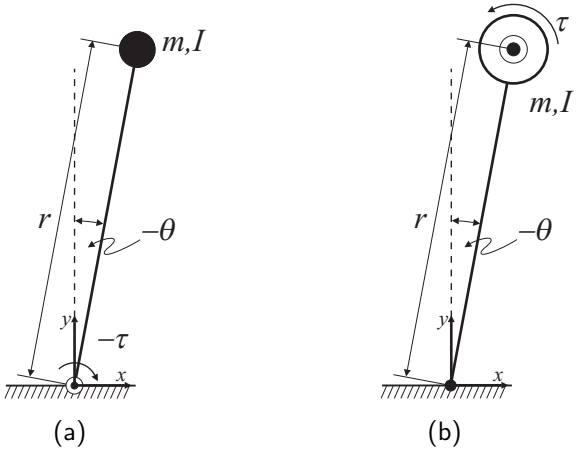

Figure 2.5: Reaction wheel pendulum equivalence: (a) an inverted pendulum is attached to the floor and it moves by applying a torque against the floor, and (b) if the torque applied to the flywheel is able to accelerate it, then both models are dynamically equivalent.

In Figure 2.5 two different pendulums are represented. In Figure 2.5(a) there is a simple inverted pendulum attached to the floor by a rotational joint, the joint is able to apply torque in order to move the pendulum as desired. The system is described by:

$$(I + mr^2)\ddot{\theta} + \tau - mgl\sin\theta = 0 \tag{2.10}$$

The other pendulum, shown in Figure 2.5(b), cannot apply a torque directly to the floor, instead it can accelerate a flywheel, its mathematical description is:

$$(I + mr^2)\ddot{\theta} + \tau - mgl\sin\theta = 0 \tag{2.11}$$

$$I\ddot{\theta}_{fly} = \tau \tag{2.12}$$

Where I is the inertia of the mass and θ_{fly} is the absolute angle of the flywheel, the other variables are described in Figure 2.5. It should be noticed that equations 2.10 and 2.11. The interesting fact here is: If the position of the flywheel is dismissed, both models are equivalent, as long as the flywheel can be accelerated[1]. Therefore, it is possible to

[1]If friction is present and the flywheel reaches its maximum speed the equivalence is no longer true.

adjust the position of the pendulum with a flywheel despite the fact that no motor exist between the floor and the support. These models improve some limitations present in the inverted pendulum model, the fact that attitude of the pendulum is now available to control, helps to describe the reality in biped systems.

The moment of inertia in 2D is a real number, but in the case of 3D motion a tensor[1] should be used. This tensor is calculated around the center of mass of the biped, and it is composed by all the rigid links that are part of it. The tensor of inertia can also be associated with its *equinomental* ellipsoid to construct the inverted pendulum.

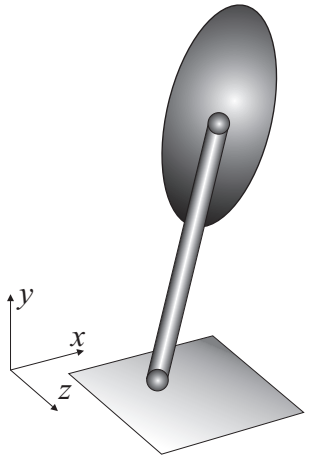

Figure 2.6: Reaction mass pendulum. The ellipsoid of the pendulum has the same mass and inertia tensor, the support is considered without mass.

In Figure 2.6 a representation of the reaction mass pendulum can be seen. In the case of a rigid body the ellipsoid of inertia is fixed. When the same ellipsoid is calculated for a multi body system[2] the centroidal moment of inertia of the complete system changes its value depending on the configuration; therefore, changing its reaction mass pendulum according to the state of the system. The last, opens the possibility to find new control strategies by *shaping* the inertia according to the requirements [65], this is better illustrated in Figure 2.7. The model discussed in the present section adds important improvements in order to keep complex dynamics of the system, but at the same time it is quite simple.

[1] The tensor of inertia is 3×3 matrix.

[2] This is the case for a biped composed by multiple links.

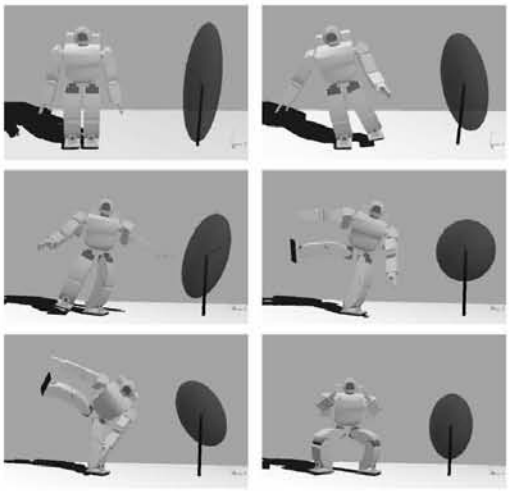

Figure 2.7: Inertia shaping method [65]. The ellipsoid of inertia changes its form and orientation according to the relative positions of the links of the robot.

2.1.4 Parametric pendulum

The parametric pendulum is a kind of driven pendulum that adds energy to the system by means of varying one of its parameters, this mechanism of adding energy is called parametric excitation. A simple pendulum is defined by two parameters, the length and the value of its point mass, because mass is normally considered as fixed, the only parameter left is length. The simplest way to control, although not a realistic one, and to maximize the energy pumped into the system is the one shown in Figure 2.8. The pendulum starts at 1, then when it is located in the lowest part of the cycle 2 it is elevated to 3. When the pendulum reaches 4 it has a wider swinging amplitude, after that it is taken to 5.

There are several applications for biped robots, the most obvious is to control the swinging of the free leg during the single stance phase [64]. This has been probed as an alternative to recover energy on passive dynamic walking [8, 6, 41]. They use an under-actuated robot with no motors at the hip, the robot has a piston that lift the leg when swinging. The robot and its gait cycle are shown in Figure 2.9.

Another well known phenomenon is the driven pendulum [16, 94]. When a pendulum is excited under certain frequency it has an stable upward position as shown in Figure 2.10(a). As was seen previously in this chapter, the biped stability problem can be summarized to the stability of an inverted pendulum, this fact is used in [50] to design the gait of a compass biped robot with extensible legs. A schematic of this robot and its gait cycle can be seen in Figure 2.10(b). The cycle is very similar to the one shown

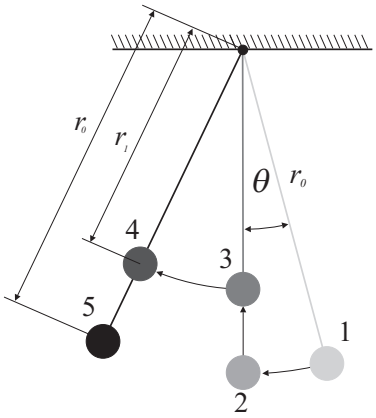

Figure 2.8: Parametric pendulum. In the figure an optimal control cycle is shown. In this case the energy into the system after one cycle is maximized.

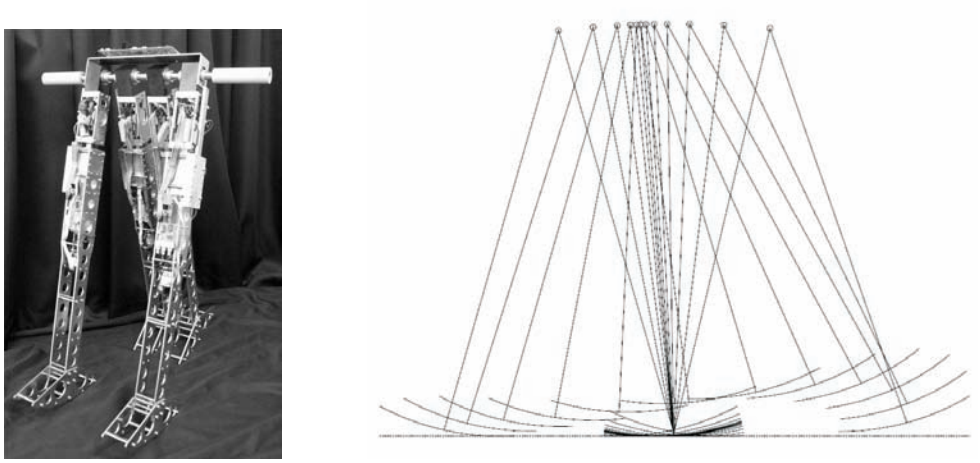

(a) (b)

Figure 2.9: Parametric excited robot [8, 6] at the Bio-mimetic Research Center, RIKEN, Japan. (a) a robot that uses the parametric excitation principle (b) stick diagram describing the gait of the robot. In this case the parametric excitation is used on the swinging leg.

in Figure 2.8, but in this case it is applied to the stance leg instead of the swinging one. Although on simulations the system works well, there are not reports of a successful working biped. The possible reason for this problem rely on the transition from point 4 to point 5. In order to achieve the transition the robot would need to pull the floor, but in reality the constraints of the stance leg can only push against it. Despite the problems, the mathematical background is interesting and it will be derived.

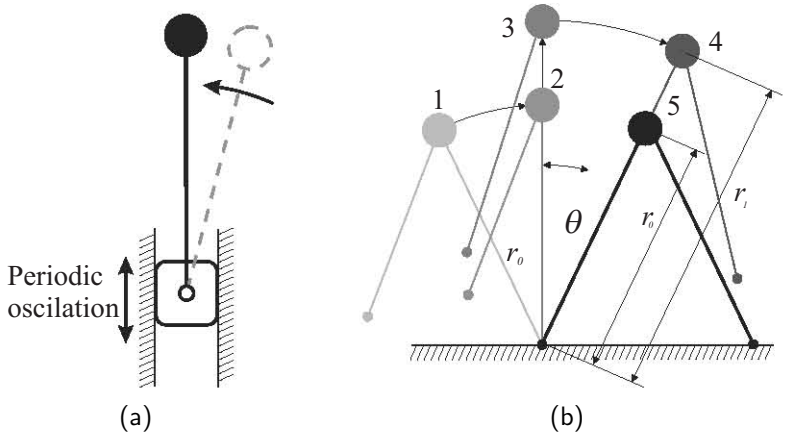

Figure 2.10: Driven pendulum model. (a) a schematic figure of the driven pendulum phenomenon (b) optimal trajectory of parametric excitation of a biped robot [50].

Let us focus on the pendulum in Figure 2.11. The angular and linear dynamics are given by:

$$mr^2\ddot{\theta} = mgr\sin\theta - 2mr\dot{r}\dot{\theta} \tag{2.13}$$

$$m\ddot{r} = F_r - mg\cos\theta + mr\dot{\theta}^2 \tag{2.14}$$

Examining term by term it is noted that the reaction force F_r does not modify the angular momentum of the pendulum, at least not directly. The reaction force can change the position of the point mass radially, therefore changing the length of the leg r. This last quantity is included in the rotational dynamics equations only when there is angular velocity. Because of that the linear actuator cannot stabilize the pendulum in the upright position. Intuitively it is possible to get more conclusions. The leg will accelerate the system when pulling the mass, because a minor length means a minor moment of inertia of the system, similar to the effect obtained by a figure ice skater, while the opposite will decelerate it.

Finally, it should be noted that there are extensive solutions for the parametric forced pendulum. The equations examined in this section only study what is happening in a single step. The reason for this decision is that a purely parametric phenomenon is not possible to achieve on a biped robot because of the low frequencies[1] present in normal gait.

[1]The frequencies are considered low when compared against the ones required to obtain an upright equilibrium, more details can be found in [16].

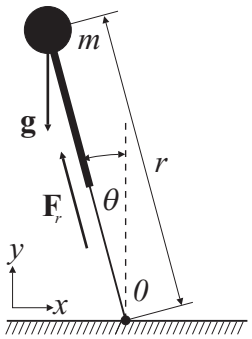

Figure 2.11: Extensible pendulum. The rotational dynamics of this pendulum cannot be affected by the leg. The change in length, instead, do have an effect on the rotational dynamics.

2.2 Ground reference points for biped robots

A biped system, because of its construction has a narrow support polygon, this particularity combined with a high center of mass produces a naturally unstable system. The interaction with the ground is not a static phenomenon as could happen with multi legged systems with low center of mass [38]. For this reason several ground reference points have been defined in order to study dynamic stability. Another motivation to define such points is the conservation of momentum principle; according to this the only way to change the momentum of a system is by external interactions. Considering the ground as the main source of those interactions, the study of these points enforce the understanding of biped dynamics.

2.2.1 Zero moment point and center of pressure

The interface between feet and ground is not over a point, but over a finite surface, this is called a pressure field. The integral of pressure with respect to the area gives the total force applied to the system by the pressure field, and the place where this force should be applied it is determined by the distance weighted of the total force:

$$r_{CP} = \frac{\int_{(A)} \vec{r} p(\vec{r}) dA}{F_{p(\vec{r})}} \tag{2.15}$$

Where r_{CP} is called the *center of pressure*, $p(\vec{r})dA$ is the position dependent pressure function, $F_{p(\vec{r})}$ is the force applied and A is the area of the pressure field. The last equation is used to determine forces over a dam, a plane wing or a sail boat where

complex pressure patterns are produced by water or air. The application in walking systems comes as an effort to summarize the complex contact forces between the floor and the feet, Figure 2.12 illustrates the last.

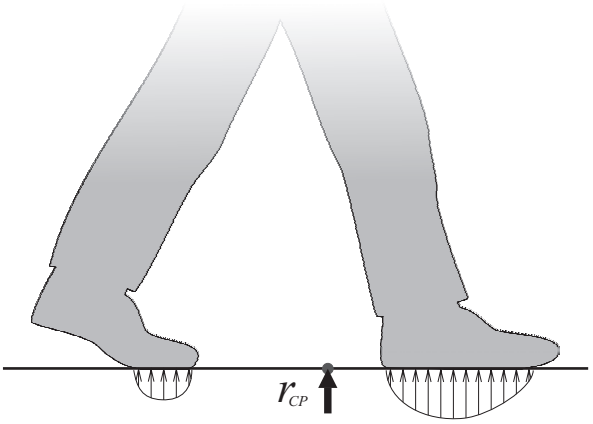

Figure 2.12: Center of pressure during the double stance phase. The center of pressure is not necessarily contained in the pressure field, but it is inside the polygon of support.

The center of pressure is often confused with the *zero moment point* (often abbreviated as ZMP), the last is due to the fact that both are in the same location during dynamic or static equilibrium states. But differences arise when looking into the definition of ZMP [103]:

> ZMP is defined as that point on the ground at which the net moment of the inertial forces and the gravity forces has no component along the horizontal axes.

Imaging a biped supported over one foot. The last definition can only exist if the whole sole is making contact with the floor, because this implies that no moment will cause rotation over an axis lying on the horizontal plane. In other words, if the body of the robot is perturbed by an external force no rotation occurs. This happens because the ZMP moves until the equilibrium is reached and the reaction forces equilibrates the horizontal moments. In Figure 2.13(a) a robotic foot is shown in equilibrium with the floor reaction R and the ankle reactions M_R and F_R. In this case the ZMP coincides with the center of pressure. If the center of pressure is located on one side of the support polygon; for example, the position of the foot in figure 2.13(b), no ZMP can be defined but instead a *fictitious ZMP* is found as the possible location of the ground reaction

force that equilibrates the system. The fictitious ZMP has been already proposed in [39] and it has been named as *foot rotation indicator*.

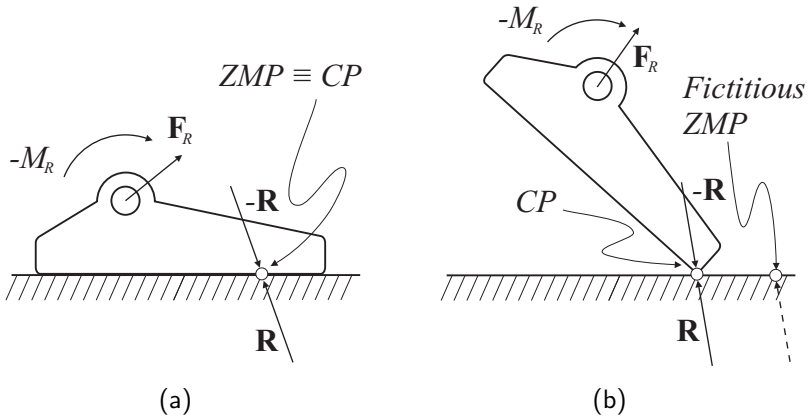

Figure 2.13: Zero moment point and center of pressure differences: (a) the whole surface of the foot makes contact, therefore the ZMP and the center of pressure are in the same position; and (b) the center of pressure is not enough to balance the biped, then a fictitious zero moment point is defined.

The previous discussion was done assuming flat surface, additional differences arise when considering the walking device over uneven surfaces. A detailed discussion can be found in [90] with a redefinition of the ZMP for the situation previously mentioned. Despite its limitations, the ZMP technique has been successfully applied to multi-legged systems [38, 81] and also applied in Asimo and HRP robots [46, 56] (All of them among the most advanced biped machines of their class). Other robots, as for example the one shown in [84], use the center of pressure concept, exploiting the dynamics of the robot beyond the restriction of the ZMP.

2.2.2 Centroidal moment pivot

The centroidal moment pivot is defined as the point where a line parallel to the ground reaction force, passing through the center of mass, intersects with the external contact surface [82], as shown in Figure 2.14. Mathematically this can be written as:

$$(\vec{r}_{CMP} - \vec{r}_{CM}) \times F_R = 0 \tag{2.16}$$

Where $\vec{r}_{CM}$ and $\vec{r}_{CMP}$ are the position vectors of the center of mass and the centroidal moment pivot. This point has been studied by different observations about the spin angular momentum during the gait cycle, the observations noted a highly regulated

angular momentum [83]. Therefore this point has been used to measure stability. Under certain conditions it also coincides with the zero moment point. Besides, it has also been used to study human gait and to compare it against artificial generated gait [83, 1].

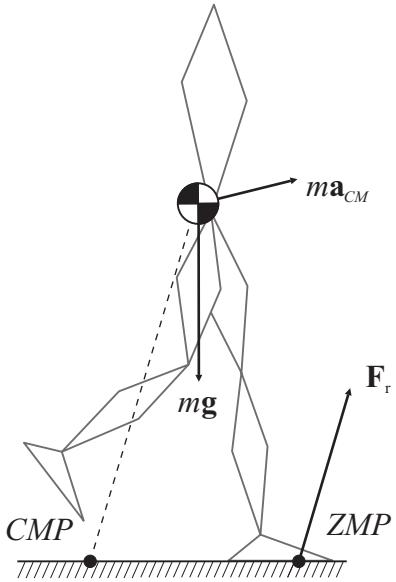

Figure 2.14: Centroidal moment pivot is the projection of the center of mass to the ground with a line parallel to the ground reaction forces. This point represent where the ground reaction forces should be applied in order to keep constant the angular momentum of the body.

2.2.3 Capture points

Ground reference points previously defined in this section are closely related, and careful interpretation of the definitions is required in order to identify them in particular situations. They are used to measure dynamic stability and as a tool to compare natural with artificial gait. But non of them can be used to predict the best position for the next step. Observations about how humans recover from large perturbations conclude that foot placement is the preferred strategy to recover balance [24]. The work in this section describes how to decide where to step in order to keep equilibrium.

A capture point is a point on the ground where the robot can step to in order to bring itself to a complete stop [85, 88]. To compute such a point in a complex robot is very difficult, besides a complex robot will have a collection of capture points. The collection of these points is called a capture region. This observation reinforce the conception that

during bipedal walking, trajectories in space do not need to be precise [87]. In this section only capture points will be discussed.

In order to simplify the estimation of capture points simple models of inverted pendulums have been used [86]. By definition a capture point is a point where all the kinetic energy is dissipated or converted into another kind of energy[1], for example converted into potential energy.

The analysis begins by computing the capture point of an inverted pendulum. In this analysis the pendulum performs a ballistic walking like gait without impacts[2], and it just stepped with speed v over a capture point that is measured from the ground projection of the center of mass by r_c, as shown in Figure 2.15. The distance r_c can be calculated by estimating the change of kinetic energy into potential energy, the total energy of the system can be written as:

$$\frac{1}{2}mv^2 + mgh = mgr \tag{2.17}$$

In Figure 2.15 it can be notice that $r_c = \sqrt{(r^2 - h^2)}$. Solving r_c in equation 2.17:

$$r_c = v\sqrt{\left(\frac{h}{g} + \frac{v^2}{4g^2}\right)} \tag{2.18}$$

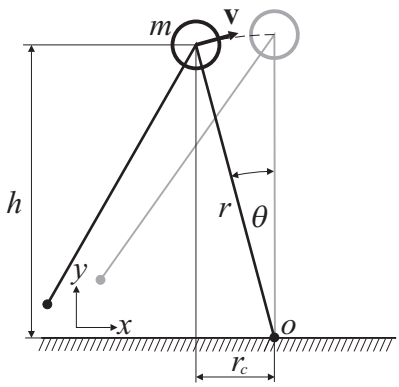

Figure 2.15: Capture point of an inverted pendulum. The distance r_c shows where to step in order to reach a full stop without any external force but the own weight.

Equation 2.18 predicts where to step respect to the ground projection of the center of mass. This is a different approach because the step length is not defined by the gait itself but by the state of the robot, therefore capture points can be used to reject large

[1] When impacts are included, it can also be a combination of both situations.

[2] An explanation of ballistic walking will be provided in section 2.3.1. More details can also be found in [33, 35, 71, 106].

perturbations. Now, the analysis will be centered around the linear inverted pendulum model.

In Figure 2.16 a biped with a point mass moving in straight line is shown. This biped obeys the following equation of motion, as was demonstrated in section 2.1.2:

$$\ddot{x} + x\frac{x}{y_h} = 0 \tag{2.19}$$

But equation 2.19 can also be interpreted as a mass-spring system with a negative-rate spring constant of g/h_0. Because of this a conserved quantity called *orbital energy* E_{LIP} of the pendulum is derived and is equal to [54, 85]:

$$E_{LIP} = \frac{1}{2}\dot{x}^2 - \frac{g}{2h}x^2 \tag{2.20}$$

This last quantity measures the amount of energy present in the linear inverted pendulum. In order to come to a complete stop the E_{LIP} should be equal to zero, therefore the two eigenvectors of the system are:

$$\dot{x} = \pm x\sqrt{\frac{g}{h}} \tag{2.21}$$

If the stable eigenvector is chosen, then the position of x found in equation 2.21 is the capture point for the given velocity:

$$x_{cap} = \dot{x}\sqrt{\frac{h}{g}} \tag{2.22}$$

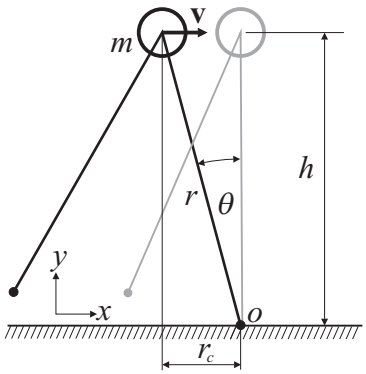

Figure 2.16: Capture point of a linear inverted pendulum. Just as happened with the inverted pendulum r_c is used as a step indicator.

In this section capture points for two systems have been found. The systems used for the derivations are under-actuated an rely on gravity and some idealizations to walk.

A complex system with more degrees of freedom is able to control every step, and therefore it is able to produce more than one capture point for a given state. This leads for a capture region, unfortunately capture points and hence capture region for such systems are really hard to compute, by the meanwhile simple models are used on different experiments on this field.

2.3 Other models

Biped systems are very complex, and as such they need different models in order to describe the phenomena present in their dynamics. The models already discussed are based in a strong simplification of the mass properties of the original robots. Although in this section the tendency to simplify is also present.

This section is dedicated to expose models that cannot be classified in the previous categories. The more complex models are preferred to be used as simulators, normally they are based on rigid body dynamics. Also simpler models can be found, as for example the rimless wheel, widely applied in the field of passive dynamics.

2.3.1 Rimless wheel

This model was originally proposed by Tad McGeer [69] to study passive dynamics walking, detailed studies are also developed in [7, 19, 18, 35, 106]. This model is based on the idea that walking is similar to rolling, considering that in both cases there is one point that serves as support and remains static during the motion. As its name suggest, a rimless wheel is a wheel without its rim, therefore the spokes serve as the only support[1]. This system does not behave like a normal wheel, instead, it looses energy after each impact, reaching zero velocity if the energy is not restored in some way. In Figure 2.17(a) a rimless wheel is lying over an inclined plane, the angular momentum just before the impact of the next spoke is:

$$H^- = (\cos 2\alpha_0 + r_{gyr}^2) m r^2 \Omega^- \tag{2.23}$$

Where r_{gyr} is the radius of gyration of the wheel, normalized with r, and Ω^- is the angular speed. The same can be done just after the impact:

$$H^+ = (\cos 2\alpha_0 + r_{gyr}^2) m r^2 \Omega^+ \tag{2.24}$$

[1] In fact, if infinite number of spokes are added a perfect wheel can be obtained.

Dividing equations 2.23 and 2.24 implies:

$$\frac{\Omega^+}{\Omega^-} = \frac{\cos 2\alpha_0 + r_{gyr}^2}{1 + r_{gyr}^2} \equiv \eta \tag{2.25}$$

It follows from 2.25 that over a series of k steps:

$$\Omega_k = \eta^k \tag{2.26}$$

On a level surface equation 2.26 shows that the wheel will decelerate exponentially. But, the analysis is performed according to Figure 2.17, then it is expected that the wheel will reach an stationary speed of Ω_0, then the period is:

$$\tau_0 = \frac{2\alpha_0}{\Omega_0} \tag{2.27}$$

This leads to the linear speed v of the wheel:

$$v = \frac{2r\alpha_0}{\tau_0} \tag{2.28}$$

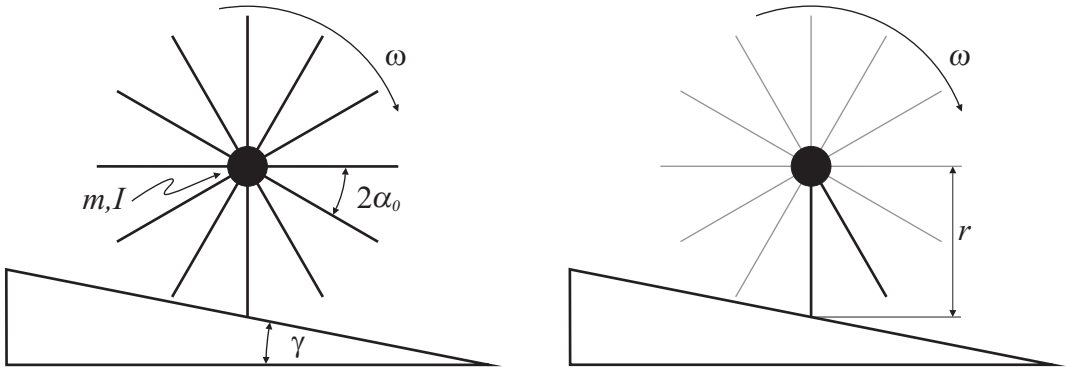

Figure 2.17: The rimless wheel: (a) a rimless wheel rolling on a inclined plane, (b) if all the spokes but two consecutive ones are removed, the result is the so called compass gait.

Finally, there is an important similarity with the inverted pendulum model. After the impact, if the moment of inertia is dismissed, both models are exactly the same. The difference is the ability of the rimless wheel to handle impacts, although intermediate dynamics can be found, the objective of the rimless wheel is to find the steady state period τ_0. In order to find such quantity, the dimensionless pendulum frequency [69]:

$$\sigma^2 = \frac{1}{1 + r_{gyr}^2} \tag{2.29}$$

The analysis is developed in dimensionless units with the mass m, leg length l, and time $\sqrt{l/g}$ as base units. Writing the equilibrium equation around the stance spoke, and taking the small angle approximation:

$$\ddot{\theta} - \sigma^2\theta \approx \sigma^2\gamma \tag{2.30}$$

θ is the angle between the stance leg and the surface normal. The rolling cycle starts when $\theta = -\alpha_0$ and $\Omega = \Omega_0$, and it finishes with $\theta = \alpha_0$ and $\Omega = \Omega_0/\eta$. When these boundary conditions are evaluated into 2.29, Ω_0 and τ_0 can be found, and the results are:

$$\Omega_0 = \sqrt{\frac{4\gamma\alpha_0\sigma^2\eta^2}{1 - \eta^2}} \tag{2.31}$$

$$e^{\sigma\tau_0} = \frac{\gamma + \alpha_0 + \Omega_0/\sigma\eta}{\gamma - \alpha_0 + \Omega_0/\sigma} \tag{2.32}$$

The previous analysis shows the behavior of a rimless wheel over an inclined plane, if all the spokes but two are removed the result is some sort of biped machine, in fact this is the base to the analysis of passive walkers [35, 106]. But it also serves as a model to develop gait in actuated machines [7, 30, 33, 106]. These machines exploit the limit cycle generated by this kind of motion, and recover the energy by the means of actuators in order to walk on level ground. The control strategies to achieve the former are endless, ranging from relatively simple state machines [47], until novel techniques that simulates the leaning plane on level ground by defining a virtual gravity vector [9, 96].

As can be seen in Figure 2.17(b) the resulting biped is similar to a geometric compass, this gives the origin of the term *compass gait*. Several studies have been develop around this, as for example 3D passive walkers [97], stability analysis focused on efficiency [66], rough terrain gait design [51], 2D and 3D stability margins [17, 18], etc. The versatility of the model allows amazing results, but unfortunately the stability of these machines depends on how fast the limit cycle can recover from disturbances, leading to a narrow stability margin. Finally, their control is very limited, because they have to stick to the dynamics of the rimless wheel, and therefore its limit cycle.

2.3.2 Complete models

Simplified models are very useful to inspire intuition, they clearly isolate complex phenomena and help to develop control strategies based on fast calculation of their reduced math. They also serve as design tool, loads can be estimated without complex calculations, and large quantities of mass properties are summarized in a few parameters. The price of all this advantages, as was mentioned above, is unmodeled dynamics that produces diverging results respect to reality. This is not always desirable, in order to probe how the real system will behave when a particular algorithm is applied more precise tools are required.

Fortunately, robots are composed by rigid links[1], in this way classical mechanics can be applied directly. The result is a detailed description of the dynamics of the system. The options to derive these equations are endless, among the most popular ones: Newton-Euler formulation, Hamiltonian mechanics, Lagrangian mechanics, bond graph approach, etc. Although any formulation can be used to derive the equations of motion, it should be notice that it is a variable topology system [31]. This is caused by the variable physical constraints that occurs during the gait cycle (i.e., ground reaction forces).

Derivation of the equations of motion

Let $q_1, q_2, \ldots, q_n$ be the generalized coordinates that completely locate our system. Let T and U be the total kinetic energy and potential energy stored in the dynamic system. The Lagrangian is defined as [5]:

$$\mathcal{L}(q_i, \dot{q}_i) = T - U \tag{2.33}$$

Since the kinetic and potential energy are functions of the generalized coordinates, the same applies to the Lagrangian. The time derivative of the Lagrangian is equal to the generalize force Q_i corresponding to the generalized coordinate q_i:

$$\frac{d}{dt}\frac{\partial \mathcal{L}}{\partial q_i} - \frac{\partial \mathcal{L}}{\partial q_i} = Q_i \tag{2.34}$$

The generalized force can be identified by considering the virtual work done by non-conservative forces acting on the system. In other words the generalized forces are the

[1] Human beings can also be considered in this way, the difference is that human joints are not purely rotational, but encompass complex kinematics. Most of the time these effects can be dismissed, and simple approximations are more than enough [105].

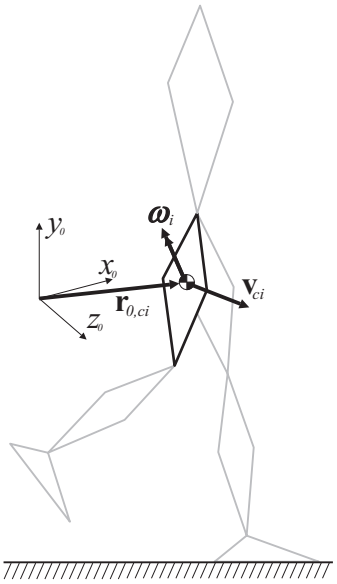

Figure 2.18: Linear and angular velocity of the center of mass of link i.

control torques and forces, friction forces, etc. According to picture 2.18, the total kinetic energy of a link is[1]:

$$T_i = \frac{1}{2} m_i \mathbf{v}_{ci}^T \mathbf{v}_{ci} + \frac{1}{2} \boldsymbol{\omega}_i^T \mathbf{I}_i \boldsymbol{\omega}_i \tag{2.35}$$

Considering the scalar nature of the energy, the total kinetic energy of the system is:

$$T = \sum_{i=1}^{n} T_i \tag{2.36}$$

Because of the constraints of each link, $\mathbf{v}_{ci}$ and $\boldsymbol{\omega}_i$ are not independent, consequently the linear and angular velocities are:

$$\begin{aligned} \mathbf{v}_{ci} &= \mathbf{J}_L^{(i)} \dot{q} \\ \boldsymbol{\omega}_i &= \mathbf{J_A}^{(i)} \dot{q} \end{aligned} \tag{2.37}$$

Where $\mathbf{J}_L^{(i)}$ and $\mathbf{J}_A^{(i)}$ are the Jacobian matrices for linear and angular velocities of link i, respectively[2]. Now, equation 2.36 is expanded:

[1]The total kinetic energy is the sum of the energy resulting from the translational and the rotational motion.

[2]Each element in the Jacobian is the derivative of a corresponding kinematic equation with respect to one of the variables [77].

$$T = \frac{1}{2}\sum_{i=1}^{n}\left(m_i\dot{\mathbf{q}}^T\mathbf{J}_L^{(i)T}\mathbf{J}_L^{(i)}\dot{\mathbf{q}} + \dot{\mathbf{q}}^T\mathbf{J}_A^{(i)T}\mathbf{I}_i\mathbf{J}_A^{(i)}\dot{\mathbf{q}}\right)$$
$$T = \frac{1}{2}\dot{\mathbf{q}}^T\mathbf{H}\dot{\mathbf{q}} \tag{2.38}$$

H is equal to:

$$\mathbf{H} = \sum_{i=1}^{n}\left(m_i\mathbf{J}_L^{(i)T}\mathbf{J}_L^{(i)} + \mathbf{J}_A^{(i)T}\mathbf{I}_i\mathbf{J}_A^{(i)}\right) \tag{2.39}$$

Where **H** is the $n \times n$ matrix that incorporates all the mass properties of the whole robot, and is called the *inertia tensor matrix* of the system. This matrix is based on the individual inertia tensor of each link[1]. Because the Jacobian of the system is involved, this matrix is configuration dependent. In order to continue, let us write equation 2.38 in scalar form:

$$T = \frac{1}{2}\sum_{i=1}^{n}\sum_{j=1}^{n}H_{ij}\dot{q}_i\dot{q}_j \tag{2.40}$$

Where H_{ij} is the $[i, j]$ component of the inertia tensor **H**. To continue the analysis, the first term of equation 2.34 is written as:

$$\begin{aligned}\frac{d}{dt}\left(\frac{\partial T}{\partial \dot{q}_i}\right) &= \frac{d}{dt}\left(\sum_{j=1}^{n}H_{ij}\dot{q}_j\right)\\ &= \sum_{j=1}^{n}H_{ij}\dot{q}_j + \sum_{j=1}^{n}\frac{dH_{ij}}{dt}\dot{q}_j\end{aligned} \tag{2.41}$$

The time derivative of H_{ij} is:

$$\frac{dH_{ij}}{dt} = \sum_{j=1}^{n}\frac{dH_{ij}}{\partial q_k}\dot{q}_k \tag{2.42}$$

The second term of equation 2.34 is computed as follows:

[1] In fact, the inertia tensor matrix represents the instantaneous composite mass properties of the whole robot.

$$\frac{\partial T}{\partial q_i} = \frac{\partial}{\partial q_i}\left(\frac{1}{2}\sum_{j=1}^{n}\sum_{k=1}^{n} H_{jk}\dot{q}_j\dot{q}_k\right)$$
$$= \frac{1}{2}\sum_{j=1}^{n}\sum_{k=1}^{n}\frac{H_{jk}}{\partial q_i}\dot{q}_j\dot{q}_k \tag{2.43}$$

Now the potential energy part of the Lagrangian is computed. Defining as $\mathbf{g}$ as the 3×1 gravity vector with reference to the base coordinate frame[1]. The potential energy of the link is given by:

$$U = \sum_{i=1}^{n} m_i \mathbf{g}^T \mathbf{r}_{0,ci} \tag{2.44}$$

Because the potential energy does not depends on $\dot{q}_i$ the first term of equation 2.34 is zero. But, it does depends on q_i therefore the second term for the potential energy is:

$$\frac{\partial U}{\partial q_i} = \sum_{j=1}^{n} m_i \mathbf{g}^T \frac{\partial \mathbf{r}_{0,ci}}{\partial q_i}$$
$$= \sum_{j=1}^{n} m_i \mathbf{g}^T \mathbf{J}_{L\ i}^{(j)} \tag{2.45}$$

Where $\mathbf{J}_{L\ i}^{(j)}$ is the $i-$th column vector of the Jacobian matrix $\mathbf{J}_{Li}^{(j)}$ Finally the equations of motion of the robot are found by substituting each term in 2.34. After reordering terms the result is:

$$\sum_{j=1}^{n} H_{ij}\ddot{q}_j + \sum_{j=1}^{n}\sum_{k=1}^{n}\left(\frac{H_{ij}}{\partial q_k} - \frac{1}{2}\frac{H_{jk}}{\partial qi}\right) + \sum_{j=1}^{n} m_i \mathbf{g}^T \mathbf{J}_{L\ i}^{(j)} = Q_i \tag{2.46}$$

Short discussion about the equations of motion

Equation 2.46 is a detailed description of a multi-body system. The first term corresponds to the inertial torques, as seen between joints. The second term corresponds to Coriolis and centrifugal accelerations, and the last term represents gravitational torques. Such detailed description produces a complex solution, rarely found analytically. In-

[1]The base coordinate frame is an inertial reference frame, this is required to apply Lagrangian mechanics.

stead, it is often used to develop simulators of the original systems, some examples are found in [36, 76, 93, 109].

Despite the complexity of the solution such a model can also be used to design gait. The flexibility of a virtual model allows the implementation of trial and error algorithms without damaging of the actual robot, as for example a neural network implemented in [104]. Also optimal solutions can be developed, the major challenge is how to solve topology changes. A possible solution is to define piecewise boundary constraints, separating the gait cycle in well defined phases [99].

The precision of the model is limited by what is implemented in it. Backlash, friction and other phenomena can be added, at the cost of adding complexity to the model. Compliance of the links, instead, are more difficult to implement because the analysis has been done assuming rigid ones. Other source of errors is the determination of the parameters of the robot. Measuring the inertia tensor of the links and location of its center of mass is not a simple task, leading to differences between the reality and the simulations; although, the results are quite accurate.

2.3.3 Reduced models

In the previous section a highly detailed and scalable model was shown. Its objective is to provide a faithful description of the system it represent. Depending of the objective, some effects can be dismissed and a simplified model can be constructed. For example, if rotational displacements are expected to be low, the inertia tensor matrix does not need close attention. In other situations the simplification is convenient in order to reduce the number of present equations. Whatever it is the case, the simplification it is required to keep most of the properties to validate the experiments.

The most common simplification is to consider rigid bodies as point masses located in its own center of mass. This is a common approach when modeling passive dynamic systems, or robots based on their limit cycles. Usually, these machines have light structures with low radius of gyration, dismissing some rotational dynamics does not compromise the results obtained by the model. Some examples of the former can be found in [51, 91]. Considering that this kind of walkers rely strongly on the natural frequency of the system, such simplification could seem excessive. In fact in [32] a pretty detail model is proposed for a passive like system. But depending on the robot other effects as actuation, friction, impact, etc. seem to be more important and override possible problems.

The simplifications also include variations of the topology of the system depending on the gait phase. An example is shown in Figure 2.19 where the system changes from

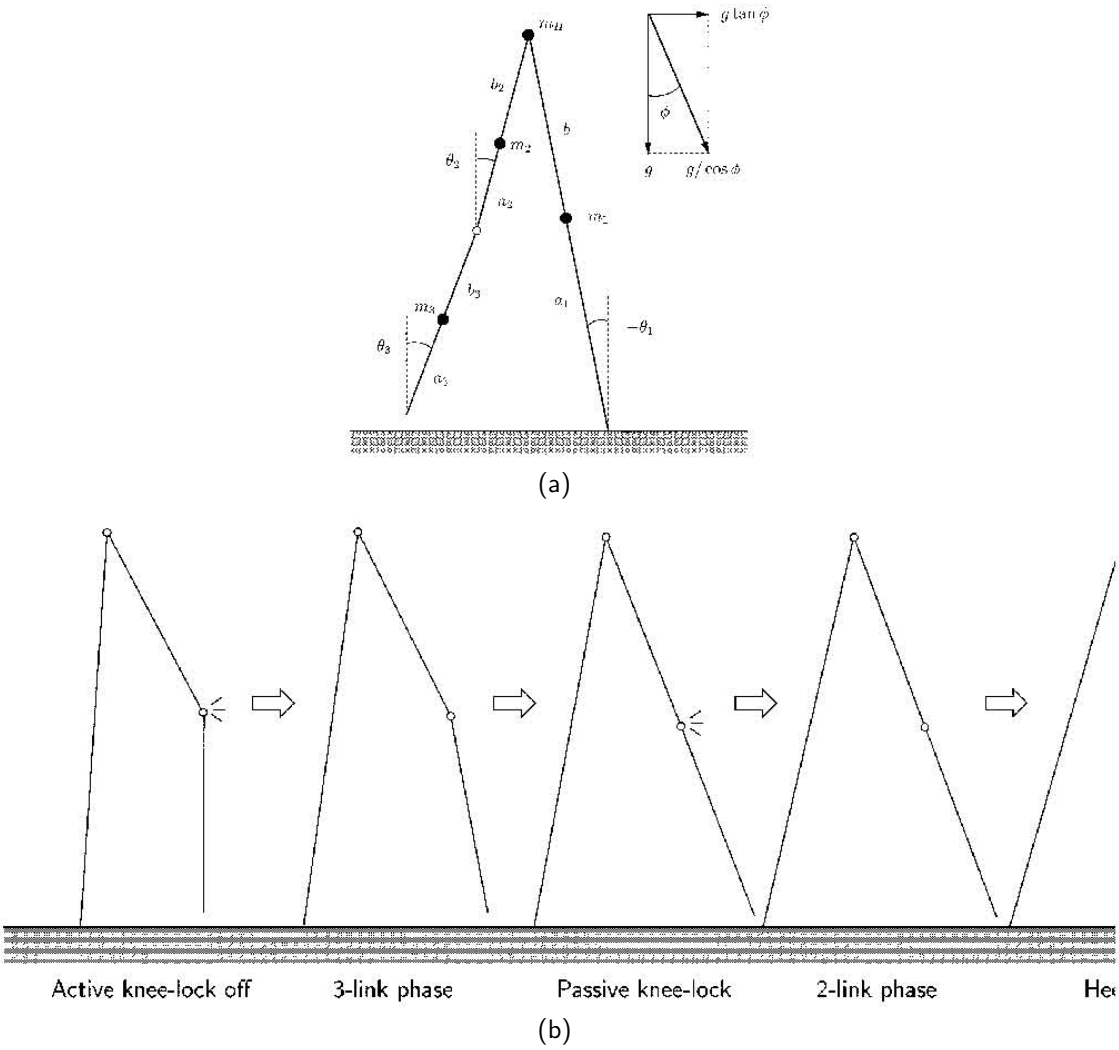

Figure 2.19: A variable topology system [9]. (a) the model changes its structure according to the gait phase, from two to three links when the knee lock is not active.

two to three links depending on the phase of the gate. The change occurs when the knee lock is active, then the two links of the leg behave like one. The difference between a real knee lock and the implementation in Figure 2.19 is that in the case of a knee lock implemented inside a model, the reaction force of the lock is computed. In the Figure the equations of motion are modified by modeling the leg as one link with one point mass instead of two. The new leg will not longer have the same moment of inertia, although it will share the same center of mass.

The torso is also added as a point mass, considering that its rotation is very limited when walking in normal conditions [65], only the center of mass plays a major role during

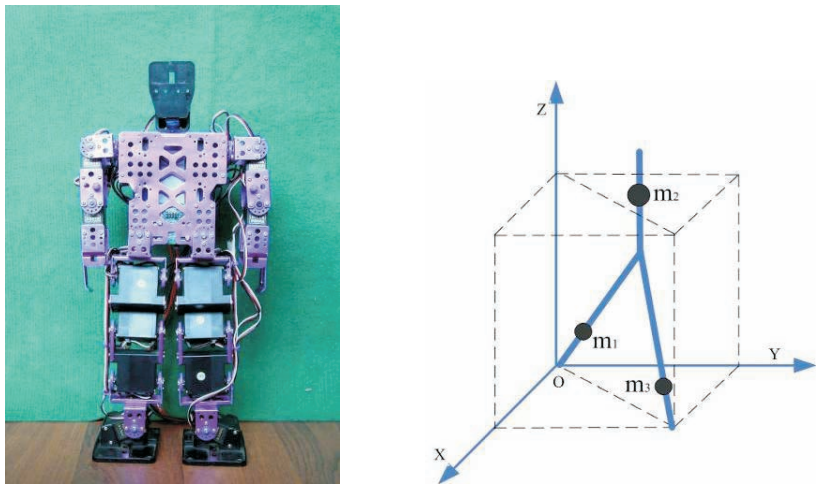

(a) (b)

Figure 2.20: A three mass model of a robot [26]. (a) the real system where the model was applied. (b) the model used to design the control algorithms.

gait cycles. Several authors have follow this way to produce their models, some examples includes [58, 91, 104]. An interesting application is done in [26] where an algorithm is developed based on the linear inverted pendulum, and then applied to a real robot with satisfactory results, according to the authors. The robot and the model are shown in Figure 2.20. Actually the point mass corresponding to the trunk summarizes the so called HAT (Head, arms and trunk). Such a harsh simplification invites to think that the model is dismissing important dynamical effects. Later in this thesis this aspect will be studied in detail when showing alternative dynamic equivalences.

The models proposed in this section are not mathematically different from the one already proposed in section 2.3.2. Their formulation has the same basis, the difference is the assignation of the parameters. While in section 2.3.2 all the mass parameters are considered, in this section arbitrary mass properties were selected, leading to simplified equations of motion, and therefore not all the dynamic effects are reflected. Yet, important similarities to the original system are maintained.

3

Theoretical Framework and Methods

In Chapter 2 a pretty clever group of mathematical models for bipeds was exposed. Those models have been the base of bipedal research during many years. In general, they have been able to probe usefulness in different conditions, as shown in the references cited in this document. Despite all the research done around the previous models, they clearly dismiss part of the dynamics by assuming the mass concentrated at the center of mass[1].

In this chapter the concept of *dynamic equivalence* is introduced as an alternative to improve the point mass simplification widely used in biped literature. The objective is to keep the point mass approach, but at the same time conserve rotational dynamics. This is done by means of the *center of percussion*, a concept widely used to study impacts of long and thin elements and also in the balancing of engines and other alternative machines.

The methods used in this thesis to perform the simulations of the following chapters are also exposed. The selected tool is the language simulation Modelica® using Dymola® implementation. Modelica® allows object oriented modeling to avoid problems like computational causality assignation. In this way completely non-causal models are generated guarantying the validity of the results for future developments.

The complexity of a biped robot has been the source of inspiration of very ingenious models described in chapter 2. Except for the model described in section 2.3.2, simplification is a common quality among all of them. The most practical approach is to only consider the effects of the center of mass. In fact, in a quasi-static situation this approach is almost an exact solution, this is a very useful concept in civil engineering. But, when studying dynamic walking it would of interest to have better tools to define alternative models.

[1]The models shown in section 2.3.2 are an exception for this statement.

In this chapter an alternative method of simplification of rigid bodies and kinematic chains is developed. As was said before, the foundation of it is the center of percussion. In summary, the idea is to keep replacing the original system by point masses. In this way, the original approaches developed in the literature of this thesis could be applied with minor modifications. The simplicity of the dynamics of a point mass is a very attractive motivation in order to find alternative ways to propose such models.

3.1 Dynamic equivalence

By definition, equivalent means that under the same conditions the result will be the same between two systems, in other words it does express an state of equality. The concept can be extended to classical mechanics. In this context it is necessary that the systems under comparison will behave in the same way under the same boundary conditions and forces, that means both systems will share the same equations of motion.

The previous paragraph can be summarized under three statements as follows:

1. The total mass of the systems is the same.
2. Both systems share the same first moment of mass.
3. And, the second moment of mass it is also the same.

The meaning of the first statement is explained by itself. The second statement means that the systems will have the same center of mass, and the final statement speaks about the equality between the moment of inertias. Clearly, if those quantities are the same, the equations of motion will be also the same, under dynamic and static conditions. When the static case is considered only the first and second statement need to be considered.

3.1.1 Center of percussion

There are countless ways to define equivalent systems, but one of the simplest is to define it in terms of point masses. A rigid body can be reduced to a minimum of two point masses[1]. In order to find the position and the value of those masses it will be necessary

[1] A system equivalence with one mass would be impossible, this comes out when thinking that every body has a finite place in space, a point by itself is infinitely small, but a system with two points could be considered that posses finite parameters, and therefore could represent a real system. Another observation is done when considering a point mass rotating around itself: The moment of inertia is zero.

to use the conditions mentioned in section 3.1. Considering the rigid body in the Figure 3.1, where the rigid body is represented by two point masses m_1 and m_2, those three conditions can be written mathematically as follows:

$$m_1 + m_2 = m \tag{3.1}$$

$$m_1 r_1 = m_2 r_2 \tag{3.2}$$

$$m_1 r_1^2 + m_2 r_2^2 = I \tag{3.3}$$

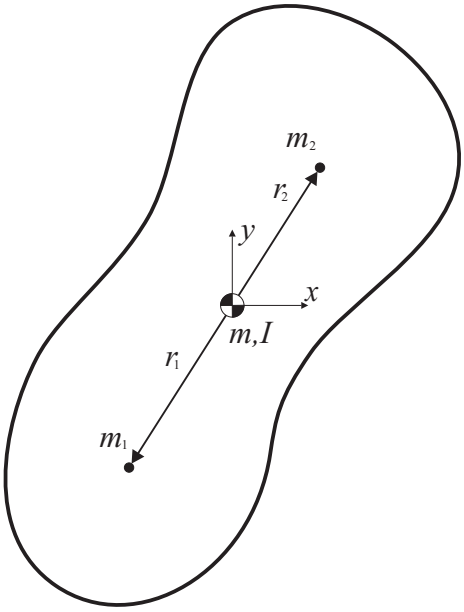

Figure 3.1: Rigid body with its equivalent point masses. A rigid body can be reduced to two point masses, both systems are dynamically equivalent.

In order to reduce the dimensionality of the system to three, instead of four, the position of m_1 is arbitrarily fixed. Now equations 3.1, 3.2 and 3.3 form a system of tree equations with three unknowns m_1, m_2 and r_2. A detailed solution of the nonlinear system is developed in Appendix A. Once the system is solved the result is:

Therefore a rigid body cannot be represented by a single mass because its moment of inertia is always greater than zero.

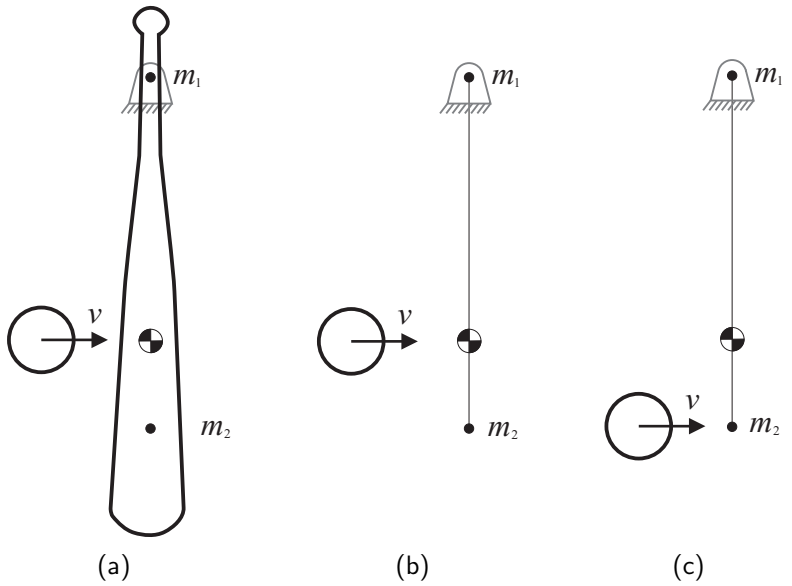

Figure 3.2: Center of percussion of a baseball bat. (a) a baseball bat, (b) equivalent model hit at the center of mass and (c) the same model hit at m_2 . Remember that all models are pivoted around m_1.

$$m_1 = \frac{mr_2}{r_1 + r_2} \tag{3.4}$$

$$m_2 = \frac{mr_1}{r_1 + r_2} \tag{3.5}$$

$$r_2 = \frac{I}{mr_1} \tag{3.6}$$

Equation 3.6 represents the center of percussion of the rigid body when the system is rotated around m_1. When the system has been reduced to two point masses it becomes more obvious the meaning of this quantity. Consider the baseball bat in Figure 3.2(a) pivoted around m_1 being struck by a ball. The behavior of the bat will change depending on the location of the hit, it is well known that the reactions becomes zero when the impact happens at the center of percussion and not the center of mass as many people tends to think. The reason for this is the one just explained in this section: A rigid body can be reduced to a minimum of two point masses. To understand this phenomenon the equivalent system depicted in Figure 3.2(b) and 3.2(c) will be used. It is composed by two point masses connected by a massless rigid rod.

When the ball hits at any point different from m_2, the reaction forces produce a moment in order to be balanced[1]. Because the system is pivoted around m_1, it is not affected by the impact. But, if the ball is pointed directly over m_2 the momentum is entirely transmitted to this mass and no reaction moment is produced. Therefore the reaction forces are minimized.

When considered the bat as a rigid body, the point where to hit in order to minimize reaction forces was not clearly defined. The solution can be found by angular momentum equilibrium [100], although correct, it is not intuitive. But, in the second case, when the equivalent system composed by only point masses is considered, the point where to hit becomes more obvious. Everybody will agree that working with point masses is far simpler than working with rigid bodies. From this analysis arise the question: Is it possible to use the center of percussion instead of the center of mass to simplify the system?. For a rigid body this question is clearly true, but in a more complex situation it needs a little more work to be answered, and it will developed in the following sections.

3.1.2 What is missing?

If only one rigid body is considered, its equations of motion are quite simple. Thus, it is possible to establish comparison using different simplifications in order to provide an objective measure of what is missing when doing such operations. Consider the rigid body in Figure 3.3(a), the body is pivoted around its base.

Now, consider the model in Figure 3.3(b). This is equivalent to what is normally done when dealing with complex kinematic chains such as a biped robot: The system is assumed to be concentrated at the center of mass. The value and location of the point mass are equal to the total mass of the original system, and there the similarities are finished. The angular momentum around the pivot of the simplified system is written as:

$$\mathbf{L}_{CM} = \mathbf{r}_{CM} \times m\mathbf{v}_{CM} \tag{3.7}$$

Where $\mathbf{L}_{CM}$ is the angular momentum, $\mathbf{r}_{CM}$ is the position vector of the point mass, m is the mass of the original system and $\mathbf{v}_{CM}$ is the velocity vector of the point mass. Remember that angular velocity is defined by $\boldsymbol{\omega}_{CM} = (\mathbf{r}_{CM} \times \mathbf{v}_{CM}) / |\mathbf{r}_{CM}|^2$, replacing this quantity in equation 3.7 leads to:

[1] Remember that the system is pivoted around m_1.

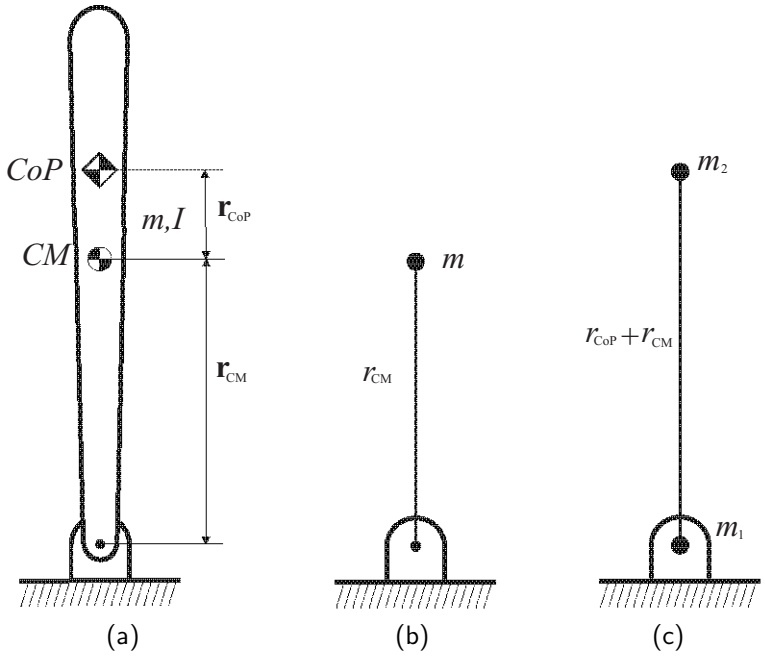

Figure 3.3: Comparison of different simplifications of a rigid body. (a) the original model, (b) a model using the center of mass approach and (c) a model using the center of percussion approach.

$$\mathbf{L}_{CM} = m\left|\mathbf{r}_{CM}\right|^2 \boldsymbol{\omega} \tag{3.8}$$

$$\mathbf{L}_{CM} = m r_{CM}^2 \boldsymbol{\omega} \tag{3.9}$$

Here, r_{CM} is the norm of $\mathbf{r}_{CM}$. Next, the same analysis will be performed to the system shown in Figure 3.3(c). Analogously, the angular momentum is written as:

$$\mathbf{L}_{CoP} = (\mathbf{r}_{CM} + \mathbf{r}_{CoP}) \times m_2 \mathbf{v}_{CoP} \tag{3.10}$$

$$\mathbf{L}_{CoP} = m_2 (r_{CM} + r_{CoP})^2 \boldsymbol{\omega} \tag{3.11}$$

from section 3.1.1 the value m_2 and r_{CoP} are equal to:

$$m_2 = \frac{mr_{CM}}{r_{CM} + r_{CoP}} \tag{3.12}$$

$$r_{CoP} = \frac{I}{mr_{CM}} \tag{3.13}$$

replacing equations 3.12 and 3.13 into equation 3.11:

$$\mathbf{L}_{CoP} = I\boldsymbol{\omega} + mr_{CM}^2\boldsymbol{\omega} \tag{3.14}$$

Now compare equations 3.9 and 3.14. The conclusion is that equation 3.14 has an additional term representing the rotation around the center of mass. In the first case the system was assumed to be composed by only one point mass, therefore no such a rotation could be modeled. In the second case, despite the fact of still being a system with only one moving mass[1] it is able to take into account the effects of the moment of inertia. Actually, equation 3.14 represents the exact dynamics of the original system, it is quite remarkable how a point mass with a smaller value, but located farther from the pivot can gather all the original dynamics of the rigid body. In the next section this concept will be extended to a kinematic chain.

3.1.3 Center of percussion of a system of particles

Section 3.1.1 depicts how to obtain the minimum number of point masses at which a rigid body can be reduced. The same methodology can be applied to a system of particles. This can be done by selecting proper reference frames when finding the couple of point masses. The result is a system of particles as depicted in Figure 3.4, here a system of particles equivalent to the kinematic chain drawn in dotted lines is illustrated. Applying the equations of motion the ith particle produces the following equations:

$$\mathbf{F}_i + \mathbf{f}_i = m_i\mathbf{a}_i \tag{3.15}$$

where $\mathbf{F}_i$ is the resultant external force acting over the ith particle, $\mathbf{f}_i$ represents the internal force, m_i is the ith mass and $\mathbf{a}_i$ is the corresponding acceleration. Adding the equations of each particle:

$$\sum \mathbf{F}_i + \sum \mathbf{f}_i = \sum m_i\mathbf{a}_i \tag{3.16}$$

[1] Although the system is composed by two point masses, only one of them is moving. The other mass is located at the pivot.

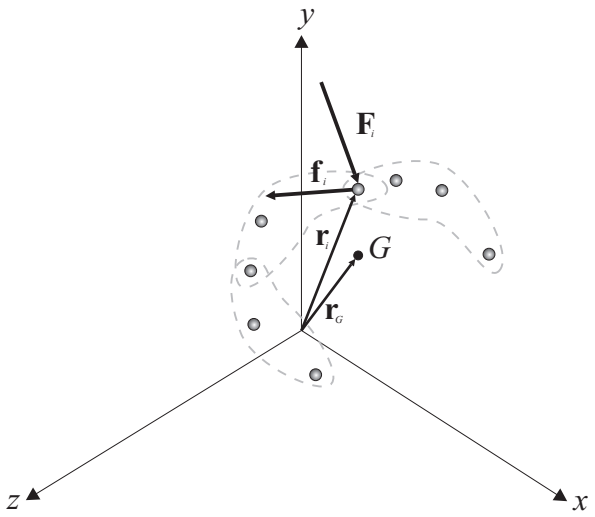

Figure 3.4: Kinematical chain represented by a system of particles. The figure shows a kinematic chain represented by an arbitrary number of particles.

The summation of the internal forces will equal zero, since internal forces between any two particles occur in equal but opposite pairs. Consequently, only the external forces are considered. Equation 3.16 is reduced to:

$$\sum \mathbf{F}_i = \sum m_i \mathbf{a}_i \tag{3.17}$$

In Figure 3.4 $\mathbf{r_G}$ indicates the center of mass of the system of particles. Remember that the definition of the center of mass is $m\mathbf{r_G} = \sum m_i \mathbf{r_i}$. Differentiating this equation twice with respect to time and assuming that the mass change in the system is zero, yields:

$$m\mathbf{a_G} = \sum m_i \mathbf{a_i} \tag{3.18}$$

replacing this result into equation 3.17:

$$\sum \mathbf{F}_i = m\mathbf{a}_G \tag{3.19}$$

From Section 3.1 a dynamically equivalent system must satisfy[1]:

$$m\mathbf{r}_G = m_a \mathbf{r}_a + m_{CP}\mathbf{r}_{CP} \tag{3.20}$$

[1]The subscripts 1 and 2 of Section 3.1 have been replaced by a and CP to avoid misunderstandings.

Also remember that one reference is selected arbitrarily in order to calculate the other point that becomes the center of percussion. Fixing m_a at the origin of coordinates and differentiating equation 3.20 twice with respect to time, the result is:

$$m\mathbf{a}_G = \ddot{m}_{CP}\mathbf{r}_{CP} + 2\dot{m}_{CP}\mathbf{v}_{CP} + m_{CP}\mathbf{a}_{CP} \tag{3.21}$$

If the derivatives of $\dot{m}_{CP}$ are assumed to be small, and therefore not considered, equation 3.21 is replaced into equation 3.19 to obtain:

$$\sum \mathbf{F}_i \approx m_{CP}\mathbf{a}_{CP} \tag{3.22}$$

Equation 3.22 states that a system of particles can be represented by a single point mass. What is not represented in the equation are the restrictions applied to that mass in order to faithfully represent the original system, in fact the restrictions are what defines the topology of the system.

As final words it should be noticed that the moment of inertia of the system of particles equals the total moment of inertia of the kinematic chain. This is consequence of how the point masses are found, they are required to maintain equality with the second moment of mass as defined in equation 3.3. The previous demonstration pretends to explain how a system can be reduced to a system of point masses, to complete the explanation in the next section the methodology will be applied to a mechanism.

Center of percussion of a kinematic chain: An application

When a rigid body is replaced by its equivalent two point mass system, we assume that all the interactions with other dynamic systems will be the same as if the original rigid body would be used. In fact this is quite easy to demonstrate and it was done partially in section 3.1.2, this is concluded after comparing the equation of motion of the original system and the equivalent one. In the case of a kinematic chain is hard to compare them. The problem arises when the equivalence is found, it happens that the topology of both systems is too different to make a direct comparison. To avoid this problem, the comparison will be done with the reaction forces produced by both systems. In fact the reaction forces could be considered as a set of generalized forces describing a system, when suitable generalized coordinates are considered.

Consider the mechanism in Figure 3.5(a), the only force acting over the mechanism is the force of gravity. The system is considered frictionless and the bars have distributed mass. In Figure 3.5(b) the equivalent system is shown, it is composed by two point

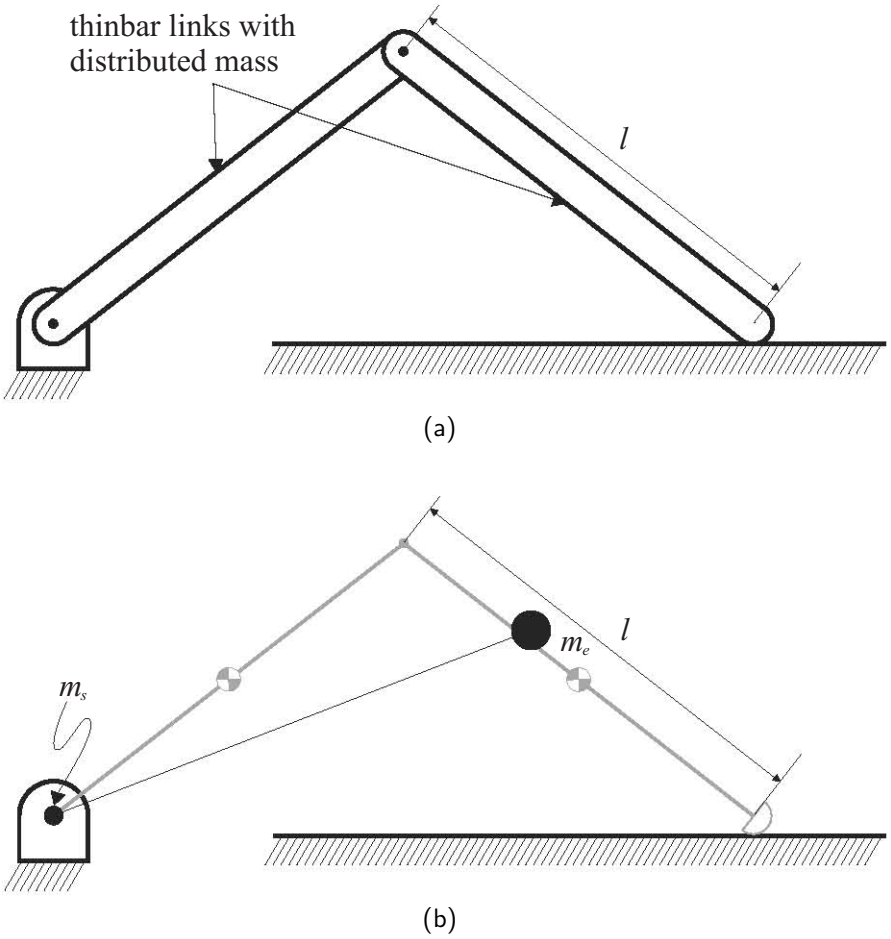

Figure 3.5: Center of percussion of a mechanism. (a) real mechanism composed by thin bars, (b) idealized equivalent mechanism.

masses calculated out of the original system drawn in gray. One of the point masses is fixed at the pivot of the mechanism, and the other is located at the center of percussion. They are calculated with the techniques already discussed in this chapter with some modifications.

The center of percussion of a rigid body is defined in equation 3.6, here the inertia of the body and the center of mass vector is required. In the case of a kinematic chain the same quantities are required, and the same formula is applied, the difference is that the center of percussion is not constant and it is configuration dependent. This is because all the quantities: Moment of inertia, mass, and center of mass vector are considered for the whole mechanism, and except for the mass they need to be calculated according to the configuration of the system.

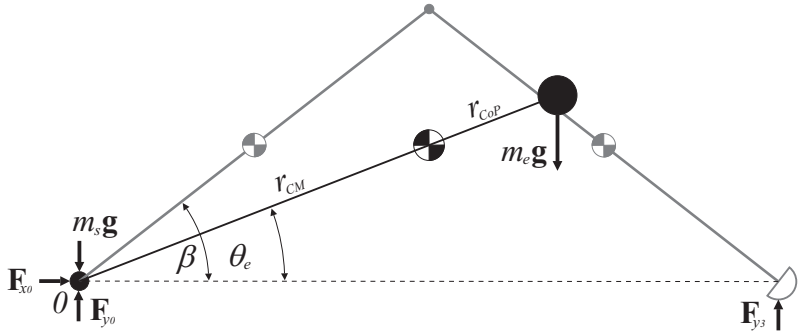

Figure 3.6: Free body diagram of the equivalent mechanism. The original mechanism is shown in gray to illustrate where the reaction forces are applied.

The point mass in Figure 3.5(b) is restricted to move according to the location of the center of percussion of the original chain, depicted in Figure 3.5(a), the point mass moves according to the parametric path described in the Appendix B.2. The equations of the path express the position of the center of percussion of the mechanism using the angle β shown in Figure 3.6 as independent variable.

Once the point mass is restricted the reaction forces can be calculated, using the free body diagram of Figure 3.6 the forces are:

$$F_{x_0} = -2m_{bar}l(\dot{\beta}^2 \cos\beta + \ddot{\beta}\sin\beta) \tag{3.23}$$

$$F_{y_0} = m_{bar}g - m_{bar}l\ddot{\beta}^2 \sin\beta + m_{bar}l\ddot{\beta}\left(\cos\beta - \frac{2}{3\cos\beta}\right) \tag{3.24}$$

$$F_{y_3} = m_{bar}g + \frac{2m_{bar}l\ddot{\beta}}{3\cos\beta} \tag{3.25}$$

In Appendix B the details of the calculation of the reaction forces for both systems are exposed. Those forces are exactly the same for both mechanisms, therefore we can conclude that both systems are dynamically equivalent, and that a kinematic chain can be expressed with a point mass restricted to the center of percussion of the original system.

It should be noticed that in this application the result is exact, this happens because the value of m_e is not dependent of β as calculated in Appendix B, therefore equation 3.22 becomes exact. Although this is not the common situation, when small movements of the system are considered the results are satisfactory as experienced at the end of this thesis.

3.2 Object oriented modeling

Throughout this thesis, simulation will be extensively used. In order to provide good simulation results object oriented modeling techniques will be used. This allows faithful reproduction of the original system with low effort. Besides scalability is also possible while reusing most of the model. The idea is to provide a tool that can produce understandable results as close as possible to the reality. General purpose simulation tools have the drawback that they are based in ordinary differential equations, therefore their causality is fixed. In object oriented modeling the causality is defined by the system, plus more properties explained in detail in the following lines.

Object oriented modeling is a method in computer science to analyze a system as a group of objects that interact between each other. The method is based in the following concepts:

- *Abstraction*: Every object can be used without knowledge of its internal structure[1].
- *Encapsulation*: All the knowledge of the model is encapsulated, and only the elements of its interface can be accessed from outside.
- *Modularity*: The objects can be described independently, the description of the system the object belongs is not required. This helps re-usability of the models.

When a model is constructed following this method a hierarchical structure is generated. This structure has proved as an appropriate mean to cope with large-scale systems, the independence of the objects stated in the three concepts previously mentioned facilitate error detection and maintenance of the model. Abstraction and encapsulation also help when dealing with large systems, because the complexity is down to the object itself.

The fact that the objects interact trough their interfaces introduces the graph theory to analyze the systems, therefore the representation can be seen as networks, block diagrams, bond graphs, etc. Actually bond graphs are a special case of object oriented modeling [13].

Modularity means that objects can be replaced by others according to different requirements. This characteristic is called polymorphism and happens when objects share the same interface. Therefore they can be used in the same context and interchanged without altering the rest of the system. Frequently, polymorphic objects belongs to the

[1] The objects require an interface, here parameters, inputs and outputs are defined.

same superclass. Detailed explanation of the concepts exposed in this section can be found in [11, 12].

3.2.1 Differential algebraic equations and computational causality

As mentioned before, simulation is often performed by means of ordinary differential equations. This is an obstacle to object oriented modeling because models cannot be composed by objects and therefore modularity is compromised. Object oriented modeling avoid this problem because the result is a differential algebraic equation without fixed causality.

For a given system with its constitutive equation provided, there is a problem to define which are the known and unknown variables[1]. Consider the electric resistance in Figure 3.7, its causality is defined by the power source of the circuit. In Figure 3.7(a) the voltage is provided as input and in Figure 3.7(b) the current is the input. From this example we can conclude that the causality is defined by how the elements are interconnected, therefore it is a global property of the system.

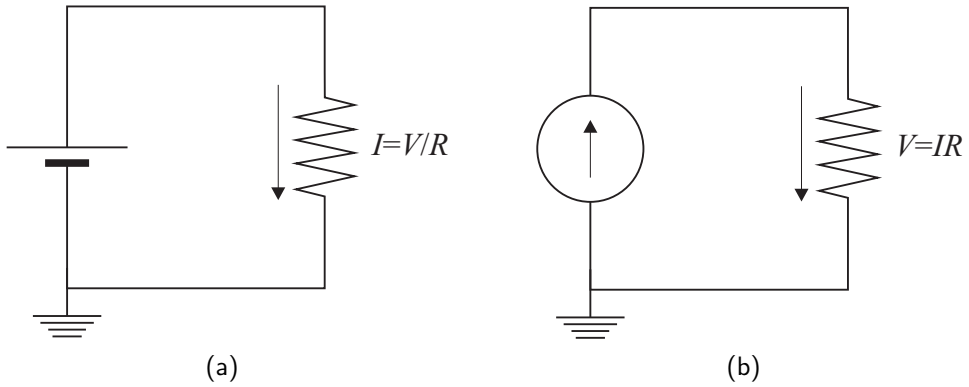

Figure 3.7: Causality of a simple circuit. Depending on the power source the causality of the this system changes.

When connecting objects of a model the result is a set of differential algebraic equations. To introduce these equations in an standard solver they can be converted into an ordinary differential equation, once the conversion is done the causality is defined. Unfortunately the conversion is not trivial and special techniques are required to perform

[1] Usually, when dealing with simple systems this is not a problem.

the conversion [101], this reduction involves a problem of index reduction of the system and it is classified as follows:

- *Problems of index 0*: When the causality has unique solution.
- *Problems of index 1*: When the problem is non singular but it contains algebraic loops[1].
- *Problems of higher index*: There is no solution of the causality that keeps all the variables that have derivatives as state variables.

Once the index reduction has been performed, the causality has been defined according to the system's structure. This is a big advantage when modeling a system because the equations are introduced without requiring a defined causality. This is the reason why object oriented modeling is often referred as *non-causal modeling*. Thanks to this property it is possible to achieve the properties of abstraction, encapsulation and modularity, mentioned in the beginning of this section.

3.2.2 Modelica

The main problem when selecting the appropriate tool to develop the present thesis was to have a fully modular simulator that captures all the phenomena related with this research, traditional simulation techniques lack of the advantages mentioned in the previous section. Most of the simulation tools (ACSL, Simulink, etc.) force to provide explicit description of the causality, as consequence part of the structure of the physical process is missing when simulated. By the other hand Modelica® is free of these limitations because the causality is automatically assigned according to the structure of the model.

According to [10] the definition of Modelica® is:

> Modelica is a language for modeling of physical systems, designed to support effective library development and model exchange. It is a modern language built on non-causal modeling with mathematical equations and object-oriented constructs to facilitate reuse of modeling knowledge.

One of the most important differences of Modelica® when comparing against traditional programming languages is how the sign "=" is used. Usually in traditional

[1] In this case the algebraic loops should be solved either numerically or by symbolic manipulation.

programming languages "=" is used to denote assignation of a value to a variable, therefore equations have to be introduced explicitly. In Modelica® the sign "=" is used to express equality, therefore equations can be introduced in the form of "`<expression1> = <expression1>`".

Modelica® allows fully object oriented modeling by providing special classes to define interfaces between objects and also power-port like connections [15]. This allows straightforward mapping of other object oriented modeling techniques, like for example bond graph theory [14].

Finally, Modelica® standard library provides a complete set of classes that fill the requirements of the research presented in this thesis. The only drawback found was the impossibility to simulate contact and mechanical locks, therefore simulating a walking robot was not possible without adding or modifying some objects. In the following sections those additions are explained.

3.2.3 Ground-foot interactions

The multibody library implemented in Modelica® does not support contact interaction [80]. Although, a collision handling solution is reported in [79], it was not included in the standard library version used in this work[1]. Besides, only viscous friction is implemented in the tangential direction of the contact, this last is a major drawback because a walking robot will always slip in order to balance tangential forces.

Impulse-based contact is one of the simplest ways of collision handling. The results can be very realistic when very stiff surfaces are simulated. In exchange of the simplicity of the method the problem of chattering appears [74]. This happens because this method is based on reinitialization of the states of the colliding objects. Despite the improvements of the technique, as for example the ones shown in [61], it was found not suitable for the purposes of this work.

Gait in normal conditions requires continuous contact similar to the one found in haptics. Implementations in Modelica® are reported in [29], and similar formulations are also found in [52]. The solution adopted in the just mentioned publications is a soft contact approach. In this thesis the following solution was implemented to calculate the normal reactions between a point of the foot and the floor:

$$F_y = \frac{1}{1 + e^{5000y}}(e^{-ky} - 1 + F_v) \tag{3.26}$$

[1]The version 2.2 of Modelica is used in this thesis.

where y is the position of the point, k is the stiffness of the interface foot-floor, F_y is the normal reaction force and F_v is the friction force modeled with:

$$F_v = \begin{cases} -\nu\dot{y} & \text{for } \dot{y} < 0 \\ 0 & \text{for } \dot{y} \geq 0 \\ 0 & \text{otherwise} \end{cases} \tag{3.27}$$

here ν is the damping constant of the interaction between the foot and the floor. The term $1/1 + e^{5000y}$ is used as a continuous form of the step function. The selection was done to improve computational efficiency. According to equation 3.26 there will be interpenetration between the floor and the foot when contact happens, therefore, when the point in contact is moving away from the floor the damping should be zero, for this reason equation 3.27 was formulated with conditional statements to avoid a *sticky*[1] effect when high values of ν are used.

The tangential forces are simulated assuming that there is not slippage between the points in contact. In order to achieve this effect the point where the contact occurs is registered in the vector `x_td` by the following code:

```
when frame_b.r_0[2]<0 then
x_td=frame_b.r_0;
end when;
```

`frame_b.r_0` refers to the position of the contact point and `frame_b.r_0[2]` to its vertical component. Once `x_td` has been set the tangential forces are calculated with the following equation:

$$F_x = \begin{cases} k(x - x_{td}) - \nu\dot{x} & \text{for } y < 0, \\ 0 & \text{otherwise} \end{cases} \tag{3.28}$$

x is the horizontal position of the contact point, and k and ν are the stiffness and damping constants respectively. The code implemented in Modelica® can be found in Appendix C.3, other variants of the model using more traditional approaches are also found in Appendix C.

[1] This is not the same of the sticky friction used to calculate tangential forces, tangential forces are calculated assuming that slippage does not occurs. When high values of ν are used it could happen that the viscous force is larger than the elastic force, in this case the contact point feels a sticky effect in the normal direction.

3.2.4 Joint simulation

Joints in human beings cannot rotate 360°, instead they have stops that vary in construction according to each joint. During gait the knee lock plays an important role[1], for this reason some elements of the Modelica® standard library were modified.

Modelica® standard library provides a complete set of joints that allows most of the constructions required in general problems of rigid body dynamics. The limitation found during the development of this thesis was the impossibility to model knee locks, therefore a modification of the rotational joint was implemented.

Similar to the model in Section 3.2.3 the stops are implemented avoiding event generation by using the logistic function as a mean to activate or deactivate the contact. The lock is modeled as a reactive torque with the following equation:

$$\tau_{r_1} = \frac{1}{1 + e^{-b(\theta - \theta_s)}}(-k_r(\theta - \theta_s) + \tau_{\nu_1}) \tag{3.29}$$

$$\tau_{\nu_1} = \begin{cases} 0 & \text{for } \dot{\theta} < 0 \\ -\dot{\theta}\nu & \text{otherwise} \end{cases} \tag{3.30}$$

were θ_s is the position of the lock, k_r and ν_r are the stiffness and damping respectively and τ_{ν_1} is the damping force of the lock. Similar to Section 3.2.3 τ_{ν_1} is conditionally activated to avoid sticky effects when high values of ν are used.

The implementation is done by using the modularity of Modelica®. The object oriented characteristic allows to extend the original rotational joint, provided in the standard library, and modify it by adding additional inputs and outputs. The details of the implementation and the entire code of the joint is explained in Appendix D.2.

[1] In fact, passive walkers rely on this biological adaptation to work [69].

4

Center of percussion and gait design of biped robots

In Section 3.1.1 the concept of the center of percussion was introduced and later, in the same chapter, extended to a kinematic chain. One of the most important characteristics of this point is that it is not unique, it depends on the reference used to calculated it. In consequence, different references can be used depending on the necessities. Gait generation requires a smart selection of such references, in order to calculate a center of percussion that can be used for such task.

In this chapter a method to generate gait using the center of percussion is exposed, also the references used to calculate the center of percussion of a simplified biped are explained. The biped uses a flywheel as a body and point feet to simplify the calculation of the center of pressure. The flywheel body is used to dismiss the orientation thereof, and therefore avoid the problem of an under-actuated system. Besides it allows other dynamic equivalences to exert torque against the floor. The work developed in this chapter can be found in [3].

4.1 Finding the equivalent inverted pendulum of a biped robot

The following analysis has been developed assuming the floor is flat and even. This is required because under these conditions zero moment point has the same location of the center of pressure [90]. In this context, center of pressure refers to the distance-weighted average location of the individual pressures on the foot. More details are described in [84]. However, in simple terms, the center of pressure is the point where the distributed force on the sole of the foot can be replaced by a point force of the same magnitude.

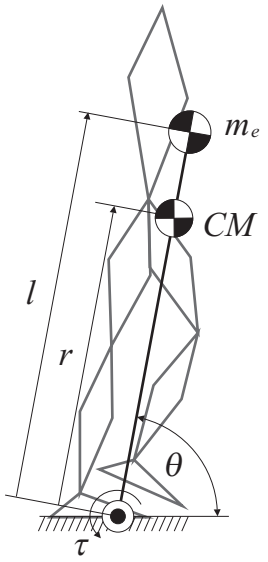

Figure 4.1: Biped with its equivalent inverted pendulum; l is the distance from the center of pressure to the center of percussion, r is the distance from the pivot to the center of mass CM. Notice that the position of the pivot and the center of pressure are the same. Also remember that the pendulum is composed by two point masses, the other mass is located at the center of pressure and it is not drawn in this figure.

Figure 4.1 shows a biped with its equivalent simple pendulum. The pendulum has length l and a point mass m_e, which is aligned with the line formed by the center of pressure and the center of mass (CM). m_e is calculated to maintain the equivalence of mass and inertial properties between the pendulum and the whole biped, just as shown in equation 3.5. Rewriting the equation with the parameters of Figure 4.1:

$$m_e = \frac{m_{robot} r}{l} \tag{4.1}$$

The distance l corresponds to the location of m_e, and also to the center of percussion as explained in section 3.1.1. As was mentioned before, this point is pivot dependent; it varies according to the position of the selected center of oscillation. Its use in walking robots results from the fact that the center of percussion is the length of the equivalent simple pendulum, the one having the same period as the original system. The center of percussion can be calculated using the moment of inertia I_{ZMP} around the ZMP, the mass m_{robot} of the system, and the distance r from the pivot to the center of mass; repeating equation 3.6 with robot parameters:

$$l = \frac{I_{robot} + m_{robot} r^2}{r m_{robot}} \tag{4.2}$$

The equivalent pendulum of the robot is composed by two point masses, but in Figure 4.1 only one is depicted [1].This approximation is possible if the system rotates around the location of the second mass. Therefore, in order to make equation 4.2 valid, the center of pressure should be in a fixed position during the stance phase. Imagining the biped of Figure 4.1 hung upside down from its center of pressure, the period of oscillation of this system is the same as the simple pendulum with length l, according to the definition of center of percussion. Then the equation of motion of the biped at this exact instant can be expressed as:

$$m_e l^2 \ddot{\theta} + m_e g \sin\theta = 0 \tag{4.3}$$

Equation 4.3 does not describe the biped in Figure 4.1. In order to do so, two terms are included, the torque τ due to the actuation of the motors, and the torque τ_d due to the dynamic effects of the moving links. The resulting equation is:

$$m_e l^2 \ddot{\theta} + m_e g l \sin\theta + \tau + \tau_d = 0 \tag{4.4}$$

τ is the input control of the system. Although it seems difficult to apply torque to this point, the fact is that any torque applied to the robot is reflected in its center of percussion. To illustrate this fact, Figure 4.2 shows the dynamic equivalence between an inverted pendulum with torque applied to its pivot, and an inverted pendulum with a free pivot but with a flywheel instead. The details of this deduction can be found in [84].

[1]The mass that is not drawn corresponds to m_1 in section 3.1.1.

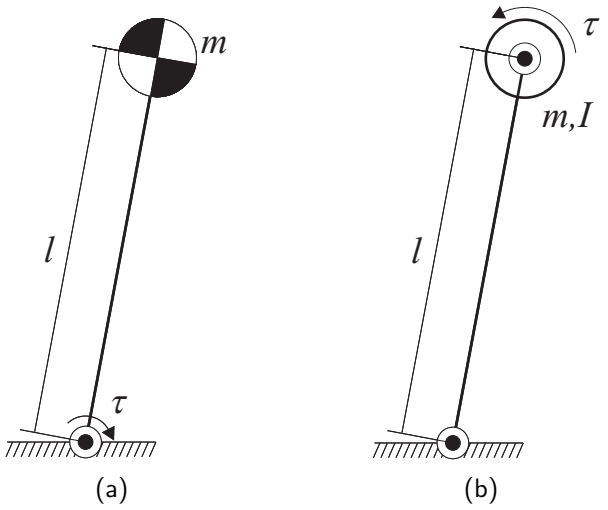

Figure 4.2: (a) Inverted pendulum (b) Inverted pendulum with a flywheel. Both models have the same dynamics.

4.2 Description of the model

The equations of the previous section can be applied to any biped, but at this point several simplifications will be made. The model can be seen in Figure 4.3, where the body has been replaced by a flywheel. It then becomes a source of torque by changing its angular momentum in such a way that the body orientation is not a variable to control. Each leg is connected independently but concentrically to the flywheel, providing the model with a bisecting hip. Knees have been added to allow correct foot clearance, providing two degrees of freedom to each leg (hip and knee), so the whole model has a total of four degrees of freedom of movement.

The feet are modeled as one contact point, allowing an exact location of the center of pressure when the robot is being supported by one foot. The location of this point on a foot with distributed contact (for example, a planar one) is easily computed, but for the sake of simplicity and for transparency of the algorithms, the one point solution was chosen. Besides point feet fix the position of the center of pressure as required in section 4.1.

Ankle torques contribute to the equilibrium of a biped [19], but ankles are fragile elements. Changing the equilibrium strategy will contribute to relief the stress in this articulation. Point feet cannot exert torque directly onto the floor, but instead they rely heavily on the dynamic equivalence shown in Figure 4.2. This is coherent with the fact

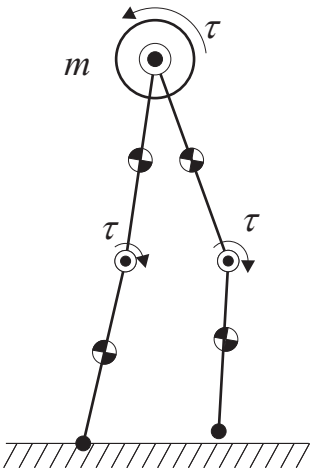

Figure 4.3: Flywheel biped. Each motor of the legs can apply torque to the flywheel independently. The knees have been added to perform foot clearance.

that the human body has its most powerful muscles in the upper part of the legs. In fact, dance and creative movement instructors teach their pupils how to balance with their hips and not with their ankles.

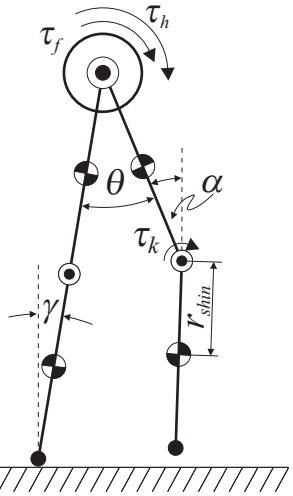

Figure 4.4: Angles of the flywheel biped: θ angle between legs, α angle of the knee joint, γ angle between the stance leg and the normal vector of the floor. τ_h is the torque between the stance leg and the flywheel, and τ_f then one between the swinging leg and the flywheel.

Figure 4.4 shows variables and control inputs. γ is the angle between the shin and the normal vector to the floor. θ is the angle between legs and is measured from the

stance leg, which means that its sign changes after each step. α is the angle of the knee and is different from zero only when the leg is swinging for foot clearance.

τ_f, τ_h and τ_k are the control inputs. τ_f is the torque necessary to actuate the swinging leg, while τ_h is the input control for body attitude and is produced by the stance leg over the flywheel. Just as with the angles, their definition depends on which leg is the stance one at that time. Finally τ_k is the knee actuation.

4.3 Gait generation

Gait can be divided into two stages. The first one is when only one leg is in contact with the floor, and the other is when the robot is in double stance phase. However, several restrictions will be applied to produce gait in order to simplify double stance phase. The first restriction is that the stance leg has to be in a straight position all the time. Consequently, the swinging leg will be straight before touching the floor, and then become the new stance leg. That will put the robot in the position shown in Figure 4.5, making the double stance phase take place within in an infinitesimal space of time. This situation is similar to the synthetic wheel described in [69]. Another advantage of this approach is that only one algorithm is required, the one for the single stance phase.

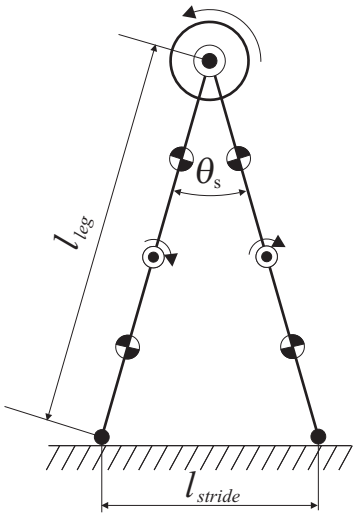

Figure 4.5: Some parameters of the gait: l_{leg} is the length of the leg, θ_s is the angle of the legs at the double stance phase, and l_{stride} is the length of the stride. The robot is in the double stance position.

This algorithm will be divided into two tasks: One to control body attitude and another for the swinging leg. The idea is to compensate the major sources of nonlinearities in order to apply linear controllers for both cases. A state machine switches the controller when the swinging leg becomes the new stance leg.

4.3.1 Gait parameters

Walking is not a regular task. In fact, complex limit cycles are described in the study of passive dynamics. However, despite its complexity, the periodicity quality makes it susceptible to parameterizing, thereby simplifying the description of the gait.

Figure 4.5 shows the robot during double stance phase. This position is repeated at the beginning of every cycle. Thus, the angle θ_s defines aperture between the legs before the double stance phase. This can define the stride length with simple trigonometry. The period t_s of each step is also of interest. In combination with θ_s the gait is completely described for regular terrain. Because the double stance phase is assumed to be infinitesimal, then t_s accounts for the total time of a single step. With this in mind, more intuitive quantities can be estimated such as the average walking velocity.

$$v_{avg} = \frac{l_{stride}}{t_s} \tag{4.5}$$

4.3.2 Swinging leg control

In order to generate gait correctly, the robot is supported by one leg, while the other leg reaches its position to become the new stance leg. During this time the swinging leg performs two tasks: The first is to position the thigh in front of the body, i.e. to reach angle θ_s shown in Figure 4.5; the second is to bend the knee to avoid foot scuffing.

The swinging leg has to reach its position in a time less than or equal to the period t_s of the gait. To ensure that the leg is ready to support the robot a shorter time is chosen. A fixed fraction of the period is defined for the time required to swing the leg:

$$t_f = ct_s \tag{4.6}$$

where $0 \leq c \leq 1$ is a constant selected to leave enough safety time gap. If the leg gets hung at a fixed point it will behave like a pendulum. Because it is actuated, it is possible to design a PD controller once the appropriate objectives have been selected. The control law for this controller is:

$$\tau_f = k_p(\theta - \theta_s) + k_d\dot{\theta} - m_{leg}\,|\vec{r}_{leg} \times \vec{g}| \tag{4.7}$$

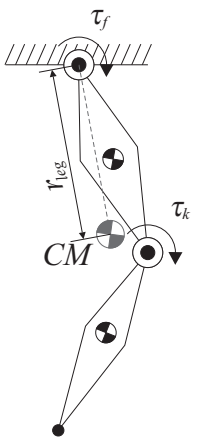

Figure 4.6: Swinging leg. τ_f is the torque at the hip, τ_k is the torque at the knee, and r_{leg} is the distance from the hip to the *CM*.

The first and second terms of equation 4.7 are the proportional and derivative part of the controller. The third term is a gravity compensation term to get rid of nonlinearities introduced by the large angle between the legs. To avoid foot scuffing the knee needs to be bent just at a small angle, and therefore the dynamic effects of knee movements are neglected.

k_p and k_d are selected to produce critical damped movement on the leg. Thus the solution for the equation of movement is $\theta(t) = (A+Bt)e^{-\omega_0 t}$; ω_0 is the natural frequency of the system when k_d is equal to zero. The inverse of ω_0 is the time constant τ of the system, an important quantity to measure the stabilization of linear systems. A common criterion is to use 7 times τ as the stabilization time [78], thus this is the time required to swing the leg:

$$t_f = 7\tau \tag{4.8}$$

$$t_f = \frac{7}{\omega_0} \tag{4.9}$$

ω_0 is defined as:

$$\omega_0 = \sqrt{\frac{k_p}{I_{leg}}} \tag{4.10}$$

Where I_{leg} is the moment of inertia of the leg around the hip. Equations 4.9 and 4.10 are combined to find k_p:

$$k_p = I_{leg}\left(\frac{7}{ct_s}\right)^2 \tag{4.11}$$

Now k_d can be defined in terms of k_p and the damping ratio ζ. The last one is defined as:

$$\zeta = \frac{k_d}{2\sqrt{k_p I_{leg}}} \tag{4.12}$$

As was mentioned previously in this section, the system is designed to have critical damping, which is interpreted as ζ having a value of 1. From equation 4.12, k_d is calculated:

$$k_d = 2\sqrt{k_p I_{leg}} \tag{4.13}$$

Because knees were added to prevent foot scuffing, their control is carried out by coupling the movements with angle γ. The equation can then be written:

$$\tau_k = k_{kp}(\alpha - f(\gamma)) + k_{kd}\dot{\alpha} - m_{shin}\left|\vec{r}_{shin} \times \vec{g}\right|$$

where k_{kp} is a stiffness value, and k_{kd} is a viscous friction term. $f(\cdot)$ bends the knee most of the time, and then blocks it near the end of the swinging of the leg. Many functions satisfy these conditions. The function chosen was $\mathrm{A}xe^{-\mathrm{b}x}$ where A and b are constants conveniently selected for the system. Better $f(\cdot)$ can be designed considering the whole kinematics of the robot. A good criterion could be constant foot clearance in a region of interest, however this is beyond the scope of the analysis developed in this chapter, and the selected function worked fine in the simulations.

Equation 4.7 is valid if the knee is blocked; because the movement of the shin is small, their dynamic effects have not been considered. However, the actuation of the knee is an easy term to compensate. Therefore, equation 4.7 is modified as follows:

$$\tau_f = k_p(\theta - \theta_s) + k_d\dot{\theta} - m_{leg}\left|\vec{r}_{leg} \times \vec{g}\right| - \tau_k \tag{4.14}$$

4.3.3 Stance leg control

The swinging leg was controlled using an adaptive PD controller. The values of the proportional and derivative gain are recalculated in real time according to the changes

in mass and inertia properties. These changes are produced by the reconfiguration of the leg when swinging, because of knee bending. The actuation to control the swinging leg is applied directly to the hip, which is the center of the arc, to measure the controlled variable θ.

The stance leg is the one responsible for body attitude, i.e the angle γ between the stance leg and the floor, as described by Figure 4.4. However, direct actuation on the support point is not possible. Even for robots with extended feet this is a major problem because the torque required to control the body only with the ankle joint, is too large. That is the reason for the dynamic equivalence mentioned in Section 4.1 and illustrated in Figure 4.2.

The stance leg only applies torque over the flywheel and this torque is reflected on the support point, also defined as the center of pressure, as an opposite reaction. The objective is to reach the double stance phase; as shown in Figure 4.5, in this position γ has a value of $\theta_s/2$.

Controlling body attitude is quite similar to controlling the equivalent inverted pendulum of the system, i.e using equation 4.4. But some changes are necessary. First, the variable to measure is not the angle of the equivalent pendulum, but angle γ, and only reactions τ_f and τ_k, due to the movement of the swinging leg, are considered. Thus, the torque at the hip joint applied by the stance leg is:

$$\tau_h = k_{po}(\gamma - \theta_s/2) + k_{do}\dot{\gamma} - m_{robot}\,|\vec{r}_{robot} \times \vec{g}| - \tau_f - \tau_k \tag{4.15}$$

The equation of motion of the system according to equation 4.4 is rewritten to match the parameters of the robot. $m_e l^2$ is the inertia of the robot I_{robot} with respect to the center of pressure, $m_e g l \sin\theta$ is the torque of the gravitational force applied to the center of mass, τ is the summation of joint torques τ_h, τ_f and τ_k, τ_d are the torques produced by centrifugal and Coriolis accelerations, and θ is replaced by γ. The terms k_{po} and k_{do} are the gains of the controller. After applying all the changes the expression is as follows:

$$I_{robot}\ddot{\gamma} + m_{robot}\,|\vec{r}_{robot} \times \vec{g}| + \tau_h + \tau_f + \tau_k + \tau_d = 0 \tag{4.16}$$

In order to find the equations of movement of the system, equation 4.15 is replaced in equation 4.16. The gravitational term is cancelled, and only τ_d remains. The final equation is:

$$I_{robot}\ddot{\gamma} + m_{robot}\,|\vec{r}_{robot} \times \vec{g}| + k_{po}(\gamma - \theta_s/2) + k_{do}\dot{\gamma} - m\,|\vec{r}_{robot} \times \vec{g}| + \tau_d = 0 \qquad (4.17)$$

Analyzing this last expression we can conclude that except for τ_d, this equation describes a damped harmonic oscillator. If the term τ_d is small enough to be neglected, a similar method to the one used for the swinging leg controller is used to calculate the gains k_{po} and k_{do}. Analogous to equation 4.11, but with the difference that the criteria is taken based on the whole period of the walking cycle t_s instead of the fraction ct_s, k_{po} is expressed as:

$$k_{po} = I_{robot}\left(\frac{7}{t_s}\right)^2 \qquad (4.18)$$

In the same way k_d is calculated, and its expression is:

$$k_{do} = 2\sqrt{k_{po}I_{robot}} \qquad (4.19)$$

4.3.4 Putting it all together

As described previously, the walking algorithm requires only one controller for the single stance phase because the double stance happens in an infinitesimal time period. Control was divided into two tasks: one for body attitude and another to swing the leg. The swinging leg was set up to perform its task, in a shorter time than that required for the stance leg to reach its position. The final position of the stance leg, just before becoming the swinging one, is such that the robot has to end up as shown in Figure 4.4, i.e. the angle γ reaches $\theta_s/2$.

In order to walk, once the swinging leg is in front of the robot, it becomes the new stance leg, and the former stance leg starts to swing. To do so, the controllers have to switch in order to perform the required task according to the situation. Then, a state machine is used. When the swinging leg touches down on the floor, the controllers are switched, and the cycle repeats itself to produce gait. There is significant amount of work on these systems and details about such machines can be found in [48] and [87].

4.4 Simulation results

The algorithms were tested with Modelica® using Dymola® implementation. Their elements are object oriented. Hence, highly detailed models can be made with minor assumptions. Implementation of such models is done in a *bond graph* fashion, and new models or extensions thereof can be made using Modelica® language.

The models are made mostly with the rigid body dynamics library developed in [80]. This library is not designed to simulate walking robots, but new elements were created to do so. In addition, the actuated joints have limited usability for the purposes of this article, and thus, modifications of these elements were developed. The details of the programming of the model are not provided here, but they are not necessary for interpretation of the data.

The chosen mass of the different parts was 1kg, and the length of the shin and thigh were 0.35m and 0.37m respectively, the last selection was approximated to a human leg using the data provided in [105]. The mass of the shin and thigh are assumed as a point mass located at the center of each member. The flywheel has an inertia of 0.01kg.m^2. Table 4.1 shows this information.

Table 4.1: Parameters of the robot used in the simulation.

Mass of each part	1.00 kg
Inertia of the flywheel	0.01 kg.m^2
Length of the shin	0.35 m
Length of the thigh	0.37 m
Total mass of the robot	5.00 kg

The multibody dynamics library cannot handle contact. In order to simulate linkages or similar situations, an anchor point should be defined first. This is not the case for walking robots. They rely on the interaction between feet and floor because the contact point changes in every step. To solve this problem a new element was created. This element simulates point contact using a damped mass-spring model. It works by determining the coordinates x_{td} and z_{td} for the contact point when the y coordinate goes below 0. Then tangential and normal forces are calculated. This can be written as:

$$f_{ry} = \begin{cases} \text{if } y_{ft} \leq 0 \text{ then } k_r y_{ft} + b_r \dot{y}_{ft} \\ \text{else } 0 \end{cases} \tag{4.20}$$

For the tangential reaction force:

$$f_{rx} = \begin{cases} \text{if } y_{ft} \leq 0 \text{ then } k_r(x_{ft} - x_{td}) + b_r \dot{x}_{ft} \\ \text{else } 0 \end{cases} \tag{4.21}$$

In other words, what this model of contact does is determine the plane $y = 0$ as the surface of the floor, and then it calculates the reactions with an elastic model with damping. z_{td} is not described here because the simulation is restricted to the plane. The knee lock is simulated in a similar way. A reactive torque is triggered when the angle of the knee goes below a certain value:

$$\tau_{lock} = \begin{cases} \text{if } \alpha \leq 0 \text{ then } k_{kr}\alpha + b_{kr}\dot{\alpha} \\ \text{else } 0 \end{cases} \tag{4.22}$$

This approach of elastic contact solves the problem of chattering, commonly found when impact-based contact models are implemented. Furthermore, it provides a softer and more realistic behavior.

The walking parameters were chosen as θ_s=0.3rad and t_f=1.5s. The walking algorithm was designed to have critical damping, and works with a state machine. The state machine makes the controllers work as an on-off system. It is therefore expected to behave as these controllers. Figure 4.7 shows the plot of angle θ, and shows its behavior, which is similar to the differential gap found in on-off systems.

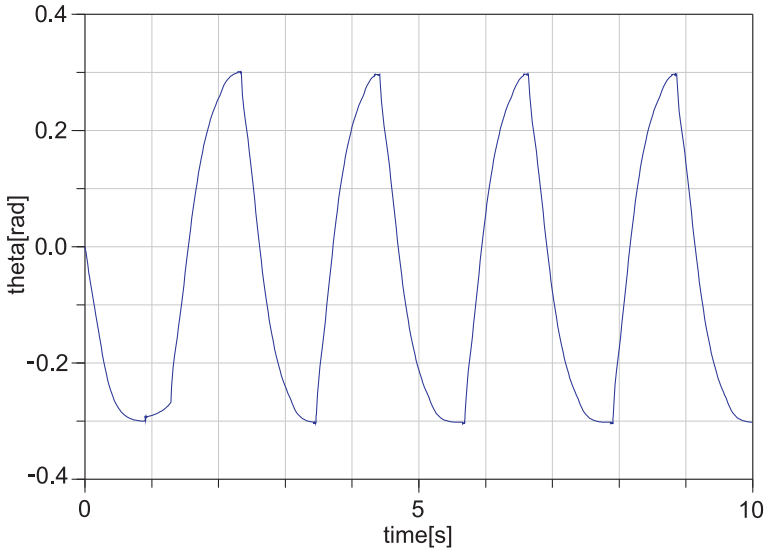

Figure 4.7: Plot of the hip joint angle. θ follows the assigned value of 0.3rad quite closely, although the period of 1.5s is less precise.

Analyzing the walking parameters, it can be found that angle θ_s is followed with remarkable precision. The period t_s has a discrepancy showing an average of 1.09s. This discrepancy is the consequence of non-modeled phenomena, principally the dynamic effects due to the swinging leg. Variation of gait parameters showed similar results, i.e. it closely followed θ_s with an appreciable variation of t_s. Carrying out a deeper analysis, the swinging leg controller which is less prone to dynamic perturbations, is responsible for the value of θ_s is. However, t_s is regulated by the stance leg controller, and withstands the dynamic effects of the whole robot.

Knee impacts due to locking of the knees cause no visible deviation of the expected performance, as can be observed in Figure 4.8. The controllers act as variable springs as can be seen in equations 4.7 and 4.11; then they can naturally reject perturbations. Other researchers have experimented with springs to obtain a more robust gait as for example [48, 84]. They have softened and improved the original McGeer models by adding springs and elastic actuation, but the adaptive nature of the controllers developed in this section provides a better disturbance rejection than those developed in previous works.

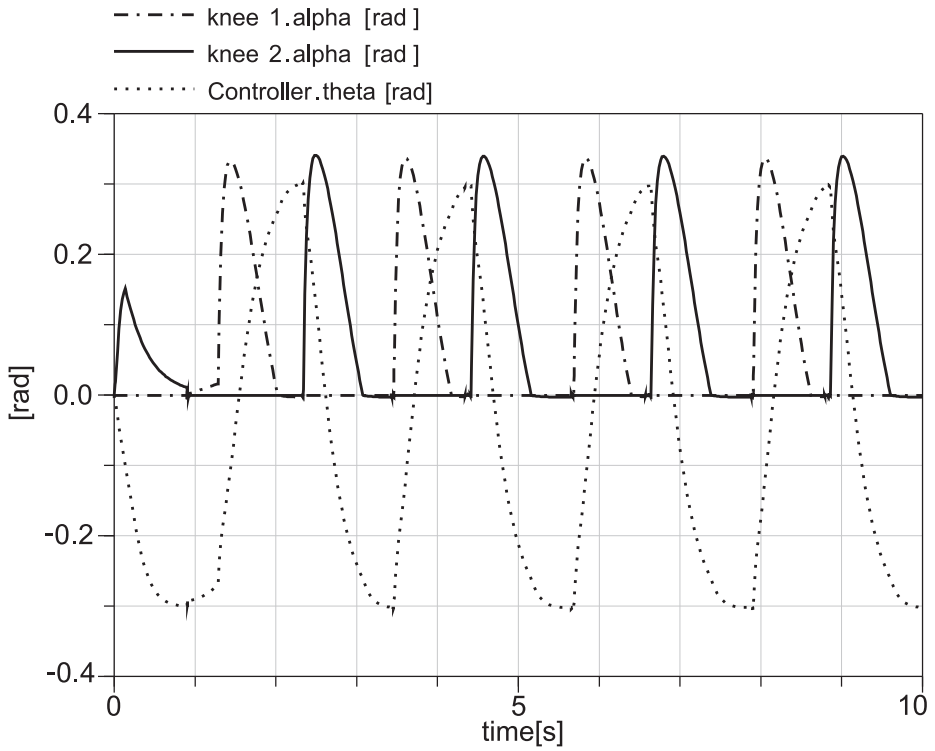

Figure 4.8: Plot of the angles of the knees plus θ, after the first step lock impacts cause no effects on the system.

The plot of angle α also shows a smooth behavior. Figure 4.9 shows this plot. The flat part at zero degrees is when the leg is swinging. Once it makes contact, it goes up to approximately 0.15rad, which is the value of $\theta_s/2$, and the lift-off occurs at about the same angle, but with a negative value. This plot shows how precisely the stance leg controller reaches the commanded angle $\theta_s/2$, as described by equation 4.15. The perturbation due to non modeled dynamics only affects the period, but not the precision of the set point of the controller.

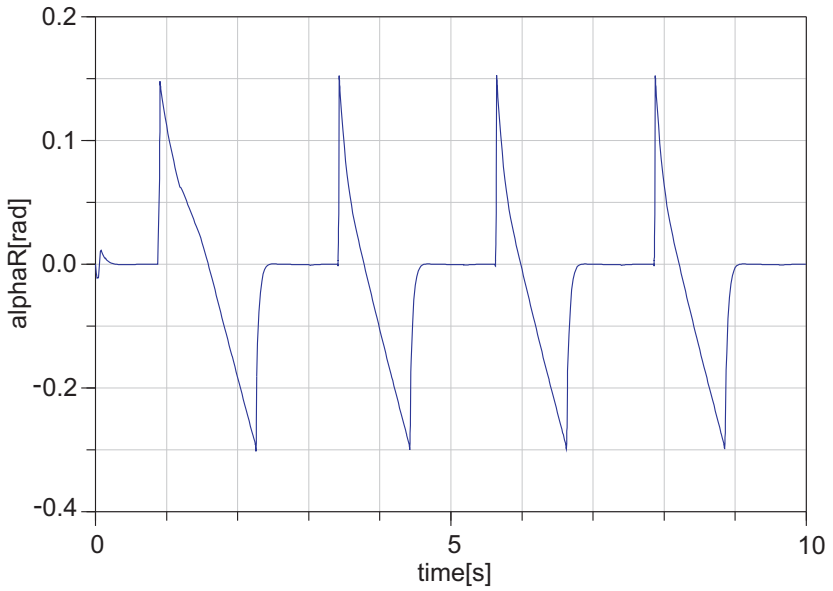

Figure 4.9: Plot of angle α for the right leg, the flat part of the plot means the leg is swinging.

The design of the system has been made attempting to follow the natural dynamics of a system, in which control is carried out around the torque of each joint. This produces a very natural and smooth gait, with a highly anthropomorphic appearance. Figure 4.10 is a stroboscopic picture of the animation. Another observation is that there are jerks at the beginning of each step. These jerks are small and are not visible in the plots, and were only observed in videos of the simulations. This can be explained by the fact that the double stance phase is almost a singularity so that the inverted pendulum changes its center of rotation (i.e ZMP) almost instantaneously. This also accounts for the variation of the simulated t_s. For a better appreciation of the foregoing a video can be found in *http://maqlab.uc3m.es/proyectos/pasibot/flywheelbiped.avi*.

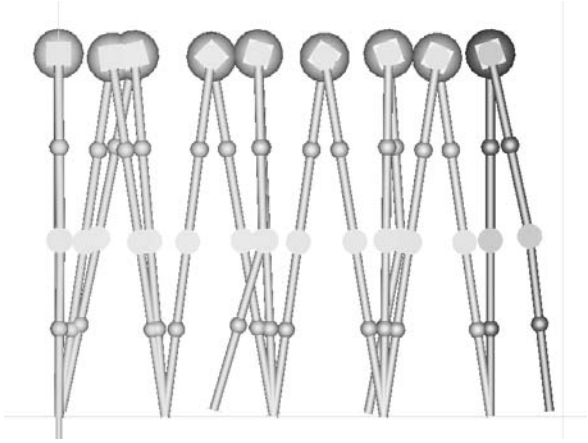

Figure 4.10: Stroboscopic picture of the animated simulation.

4.5 Conclusions of the chapter

In this chapter, a linearization of a bipedal system is developed. The tools to do so are taken from among the most popular ones such as the ZMP or the linear inverted pendulum model. The novelty is the introduction of the center of percussion of the robot in order to find the equivalent inverted pendulum of the system. With this information, the system is rewritten as shown in equation 4.16. With the linear model, adaptive PD controllers were designed. To prove the validity of the algorithms, the system was simulated using Dymola®.

Gait is characterized by two parameters: t_s that is used as the period of the walking cycle; and the length of the stride, defined indirectly with θ_s for even terrains as shown in Figure 4.5. Simulations provided good results, as shown in Figures 4.7, 4.8 and 4.9. The parameter θ_s was closely followed by the system, and the period t_s had deviations. The deviations of t_s were produced by the dynamics of the links not modeled in the control laws, described in equations 4.14 and 4.15, and the jerks observed in the animations. Only gravitational compensation was included in these equations. Given these results, including the dynamic effects in future controllers, is a priority.

Optimization of the gait has not been carried out due to the jerks that were observed in the animations. The simplification of shortening the double stance phase to negligible time takes its toll by introducing undesirable perturbations. Gait optimization requires a better double stance solution. Despite these problems, equations 4.16, 4.18 and 4.19 show the connection between the mass properties of the robot and its gait parameters.

4.5.1 Some words about stability

The stability of the controller can be evaluated with equation 4.4, because it is a linear system its poles can be always placed with a negative real part. Although in simulations the controller was stable, there are several issues that should be taken into account for a practical implementation.

Unfortunately in a real implementation the controller is expected to work in a narrow band, this is basically due to saturation problems. Because the control action relies on the acceleration of the flywheel, its action will disappear when the flywheel has reached its maximum velocity. In order to achieve a successful implementation of the controller in a real system, the gait parameters have to be carefully selected to avoid the mentioned saturation.

Other issues to be taken into account are related with friction. Just as happen with humans if one of the legs slips, the robot will fall. Because friction is not modeled in the controller, the gait parameters that produce a successful gait are limited to those that do not overcome the static friction of the system.

4.5.2 Mass distribution of the biped

Just as the classic inverted pendulum models, the pendulum obtained with the center of percussion is sensible to configuration of the biped. This issue was solved in the controller by fixing the natural frequency of the system (equation 4.18) and calculating the necessary proportional gain k_p according to the changes of I.

At first sight, the center of percussion method seems to share the same limitations of the classic inverted pendulum. The advantage over the last one is that pendulums modeled after the *center of mass* only consider the static properties of the system. When constructing the equivalent pendulum in this article, two point masses were added, one at the center of percussion and another one at the ZMP. The mass at the ZMP has not been considered for the analysis because it remains static, just as explained in section 4.1. Because the pendulum is constructed with two masses, it shares the same moment of inertia with the robot, therefore rotational dynamics of the system has been added to the model.

Another characteristic of the model is that the magnitude of the equivalent mass of the pendulum is configuration dependent. The time derivative of this equivalent mass can provide information about the inertial forces acting over the biped, but a more detailed study is required. The variation of the equivalent mass is interpreted as the

variation of the inertia of the robot, giving more information to design better controllers in the future.

4.6 Improvements of the technique

The methods proposed in this chapter need to prove its possibilities with robots having true body and feet, also the energy optimization is a point of interest. Future developments are expected to cover these improvements as described in the following lines.

4.6.1 Adding a torso and feet

In this chapter the torso was replaced by a flywheel, but in order to extend this work to other bipeds a true torso need to be added. Although the proposed control law cannot be directly applied to such bipeds, it is possible to construct a pendulum using the center of percussion. Because center of percussion based pendulums and the linear inverted pendulums are quite similar, it will be of great interest to adapt control algorithms like the one shown in [76].

Other important generalization is adding feet to the model. Again the control law will need important changes, but just as before a pendulum constructed out of the center of percussion can be obtained. But feet will introduce an interesting change: The fact that the second equivalent mass needs to be introduced in the model. In section 4.1 a coarse assumption was done by fixing the position of the ZMP. But variations of the position of ZMP will change the position of the second mass, and therefore introducing new dynamics to the system. Using both masses to model a biped introduce more significance to ZMP displacement during gait and therefore more information to design better controllers.

4.6.2 Energy optimization

Although energy efficiency was one of the motivations of this work, optimization was not performed. It is expected that the developments proposed will behave energetically acceptable by the fact that the gait is generated using the dynamics of the system similarly to [84].

For example, a first attempt of optimization can be made by selecting the period of the gait close to the average period of the equivalent inverted pendulum, during the single stance phase. This should minimize the required actuation because gravity should

do most of the work and motors will be actuated only for compensation. These are part of future developments to exploit the center of percussion applied in bipedal walking.

In addition, mass distribution could be studied with the equivalent inverted pendulum. The center of mass of the different parts could be designed to match a desired natural frequency. Even springs could be added to relieve the load of actuators. These springs could be arranged in parallel distribution, instead of a serial one similar to the ones presented in [84]. Again, the springs would be selected based on the desired natural frequency, or even the average of the kinetic energy of the system, where methods like the one proposed in [31] could provide important information.

Another future development is to use different design criteria to set the gains of the controllers. In this work, critical damping was used because of the simplicity of the analytical solutions. But under-damped oscillations or even free oscillations seem to be a better solution from the energetic point of view. The problem with them is that the phase of the movements has to be carefully studied to avoid destabilization. However their foreseeable advantages put them into the list of future improvements.

Finally, to simplify gait generation, straight leg during the whole stance phase was required. This is not efficient because heel strike will dissipate part of the kinetic energy. Therefore future control algorithms will take this into account to design better strategies to avoid such problems.

5

Four point masses equivalent model of a biped robot

In Chapter 2 different methods to simplify the complex topology of a biped robot was exposed. The most common approach was to replace rigid bodies by point masses. The simple analysis required when dealing with such simplifications is what it seems to inspire most researchers to follow this path. But, the decisions to construct the equivalent point mass system look arbitrary, due to the fact that no formal analysis is performed at the time of selecting the values and positions of the point masses.

In this chapter a methodology to simplify a biped into 4 point masses is developed. The central idea is the concept of dynamic equivalence developed in Chapter 3. Although in Chapter 4 the same approach was used, the difference here is that a different reference point is used, and as a result several centers of percussion are obtained. The system is a four point mass system.

The equivalent system is used to compensate reaction torques produced by the relative movement between the links of the robot. Several experiments are conducted and compared against a reference model, the reference model is constructed by replacing several links by point masses located at their center of mass, in a similar way as done in [26]. This comparison confirms the advantage of the center of percussion over the center of mass. These compensation experiments lead to the decoupling of the dynamics using information of the point masses of the equivalent system.

5.1 Modeling a biped with four point masses

In section 3.1 the conditions to find dynamic equivalence were determined. The result was that the original system was replaced by two point masses, but the position of one of them was dependent on the position of the other, concluding that one mass was the

center of percussion with respect to the other and vice versa. Because there were more unknowns than equations, one of the masses was fixed in a random position in order to solve the set of equations. Considering this fact a system can be replaced by an infinite number of equivalent systems according to the selected reference.

In Chapter 4 the equivalent model was done by selecting a better approximation of the inverted pendulum model. Because the topology was smartly simplified, only linear controllers were required. One important effect partially solved, was related to the internal dynamics. Not all the reaction torques were compensated, and the leg was modeled with its own center of percussion in order to find a swinging algorithm having some criterion.

Another limitation of the inverted pendulum of Chapter 4 is that the selected reference is the center of pressure, therefore at least one foot should be all the time on the floor, if that condition is broken it will cause a singularity. Considering this limitation the model cannot be used to synthesize running gait, or similar gait where a flying phase is required. Although the impossibility of the previous model of dealing with a flying phase is an important issue, to have a system that resembles the dynamics of the original biped in a more straightforward way is also desirable, and the main motivation of this chapter.

5.1.1 Selection of a suitable reference

A biped robot can be divided in several group of links according to the function of those groups. Following the common segmentations done in other publications [84, 26], where the objective is to study gait, we can conclude that bipeds are often divided in three parts: two legs and the trunk. The trunk includes the arms and the head[1]. By the other hand, for the sake of simplicity it is desirable that the minimum amount of point masses will represent the equivalent system.

Considering that the just mentioned groups intersect at the hip, and the hip is used as a permanent reference when running, hopping, walking, etc.; we should expect that the result is a system with several point masses. The hip is an excellent candidate because it belongs to the biped, and its existence is not conditioned to the foot-ground interactions like the center of pressure.

Now everything is ready to calculate the center of percussion of each group. Remember that we have decided to divide the biped into three groups, the equivalent system of each group will be composed by two masses, therefore a set of six point masses is ob-

[1] This group is often called HAT, that stands for head, arms and trunk.

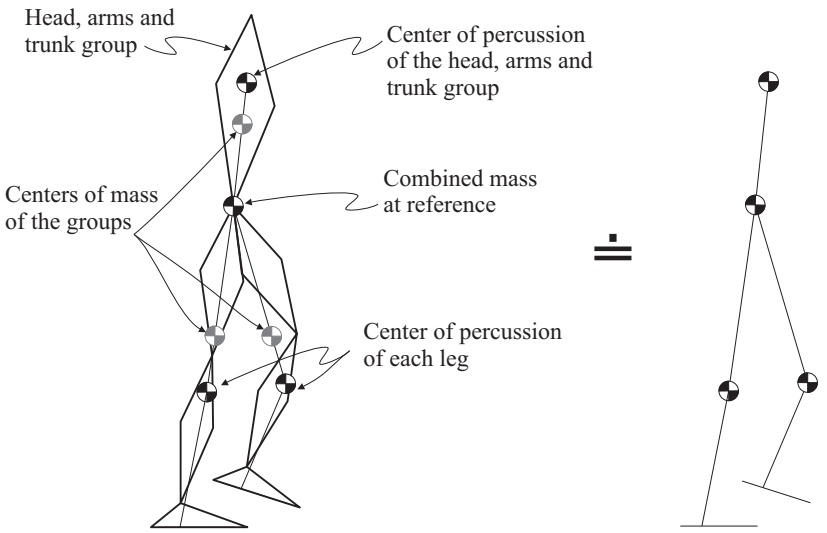

Figure 5.1: Four mass equivalent system. The biped system is reduced to four point masses. One mass in each center of percussion, and a combined mass at the hip. The combined mass is obtained out of the three masses that share the position.

tained. But, the centers of percussion were calculated with the same reference, therefore three masses share the same position and can be considered as one. To illustrate what has been explained in this paragraph, a biped and its equivalent four point system is shown in Figure 5.1.

The result is a four point mass system connected by massless links at the hip, notice that the sign of approximately equal has been used. This is done because there are effects produced by nonconservative forces, as for example the knee locks, that produce negligible non modeled effects. Details about this variations will be discussed later in this chapter.

5.1.2 Calculating the equivalent model

Once we have a suitable reference, it is possible to calculate the parameters of the equivalent model. Because there are several groups with similar parameters the author has selected the following notation for the sake of comprehensiveness. The point masses will have a subscript and a superscript m_n^x, where the subindex x refers to the part it belongs as it could be $l1$ or $l2$ for the legs, and b for the HAT group. By the other hand, n can take the value of 1 or 2; 1 is used if the mass is at the reference point, in this case it is the hip, and 2 is used when the mass is at the center of percussion. The scalar distances have the following format r_b^x, where b could be CM for the center of mass and

CP for the center of percussion. Finally the inertia and mass of each group is noted as I_x and m_x respectively, with the exception of the total mass and inertia where no subscripts are used

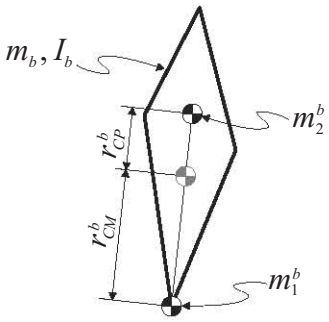

Figure 5.2: Equivalent system of the HAT group. The equivalent system is drawn on top of the HAT group. It is composed by two point masses and the reference is the hip joint.

First, the equivalent system of the HAT group will be calculated. A diagram is shown in Figure 5.2. Using the equations found in Chapter 3 the parameters of the equivalent model of the HAT group are calculated as follows:

$$r_{CP}^b = \frac{I_b}{m_b r_{CM}^b} \tag{5.1}$$

$$m_1^b = m_b \frac{r_{CM}^b}{r_{CM}^b + r_{CP}^b} \tag{5.2}$$

$$m_2^b = m_b \frac{r_{CM}^b}{r_{CM}^b + r_{CP}^b} \tag{5.3}$$

Following the same approach taken when calculating the equivalent model of the HAT group, the leg shown in Figure 5.3 has the following parameters for its equivalent model:

$$r_{CP}^{l1} = \frac{I_{l1}}{m_{l1} r_{CM}^{l1}} \tag{5.4}$$

$$m_1^{l1} = m_{l1} \frac{r_{CM}^{l1}}{r_{CM}^{l1} + r_{CP}^{l1}} \tag{5.5}$$

$$m_2^{l1} = m_{l1} \frac{r_{CM}^{l1}}{r_{CM}^{l1} + r_{CP}^{l1}} \tag{5.6}$$

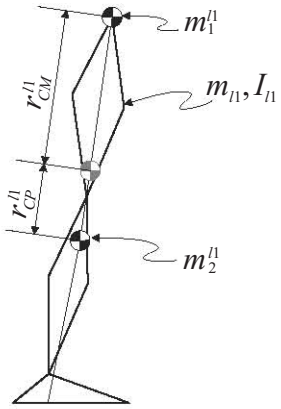

Figure 5.3: Equivalent system of the leg referred as $l1$. In a similar way as was done previously the parameters of the equivalent system for the leg are shown.

Finally the equations of the equivalent system of the leg $l2$ as shown in Figure 5.4 are:

$$r_{CP}^{l2} = \frac{I_{l2}}{m_{l2} r_{CM}^{l2}} \tag{5.7}$$

$$m_1^{l2} = m_{l2} \frac{r_{CM}^{l2}}{r_{CM}^{l2} + r_{CP}^{l2}} \tag{5.8}$$

$$m_2^{l2} = m_{l2} \frac{r_{CM}^{l2}}{r_{CM}^{l2} + r_{CP}^{l2}} \tag{5.9}$$

Equations of legs $l1$ and $l2$ are quite similar, in fact only the subscripts change. At first sight one could be driven to make the calculations regarding any of the legs, and use the same results for the other. But it should be addressed that this will lead to false results. The reason is that each leg has its own configuration during gait, therefore their moment of inertia is not the same most of the time. Checking equations from 5.4 to 5.9 the conclusion is that all the quantities are dependent on the moment of inertia of the system, therefore each leg will have its own equivalent model with different parameters.

Figure 5.5 shows the final model with all its parameters, all the quantities have been analytically exposed except for m_h. As was mentioned before, the models of each system share the same reference at the hip; therefore m_h is the combination of m_1^{l1}, m_1^{l2} and m_1^b. Finally, the last quantity of the model is:

$$m_h = m_1^{l1} + m_1^{l2} + m_1^b \tag{5.10}$$

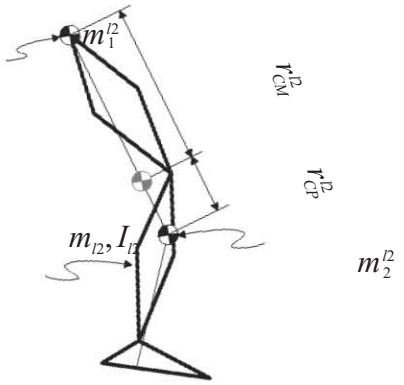

Figure 5.4: Equivalent system of the leg referred as $l2$. Although the calculations and therefore the parameters are equal to the case of leg $l1$, it has been redrawn to emphasize that the quantities are not equal. The last happens because each leg has its own configuration during the different gait stages.

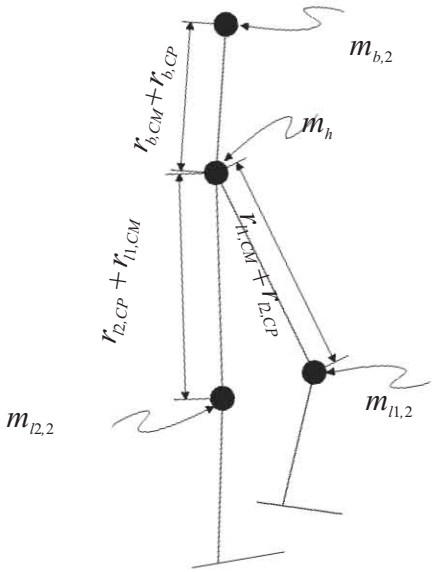

Figure 5.5: Schematic of the equivalent model with its parameters. In the figure the parameters of the model are shown, m_h is the combination of m_1^{l1}, m_1^{l2} and m_1^b.

5.2 Some words about impedance control

Originally walking robots were developed using trajectory tracking and similar techniques used to control manipulators. The major drawback was that the stiffness of the controllers did not contribute in the equilibrium of the robot. Despite this limitation the technique was refined and today impressive robots mostly Japanese [110] have been developed using high budgets. But, in mid 80's a different breed of robots also appeared, these robots depend heavily on their natural dynamics [87, 84]; therefore, *softer* control algorithms were required. Although the algorithms may vary according to the requirements, robots with dynamic gait generally use impedance control to calculate the joint torques $\boldsymbol{\tau}$ with the following law [5]:

$$\boldsymbol{\tau} = \hat{\mathbf{g}}(\mathbf{q}) - \mathbf{J}^T(\mathbf{q})[\mathbf{K}_P\tilde{\mathbf{x}} + \mathbf{K}_D\dot{\tilde{\mathbf{x}}}] \tag{5.11}$$

where $\hat{\mathbf{g}}(\mathbf{q})$ is the estimated gravitational torque, $\mathbf{J}(\mathbf{q})$ is the Jacobian, $\tilde{\mathbf{x}}$ the displacement vector, and $\dot{\tilde{\mathbf{x}}}$ is its derivative. Matrices $\mathbf{K}_P$ and $\mathbf{K}_D$ can be interpreted as the desired apparent stiffness and damping of, for example, one of the legs. Notice that equation 5.11 can be seen as the linear mapping between task space force and joint torque vector, with gravity compensation. Finally, the displacement vector $\tilde{\mathbf{x}}$ can be interpreted as a measure of the error with respect to the desired value $\mathbf{x}_d$ and the position of the reference $\mathbf{x}$ used in the Jacobian, therefore $\tilde{\mathbf{x}} := \mathbf{x} - \mathbf{x}_d$.

Equation 5.11 is the general form of a one degree of freedom PD controller, an equivalent physical system would be a spring-damper-mass system. Let us imagine that each leg is controlled by a similar controller, the main issue is that depending on the stiffness of the controller, the legs can be more or less sensitive to external perturbations, and such perturbations come as reactions torques of the relative movement of the links of the robot itself. For example, moving one leg forward causes the stance leg to move out of its equilibrium point.

The control law in equation 5.11 is also present in assistive robotics in the form of hybrid controllers [44, 25]. Kuo [63] models human muscles as elastic elements, while Pratt [84], Collins [20] and Daemen [23] use actuators with a spring connected in series to reduce the stiffness of their systems[1]. With this in mind, the common element of the previous examples is that all of them are thought to be used in human environments where low stiffness it is always desirable to reduce security issues.

[1]This configuration has been named *series elastic actuator* by its inventor Jerry Pratt.

Although the control law in equation 5.11 is stable, it is very sensible to external perturbations. This characteristic will be exploited to validate the model proposed in Section 5.1.2. The idea is to compensate the reaction torques only with the information provided by the equivalent model. It should be noticed that the reaction torques can be estimated by several methods, including solving the equations of motion described the in Section 2.3.2. But, the objective is to provide simpler models to work with.

5.3 Fast swinging of one leg

Gait in steady state can be considered as dynamically balanced, internal dynamics have been carefully tunned in order to generate locomotion. Usually, gait is generated at relatively low speeds, therefore most dynamic effects including inertial forces can be dismissed. Another way to dismiss these effects is to design robots with light links, this solution can be normally found in passive walkers and similar machines [20, 69, 106]. But thinking in walking machines as more flexible and reliable mobile robots will lead to heavier and faster designs, and the previously mentioned workarounds will no longer be valid.

In this section experiments of a biped robot standing over one leg, while the other is swung at a relative fast speed, are performed. The parameters and the speed of the movements are selected to produce no negligible reaction torques. The performed movement is like kicking a soccer ball, although no soccer ball is present. The experiment is repeated using the same controller gains compensating the reaction torques with two different techniques and comparing them against the uncompensated system.

5.3.1 Selection of the parameters

The parameters of other walking machines are difficult to find, although general parameters can be found, details about center of mass or moment of inertia of each link are not usually available. Besides, the parameters of other walking robots are the product of the wiser design available according to the selected mechanical components, though it is not their objective to reproduce human dynamics. Albeit, nondimensionalization of the equations will generalize the results, the presence of nonlinearities can restrict this technique. Despite this limitation the technique has been used to study robots [35, 24, 102] and human beings [63].

Table 5.1: Parameters of the robot calculated based on human standards.

	Thigh		Shin	
	Dimensionless parameters	Robot parameters	Dimensionless parameters	Robot Parameters
Mass	0.1 M	6.3 kg	0.0465 M	2.0925 kg
R. Gyration	0.323 S	0.1392 m	0.0302 S	0.1114 m
Inertia	–	$0.1222\,\mathrm{kg}\cdot\mathrm{m}^2$	–	$0.0260\,\mathrm{kg}\cdot\mathrm{m}^2$
S. Length(S)	0.245 H	0.4312 m	0.246 H	0.3690m
r_{CM}	0.567 S	0.2445 m	0.567 S	0.2092m
	HAT group		Foot	
	Dimensionless parameters	Robot parameters	Dimensionless parameters	Robot parameters
Mass	0.678 M	30.51 kg	0.0145 M	0.6525 kg
R. Gyration	0.496 S	0.2530 m	0.475 S	0.0278 m
Inertia	–	$1.9522\,\mathrm{kg}\cdot\mathrm{m}^2$	–	$0.0005\,\mathrm{kg}\cdot\mathrm{m}^2$
S. Length(S)	0.34 H	0.51 m	0.039 H	0.0585m
r_{CM}	0.626 S	0.3193 m	0.5 S	0.02925m
Foot length	–	–	0.152 H	0.228m

Note: The dimensionless parameter are used to calculate each robot parameter with M, H and S constants. M and H are the mass and the height, 45kg and 1.5m respectively, and S is the link segment length. Finally, r_{CM} is the distal distance of the center of mass.

Taking advantage of the possibilities of simulation, in this work properties will be selected closer to human standards in order to avoid possible errors produced by a bad selection of parameters; therefore, they will be selected based on anthropometric data. Plenty of sources, principally from the department of defense, are available; but, the information provided in Winter [105] was preferred instead. The reason is that this book has been used by the robotics community during several years. Based on the information provided in the previously mentioned reference, the parameters shown in Table 5.1 were defined, besides Figure 5.6 shows a graphic description of them. The parameters provided in [105] are nondimensionalized[1] in terms of the height and weight

[1]Nondimensionalization is used to describe the parameters in terms of measurable quantities of a human being. In other words, it is used in the sense of parameterization, and it is not used to describe dimensional analysis. Therefore, should not be confused with the scaling done by other authors to generalize their results.

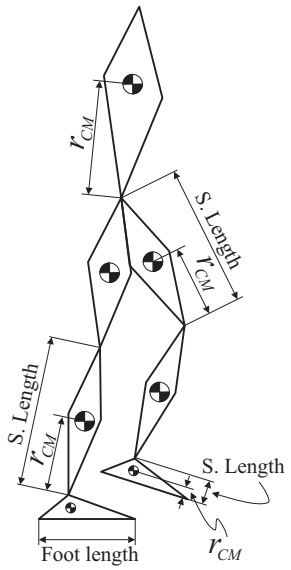

Figure 5.6: Parameters of the model. Graphic description of the parameters shown in Table 5.1. It should be noticed that the positions of centers of mass are distal distances, except for HAT group that is proximal.

of the subject. The author selected a height of 1.50m and a weight of 45kg, these parameters correspond to the height of other humanoid robots, and the weight matches the weight of healthy colleagues with that height. Albeit, the selection is not based in any scientific criterion, the requirement was to find some parameters that will describe a real human being, and the assumption was enough in order to produce realistic mass and geometric properties[1].

5.3.2 "Kicking" experiments

Once the parameters have been selected, some experiments in order to evaluate the precision of the equivalent model will be performed. In this section the robot will be standing over one leg, while the other swings similar to a kicking action, as described in Figure 5.7. Each joint will be controlled with an independent PD controller using a position control strategy. Gravitational effects will be compensated in order to study only the perturbations produced by the reaction torques. These torques will be compensated using information from different models as explained in the following lines.

[1]The properties found with the selected parameters are considered to be realistic, because a healthy human being having approximately the same weight and height can be easily found.

Figure 5.7: Stroboscopic animation of the "kicking" experiment. This experiment will compensate the torques produced by the inertia of the swinging leg. The objective is to demonstrate how precise is the four point model proposed in this chapter.

The main idea is to use only the information of point masses to compensate the reaction torques. Depending on how accurate those models are, the compensation will be more or less successful. The compensation will be done by modeling each group (legs and HAT group) by point masses, as shown in Figure 5.2, in one case the center of percussion will be used[1], the next experiment will be performed using the center of mass[2] and finally no compensation at all. The compensation takes into account only the inertial forces produced by the point masses; therefore, a compensation torque $\boldsymbol{\tau}_i^c$ with opposite sign to the reaction torque produced by the acceleration of the point mass m_j will be generated at each joint with the following value:

$$\boldsymbol{\tau}_i^c = -\sum_j m_j \mathbf{r}_{ij} \times \mathbf{a}_{ij} \tag{5.12}$$

where $\boldsymbol{\tau}_i^c$ is the compensation torque applied at the ith joint, m_j is the point mass of the group being compensated[3], $\mathbf{r}_{ij}$ is the position vector from the ith joint to the jth point mass, and $\mathbf{a}_{ij}$ is the acceleration of the jth point mass relative to the ith joint, in other words i and j are never the same. The joint and the point mass should not belong to the same group, because the point mass models the group itself. Figure 5.8 shows

[1] i.e., the black marks in Figure 5.2.
[2] i.e., the gray marks in Figure 5.2.
[3] The groups are the HAT group, and the swing leg.

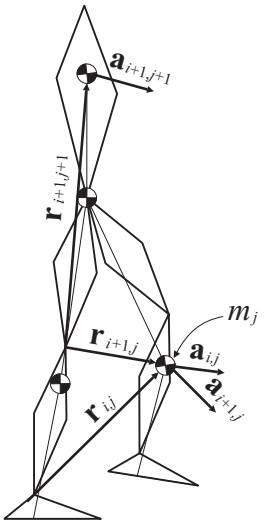

Figure 5.8: Compensation of the reaction torques. m_j is the point mass that models the group, it could refer either to the center of mass or to the center of percussion.

the meaning of equation 5.12 graphically. The compensation is done twice in each joint, because it should compensate the movements of the HAT group, and the swinging leg.

5.3.3 Results of the "kicking" experiments

As it was mentioned before, the robot is controlled using PD controllers in each joint. The controllers are set in a position control scheme, producing a steady state configuration similar to the final position shown in Figure 5.7. The stance leg has a proportional gain of $10\text{N} \cdot \text{m/rad}$ and the derivative gain has a value of $3\text{kg} \cdot \text{m/s} \cdot \text{rad}$, the gains are the same for each joint controller of the stance leg. These gains were selected to be sensible to external perturbations, therefore gravity compensation was required to avoid large steady state errors. Besides, the sensibility is a desired quality to asses the compensation techniques being evaluated in this chapter. The swinging leg has stiffer gains at the knee and the ankle joint having $40\text{N} \cdot \text{m/rad}$ and $20\text{kg} \cdot \text{m/s} \cdot \text{rad}$ for the proportional and derivative gain respectively. The reason is, as mentioned in the Section 5.3.2, there is not internal compensation in the groups, and only the effects of external groups are compensated in each joint[1]. Finally, the hip joint of the swinging leg has high gains, the values are $80\text{N} \cdot \text{m/rad}$ and $10\text{kg} \cdot \text{m/s} \cdot \text{rad}$. Table 5.2 shows the gains

[1] i.e. compensation of the inertial forces of the point mass modeling the group considered external from the point of view of each joint.

of each controller. The high gain used on the hip joint of the swinging leg produces a swing with a duration of approximately 1 second.

Table 5.2: Gains of the controllers used in the "kicking" experiments.

	Stance leg		Swinging leg	
	Proportional gain	Derivative gain	Proportional gain	Derivative gain
hip	10	3	80	10
knee	10	3	40	20
ankle	10	3	40	20

Figures 5.9, 5.10 and 5.11 show the results of the experiments of this section. There are two graphics in each figure, one shows the angular position of each joint of the stance leg and the other shows the angular position of the swinging leg. All the joints in the stance leg are set to zero radians. Therefore the perturbations due to the swinging leg are shown as a deviation from the zero position. Figure 5.9 depicts the experiments with no compensation, as expected, all the joints of the stance leg were affected by the swinging leg. The fact that all the joints of the stance leg are moving produce a non linear behavior, and consequently the joint took a longer time to reach its steady state.

Figure 5.10 uses the center of mass of the swinging leg to compensate the inertia effects. Using this approach one expects that only the linear momentum effects will be compensated, therefore the graphs will show a reduction of the disturbances produced by the swinging leg. In fact, Figure 5.10(a) shows a reduction of the amplitude of the vertical scale of 50%. This is very encouraging toward the next experiment when the center of percussion will be used. But, Figure 5.10(a) still shows non linearities, and they seem even stronger than the ones depicted in Figure 5.9(b).

Finally, in Figure 5.11(a) there is a reduction of the perturbations approximately of two orders of magnitude. This strong reduction of external effects gives as a result that the swinging leg presents no deviations from its linear behavior as shown in Figure 5.11(b). Because the stance leg, successfully rejects the perturbations from the swinging leg, its joints also reach their rest position much faster than the other cases. At this point, we can conclude that the center of percussion successfully reflects most of the dynamics involved in a complex system. But, in the next section a quantitative analysis will be performed.

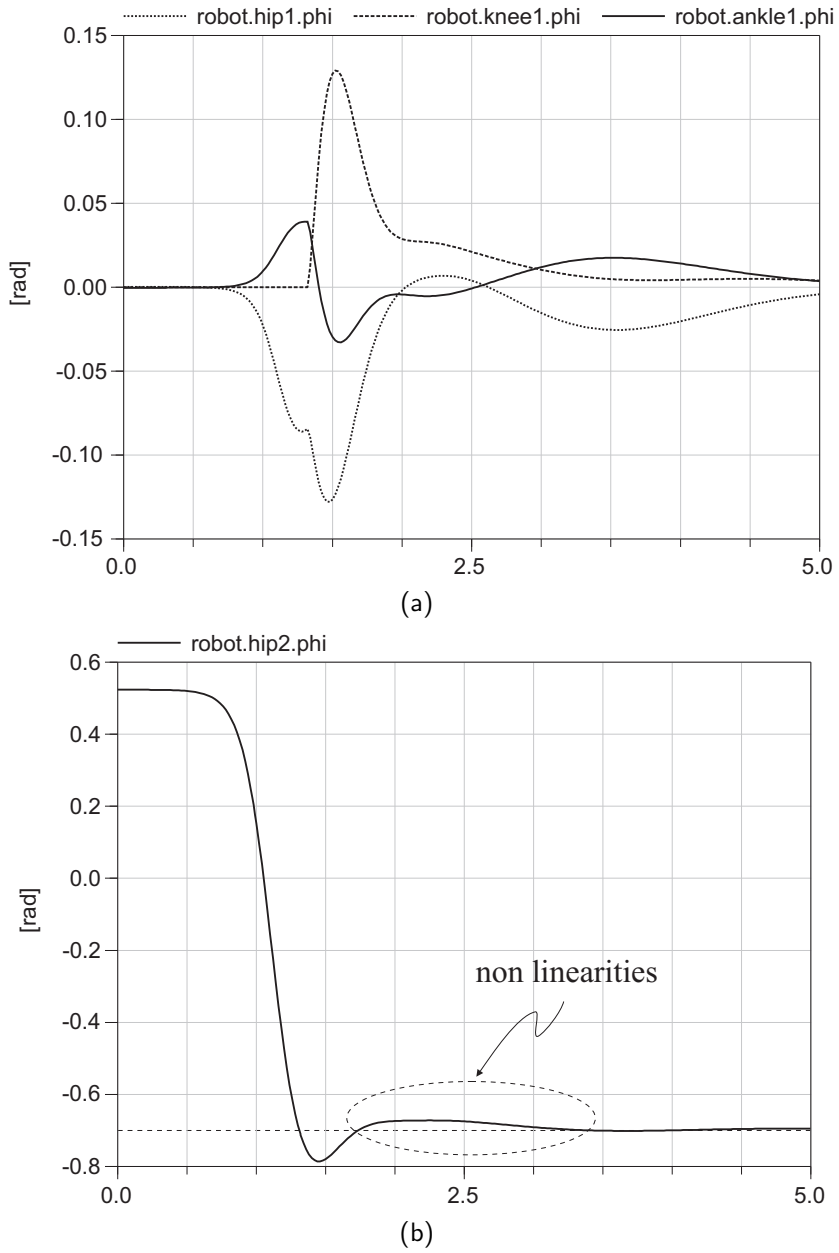

Figure 5.9: Experiments using no compensated controllers. (a) Angular position of the joints of the stance leg. (b) Angular position of the swinging leg. It can be seen that the swinging leg acts as a perturbation, moving out from the rest position all the joints. Also, the swinging leg does not behaves linearly, although it reaches its steady state position after some time. The units of the horizontal axis are seconds.

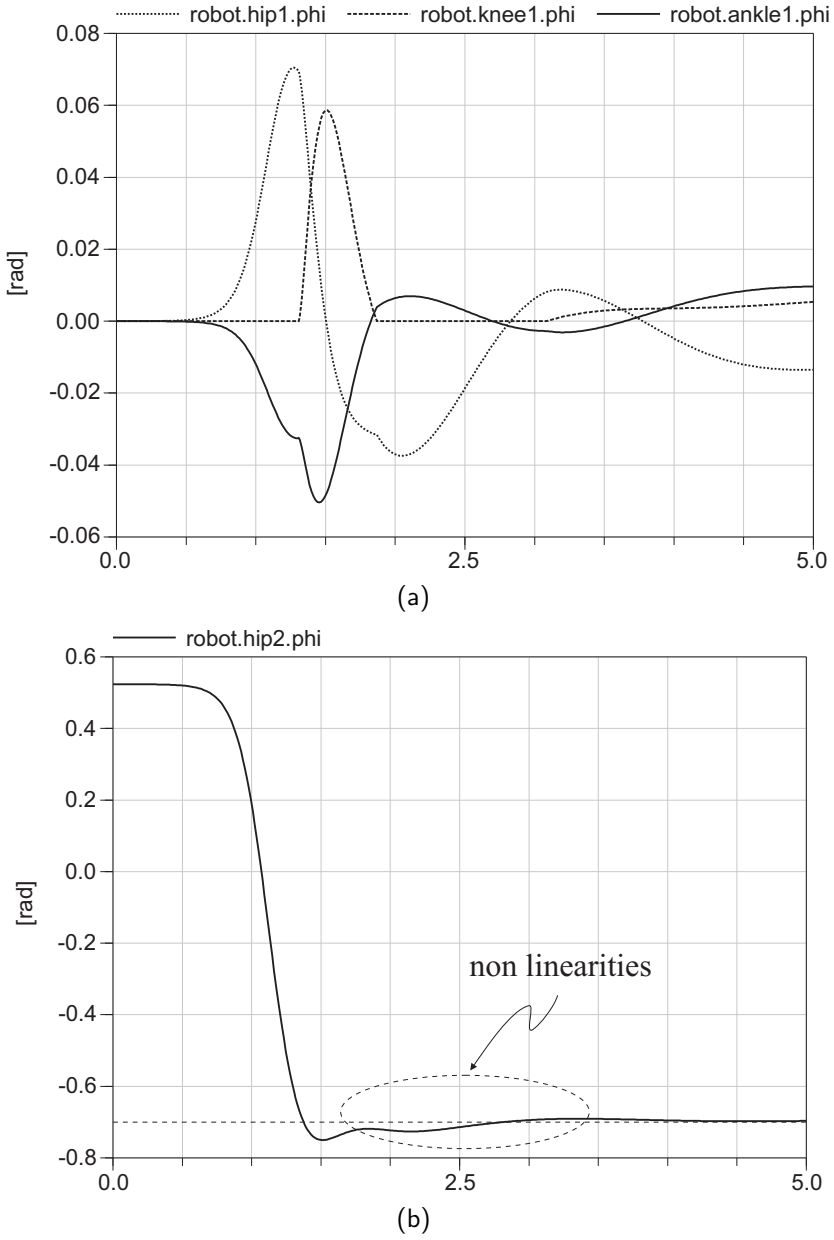

Figure 5.10: Experiments using center of mass compensation. (a) Angular position of the joints of the stance leg. (b) Angular position of the swinging leg. This figure shows that using the center of mass to compensate reaction torques does reduce the perturbations produced by the swinging leg by approximately 50%. The swinging leg still takes some time to reach its steady state position, and the nonlinearities are clearly seen. The units of the horizontal axis are seconds.

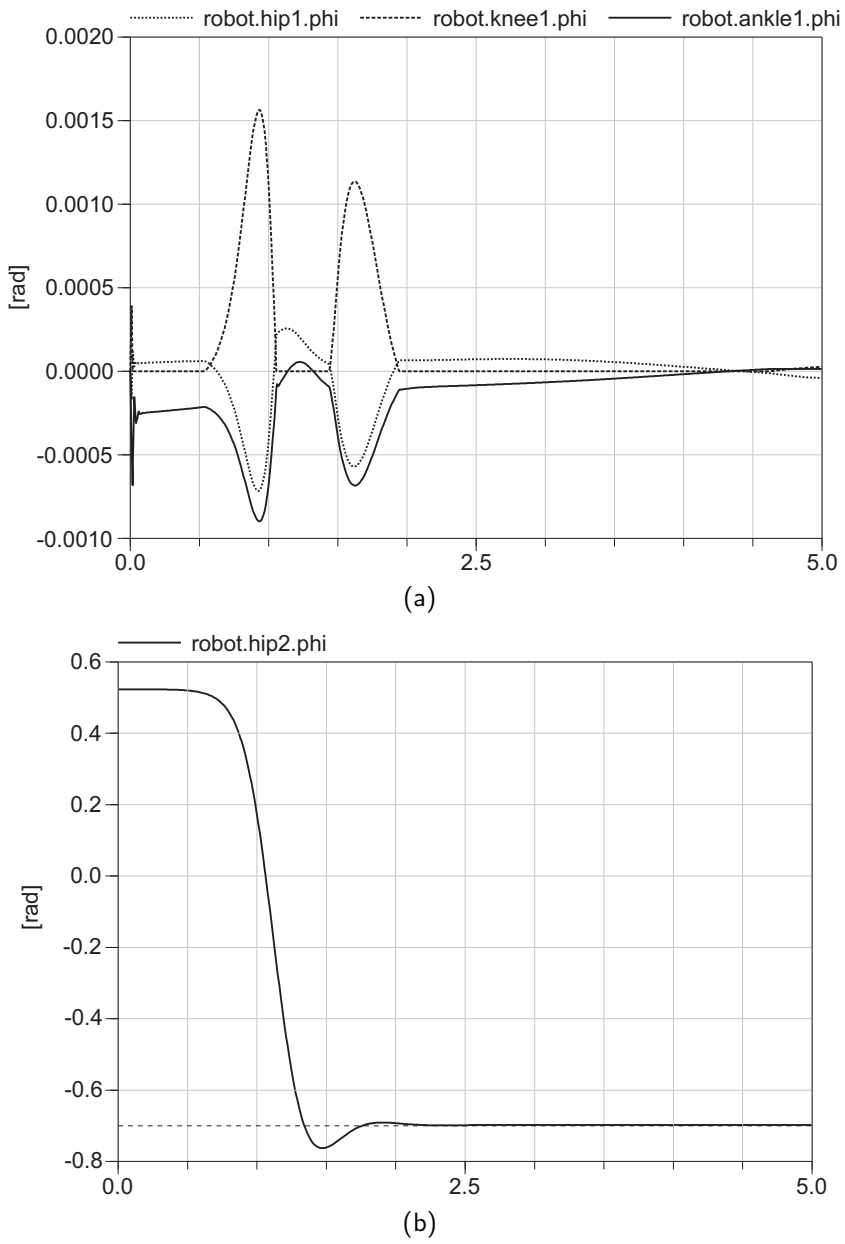

Figure 5.11: Experiments using center of percussion compensation. (a) Angular position of the joints of the stance leg. (b)Angular position of the swinging leg. Using the center of percussion to model the point masses attenuates the perturbations by at least two orders of magnitude with respect to the non-compensated controllers, also each joint reaches its steady state equilibrium almost immediately. The swinging leg shows a remarkable linear behavior, reaching its steady state with no problems. The units of the horizontal axis are seconds.

5.4 Oscillation experiments

In Section 5.3.3 experiments rejecting perturbations produced by the swinging leg were performed. The result was that the system modeled using the center of percussion was far more stable than the system using the center of mass to model the system. The results were analyzed in a qualitative way by comparing the amplitude of the perturbations in each joint of the stance leg, and by looking for artifacts in the hip joint graph of the swinging leg. But still remains the question how linear is the model, considering that equation 5.12 shows only the effects of inertial forces, dismissing other accelerations like centrifugal, or Coriolis ones. The strong attenuation shown in Figure 5.11(a) provide information that the approximation using the center of percussion is quite close to the reality, and that the effects not included can be dismissed without problems. To prove these statements measurements of the natural frequency of the controllers will be provided in this section.

The experiments take the robot in the configuration of Figure 5.13(b) and then, each group (HAT group, stance leg and swinging leg) is excited at the same time by an step function, producing undamped oscillations. The dynamics of each group is decoupled thanks to the methods used in 5.3.2, more specifically the equation 5.12. After that, each group behaves independently showing no coupling, and their controllers behave linearly.

5.4.1 Parameters used in the simulations

It is well known that the impulse response of a system determines the behavior to any input, this is true to any linear time invariant system[1]. Therefore, if such a response can be characterized, we can conclude if a system is linear or not. Also, in our case, it will confirm that the compensation done using the center of percussion can decouple the dynamics by letting each controller behave independently.

The experiments will be performed by measuring the period of the undamped controllers. The gains are the ones shown in Table 5.2 except for the swinging leg proportional gain, that is set to 80N·m/rad, and the derivative gains of the ankle of the stance leg and the hip joints that are set to zero. The last is done because, as it was mentioned before, we want to measure the undamped period. The parameters of the four point masses equivalent model are gathered in Table 5.3 and explained in Figure 5.13(a).It should be noticed that those values are configuration dependent, in Figure 5.13(b) the

[1]This concept is the basis to develop impulse response filters, those filters can be used to model complex phenomena in different domains.

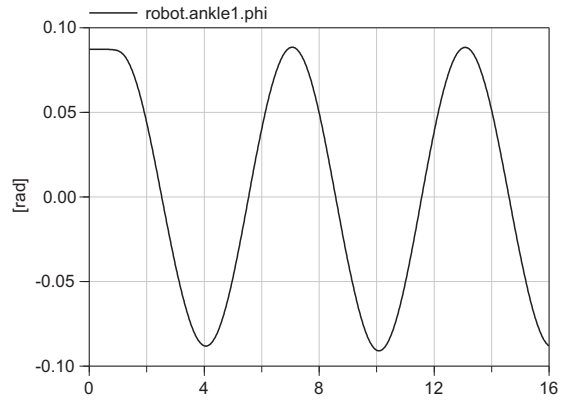

(a)

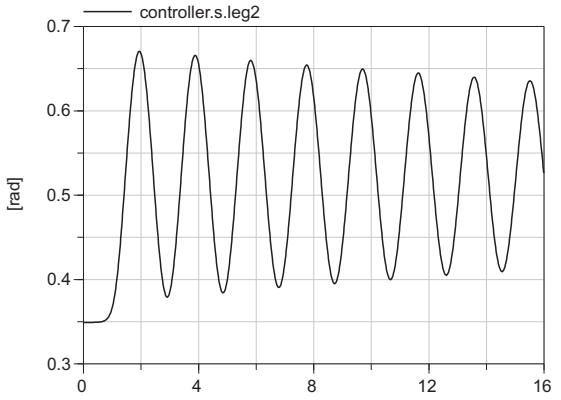

(b)

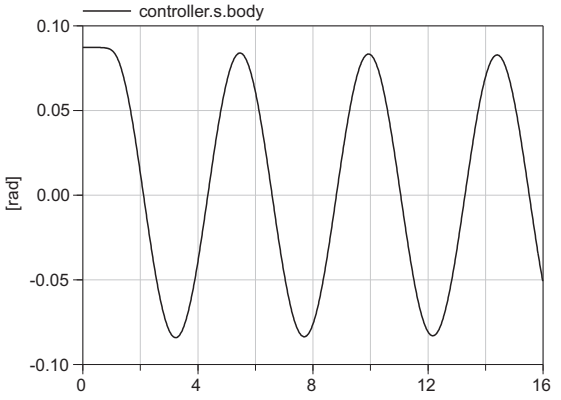

(c)

Figure 5.12: Oscillation experiments. (a) Angle of ankle joint of the stance leg. The period in this graph is approximately 6.032s.(b) Angle of the swinging leg. The observed period is 1.94s. (c) Absolute angle of the HAT group. The period according to this graph is 4.44s. The units of the horizontal axis are seconds.

Table 5.3: Parameters of the equivalent model.

	mass (kg)	r_j (m)	r_k (m)
m_{hip}	16.822	0.5197	–
m_{leg1}	4.6033	0.5037	0.2328
m_{leg2}	4.583	0.4540	–
m_{HAT}	18.7393	0.5197	–

equilibrium angles of the controllers used in the experiments are shown. Besides, the angles of the knee and ankle joints shown in the same picture plus the parameters of the robot listed in Table 5.1 produce the values listed in Table 5.3.

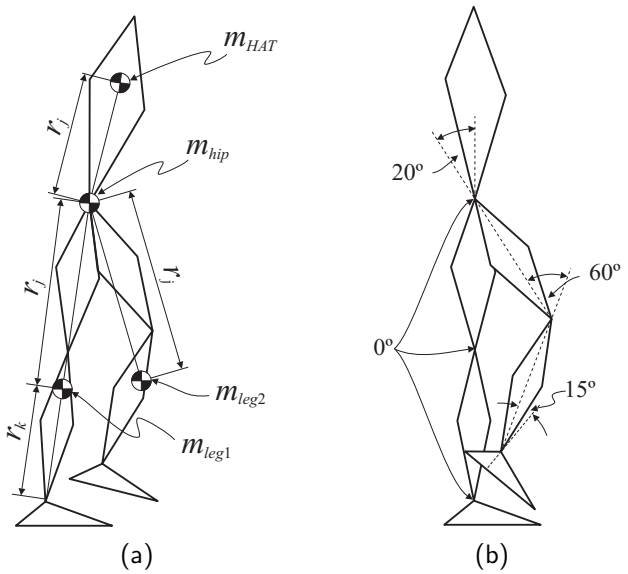

Figure 5.13: Parameters of the oscillation experiments. (a) Parameters of the equivalent model.(b) Configuration of the robot used in the oscillation experiments. It should be noticed that the angles of the knees and ankles plus the parameters of the robot listed in Table 5.1 produce the values listed in Table 5.3.

5.4.2 Results of the oscillation experiments

It is well known that biped robots are systems with high levels of coupling, i.e. moving any part of the robot will introduce perturbations and nonlinearities in the other joints. The main conclusion of Section 5.3.2 is that compensating the reaction forces using the center of percussion information could reduce such perturbations to very low levels.

Therefore, a decoupling of the dynamics can be performed, and moving different groups will not produce undesirable effects. By the other hand in Section 5.3.2 only one of the groups was moving, that was the swinging leg. In this section all the groups are moving, and the natural frequency of each group is calculated and compared against the simulations of the whole model.

Figure 5.12 shows the undamped natural frequencies of each controller. The graphs were obtained by giving starting values to the angles of the hip joints and the stance leg ankle, different from the equilibrium in order to simulate a step to excite the system. The gains, as it was mentioned in Section 5.4, for both hip joints and the ankle joint of the stance leg have a value of $10\text{N} \cdot \text{m/rad}$ for the proportional gain, and zero for the derivative gain. The other values are not modified and taken from Table 5.2. At first sight the graphs in Figure 5.12 are clearly the response of an undamped linear system, except for 5.12(b) that has some damping but low enough to be dismissed[1]. But one can conclude that no coupling is happening between the controllers. From those graphs the periods of one cycle are taken and then compared against the theoretical values of the equivalent four point masses model.

Now, we are ready to calculate the theoretical values of each controller. The HAT group rotates around the hip joint, therefore its natural frequency:

$$\omega_n^{HAT} = \sqrt{\frac{k_p}{I_{HAT}}} = \sqrt{\frac{k_p}{m_{HAT} r_j^2}} \tag{5.13}$$

$$\omega_n^{HAT} = \sqrt{\frac{10}{(18.793)(0.5197)^2}} = 1.4057 \tag{5.14}$$

And the period is:

$$T^{HAT} = \frac{2\pi}{\omega_n^{HAT}} = 4.469\text{s} \tag{5.15}$$

Because the swinging leg also swings around the hip joint it has similar equations, then its natural frequency and period is:

[1] The damping ratio can be calculated from Figure 5.12(b), using $\delta = \ln(x_0/x_n)/n$ and $\zeta = 1\Big/\sqrt{1+(2\pi/\delta)^2}$, also called the logarithmic decrement method. The damping ratio is ζ=0.0012, therefore the natural frequency is approximately the damped natural frequency.

$$\omega_n^{leg2} = \sqrt{\frac{k_p}{m_{leg2} r_j^2}} \tag{5.16}$$

$$\omega_n^{leg2} = \sqrt{\frac{10}{(4.583)(0.4540)^2}} = 3.2536 \tag{5.17}$$

$$T^{leg2} = \frac{2\pi}{\omega_n^{leg2}} = 1.9311\text{s} \tag{5.18}$$

The ankle joint at the stance leg should compensate the mass at its center of percussion called m_{leg1} and the point mass at the hip joint, this mass is composed by the combination of the point masses of the other subsystems as explained in equation 5.10. Therefore its natural frequency is:

$$\omega_n^{leg1} = \sqrt{\frac{k_p}{m_{hip}(r_j + r_k)^2 + m_{leg} r_j^2}} \tag{5.19}$$

$$\omega_n^{leg1} = \sqrt{\frac{10}{(16.822)(0.5037 + 0.2328)^2 + (4.6033)(0.2328)^2}} = 3.2536 \tag{5.20}$$

$$T^{leg1} = \frac{2\pi}{\omega_n^{leg1}} = 6.0834\text{s} \tag{5.21}$$

Comparing the theoretical periods of the controllers against the ones observed in the simulations, the result is that they differ by less than 1%.

5.5 Conclusions of the chapter

In this chapter an equivalent model composed by four point masses was proposed, the method to construct such a model were exposed and experiments to validate it were performed. The first experiment, called the “kicking” experiment, measured the ability to compensate the reaction torques by performing a fast swinging of one leg, similar to a kicking action. First, the leg was swung and no compensation was used. Once this was done, it was compared against a similar model, but using the center of mass to obtain the values and location of the point masses. In this case, and improvement over the non-compensated experiment was observed. A reduction of the amplitude of the perturbations of around 50% was reported.

Finally the point mases were modeled using the center of percussion. The result was that the center of percussion model was far more accurate rejecting the reaction torques produced by the swinging leg. The reduction was of two orders of magnitude when compared against the non compensated controller. Although the same result could be obtained by calculating the dynamics of each link, and then using those results to compensate the reaction torques. The advantage of the method proposed in this work is that everything is done by using the information provided by one point mass. Resolving the dynamics would imply monitoring several rigid bodies with several parameters, adding great complexity to the final solution.

Another relevant point of the first experiment is how accurate the reaction torques were rejected. Dismissing centrifugal or Coriolis accelerations can greatly simplify the equations of motion, this practice has been commonly implemented by several authors to make highly dynamic algorithms for walking machines [87], but there was not a formal proof about what was missing when doing such simplifications. Because in this work the concept of dynamic equivalence is extensively used, this means that using the equivalent system is equivalent to use the original one. Therefore, we can conclude that those accelerations are negligible when comparing them against the inertial forces, proving the reason why it is possible to ignore other accelerations in this kind of systems.

The second part of this chapter was focused on the behavior of the controllers. Both hip joints and the ankle joint of the stance leg were set only with proportional gains in order to avoid damping effects. In that way the HAT group and the legs were able to oscillate freely. Each group of the biped was excited and their oscillations were measured. The results are shown in Figure 5.12, and they depict decoupled systems each of them with their own natural frequency. The theoretical natural frequencies and periods were calculated using the four point masses equivalent model, and finally experimental and theoretical values were compared. The discrepancy of both values was less than 1%. With such precise results the final conclusion is that the four point mass model proposed in this work is a powerful tool to simplify the complex dynamics involved in biped robots. Besides, despite other simplifications, the amount of non-modeled dynamics is reduced to imperceptive levels as demonstrated by the experiments performed.

6
Analysis of the models

In this work a novel approach to make simplified equivalent models of biped robots has been proposed. The method is based on the dynamic equivalence criterion, this works by keeping the same values of the main parameters between the original and the equivalent system. Those parameters defines the dynamics of both systems and are the mass, the moment of inertia and the center of mass. Intuitively, one can conclude that on a rigid body those are the only parameters present in the equations of motions, consequently those are the only numbers that affect the solution of those equations. The simplification of a rigid body would not have any merit because excellent solutions are available in classic mechanics; but, when dealing with complex systems alternative analysis tools are welcomed in order to provide a better criteria.

The dynamic equivalence concept is later extended to multi-body systems, and applied to bipedal machines, producing two models: A modified inverted pendulum, and a four point masses model. Gait has not been thoroughly studied in this thesis[1] because this could distract from the main objective of this work, that is to provide a tool of analysis of biped robots. Therefore, the efforts have been focused on the usage and demonstration of the accuracy of the methods proposed in this thesis.

In this chapter additional analysis about the proposed models is described. The torque actions used in the experiments of Section 5.3.2 are analyzed. The objective is to assess where the power is used, and how much of the power is actually used to perform the actions commanded by the inputs. The fact that there is a model with decoupled dynamics, encourages to perform this kind of experiments. Besides, it is expected that this could provide information about the forces being withstood by joints and links, this could be used as input information for mechanical design for future prototypes.

[1] Gait generation is a very sensitive matter, different methods are proposed to generate it with a wide range of advantages and disadvantages, making it a subject out of the scope of this work.

Also in this chapter additional properties of the equivalent pendulum proposed in Chapter 4 are studied. Originally when this pendulum was used, the center of pressure was fixed by using point feet. In order to generalize its application this simplification is to restrictive, all bipeds are expected to have real feet in order to walk in an anthropomorphic way. Although the analysis is not performed on a biped, but a pendulum with a wide base measuring the center of pressure, the results are expected to be extensible to other systems that are able to measure the center of pressure, as it could be a biped robot or even a multi legged walking system. The analysis is done by relating the reaction forces of the original system with the dynamic forces produced by the equivalent pendulum.

6.1 Four point masses model and torque analysis

In Chapter 5 a simplified model of a biped was proposed, the difference when comparing against other similar works, like for example the ones shown in [9] or [25], where models with point masses are also used, is that in this case the masses are selected to match all the important dynamic parameters of the robot[1]. The dynamic equivalence used in the method allows that the model can be used to decoupling all the dynamics of the original system. Now, each part of the control action can be examined independently, therefore it is possible to asses what happens with the other joints when others are moving.

Depending on the applied gait design strategy, this analysis can be more or less important, but from the point of view of design, it is of interest to know how much of the power will be assigned to compensate or to provide actuation. In this section the parts that form the total control action will be analyzed, they are: The gravity compensation, the dynamic compensation and the control action itself. In Chapter 5 they were mentioned and their parameters exposed, but no graphs were shown, hence in this section plots of the control actions are exposed.

6.1.1 Components of the control action

The control law in Chapter 5 used to move the joints is composed by three torques: The torque produced by the PD controller, the gravity compensation torque and the dynamic compensation torque. Therefore, the control action at the ith joint can be written as:

[1] i.e. the total mass, the center of mass, and the moment of inertia.

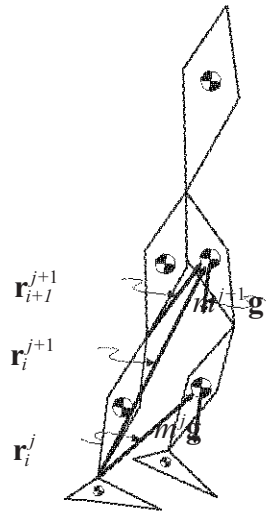

Figure 6.1: Gravity compensation. The torque produced by each link over the joints is compensated using the cross product between their relative distances and their weight force vector.

$$\tau_i = \tau_i^{PD} + \tau_i^G + \tau_i^c \tag{6.1}$$

The calculation of τ_i^c is shown in Section 5.3.2, τ_i^G is the sum of the torques produced by each link on the ith joint. Using Figure 6.1 the ith joint torque is written as:

$$\tau_i^G = \sum_j m^j \mathbf{r}_i^j \times \mathbf{g} \tag{6.2}$$

The PD control action is nothing more than a spring-damper system, and it positions the joint in the desired angle. In other words, it is the input to be controlled. Therefore τ_i^{PD} is written as:

$$\tau_i^{PD} = k_p^i(\theta_d^i - \theta^i) + k_d^i\dot{\theta} \tag{6.3}$$

6.1.2 Analysis of the torque components

Figure 6.2 shows plots of the torques calculated from equation 6.1, those plots are obtained from the experiments described in Section 5.3.2. The parameters of the robot, as well as the gains of the controllers are exposed in that section. When the experiments were shown by the first time in this thesis, the objective was to prove the decoupling of the dynamics in order to validate the four point masses model proposed in that chapter.

That objective was accomplished using plots of the position of the joints, and comparing the theoretical parameters of the system against the experimental ones obtained from those plots. The torque plots of the joints were not required for the analysis, but they still can provide additional information about the system, and that is what is pursuit in this section: Expose the significance of each of the components of the control torques.

Torques can be used as a tool for designers, the control actions provide information about the forces that will be supported by the links and joints of the robot. Examining Figure 6.2 one can notice that the total torque has almost the same value for all the joints, except for the case of the swinging leg (Figure 6.2(e)). The own weight of the robot determines the size of the actuators as well as the required resistance of the links. The other components of the torques are just a fraction of the total control action. Despite they are relatively small when compared against the total torque, they are very important because they are responsible to move the robot.

Figures 6.2(b),6.2(d) and 6.2(f) shows the torque produced by the PD controller, and the dynamic compensation action. The ankle joint, as it can be expected, applies a major compensation torque, because it stands all the moving links. In the case of the hip joint of the stance leg (Figure 6.2(d)), the compensation action is reduced and it has minor amplitude than the PD torque. Some jerks are present, but they are not significant, because they are not big enough to modify the total control action, therefore they are not taken into account. Finally Figure 6.2(f) shows the torques of the hip joint responsible of the swinging leg. The compensation torque is the least important of the previous ones. This happens because the swinging leg has the minor mass of the other groups.

It should be noticed that most of the power goes to compensation actions, more specifically to compensate gravitational forces. If this is not done, extremely high gains would have to be used in order to maintain equilibrium, other option is to avoid linear controllers. This analysis maximized the importance of wise designed structures with the least weight, because the frequency response of the actuators it is determined by the residual torque not used to compensate gravity effect. Other interesting phenomenon can be seen in Figure 6.2(e), here the control action has a minor amplitude than the gravity compensation torque. This happens because the PD torque and the compensation torque oscillates around zero N·m, while the others are offseted at approximately -5N·m, therefore the total torque takes some of the energy from the gravitational field.

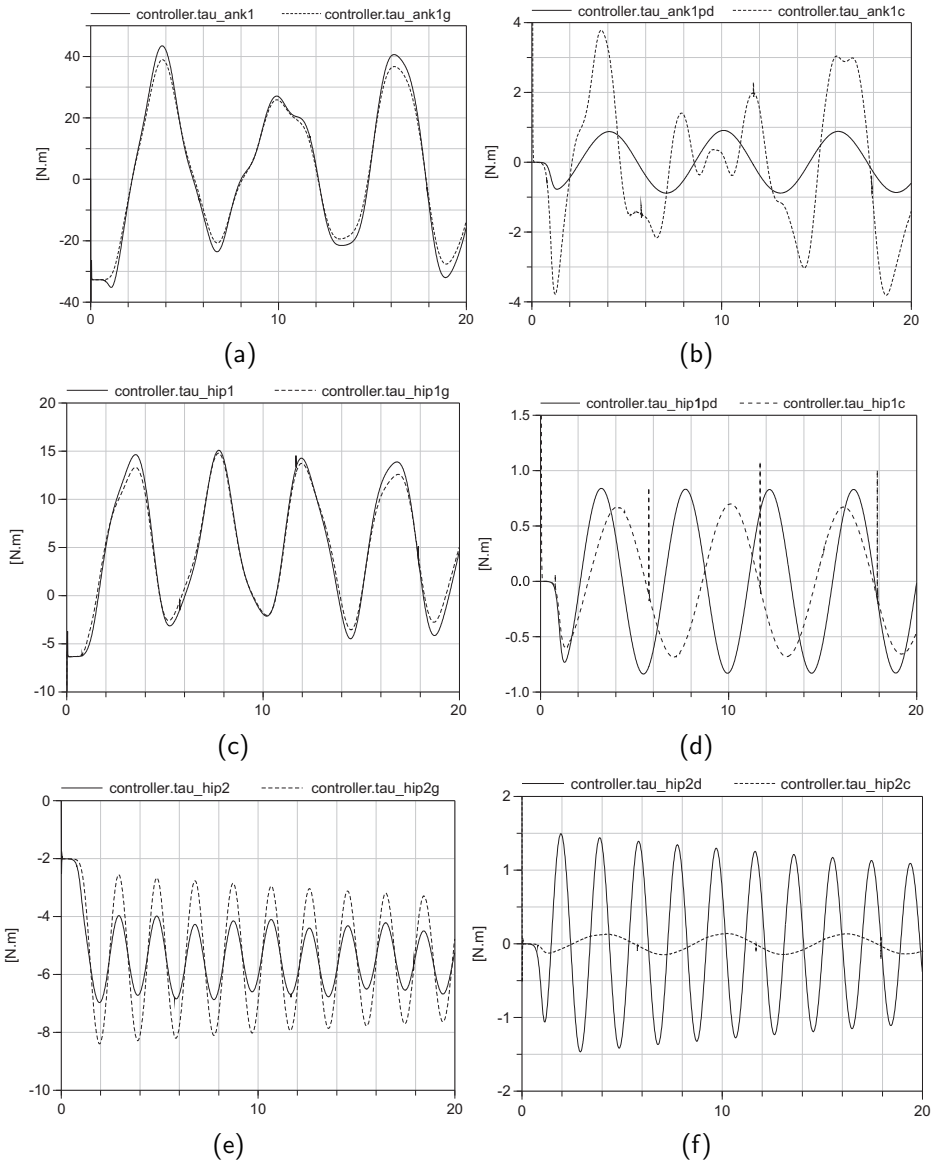

Figure 6.2: Torques at joints using propotional gains of 10N·m/rad.(a) Total (solid line) and gravitational torque (dashed line) applied at the ankle joint of the stance leg. (b) PD torque (solid line) and Compensation torque (dashed line) at the ankle joint of the stance leg. (c) Total (solid line) and gravitational torque (dashed line) applied at the hip joint of the stance leg. (d) PD torque (solid line) and Compensation torque (dashed line) at the hip joint of the stance leg.(e) Total (solid line) and gravitational torque (dashed line) applied at the hip joint of the swinging leg. (f) PD torque (solid line) and Compensation torque (dashed line) at the hip joint of the swinging leg. The units of the horizontal axis are seconds.

6.1.3 Varying the proportional gains

In this section the proportional gains will be incremented to observe how they affect the compensation actions. The increments will be done in the ankle joint of the stance leg, the hip joint moving the body, and the hip joint moving the swinging leg. The increments will be done only on one of the previously mentioned joints at the time, while the others keep their original gain values. Those values are listed in Table 6.1 that is a slightly modified version of table 5.2. The values listed in Table 6.1 are those used in the experiments of Section 5.3.2 and therefore, the Figure 6.2. Gravitational compensation torques as well as the total control actions are not analyzed in this section because the first ones depends on the configuration of the robot, and that configuration is not affected by the gains. In the case of the total control actions (i.e the total applied torques), they are not analyzed because the contribution of the actions analyzed in this section are not significant to the total torques.

Varying the gain of the hip joint of the stance leg

Figure 6.3 shows the plots obtained by varying the proportional gain of the hip joint of the stance leg from 10N·m/rad to 40·m/rad. This joint moves the HAT group, therefore it is expected changes on this group. Because it is the heavier group, a big increment in the amplitude of the compensation torque it is observed in Figure 6.3(a). Also a change on the frequency of the torque produced by the PD controller is observed in Figure 6.3(b). This happens because the increment of the gain means a stiffer system and therefore a higher natural frequency. The swinging leg does not show any change in their behavior as can be seen on Figure 6.3(c). Also, it should be noticed that PD torques of the not modified joints keep the original natural frequency. This confirms the linearity of the model, and the successfully decoupling of the dynamics.

Table 6.1: Gains of the controllers used in the oscillation experiments.

	Stance leg		Swinging leg	
	Proportional gain	Derivative gain	Proportional gain	Derivative gain
hip	10	0	10	0
knee	10	3	40	20
ankle	10	0	40	20

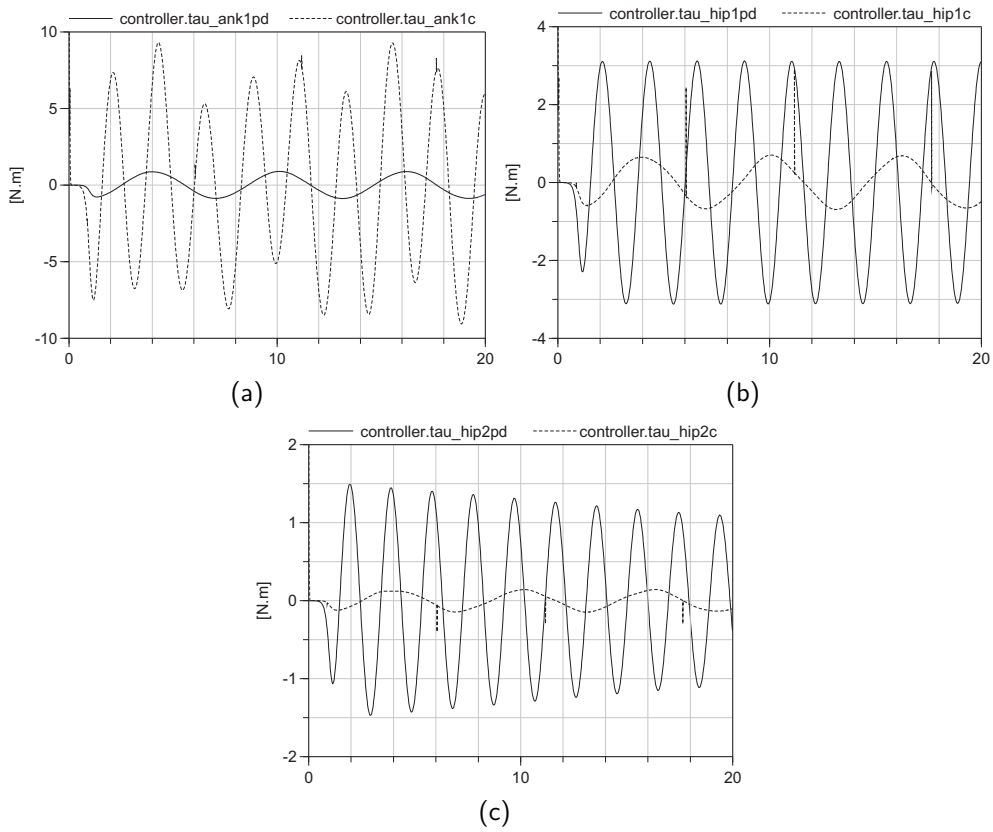

Figure 6.3: Experiments using 40N·m/rad gain at the hip joint of the stance leg. (a) PD torque (solid line) and Compensation torque (dashed line) at the ankle joint of the stance leg. (b) PD torque (solid line) and Compensation torque (dashed line) at the hip joint of the stance leg. (c) PD torque (solid line) and Compensation torque (dashed line) at the hip joint of the swinging leg. The horizontal axis units are seconds.

Varying the gain of the hip joint of the swinging leg

Now, the proportional gain of the swinging leg is set back to the value listed in Table 6.1 and the hip joint of the swinging leg is set to 40·m/rad. Figure 6.4 shows the results of this experiment. Because the swinging leg is the lightest group, a great increment on its natural frequency happens as it can be seen in Figure 6.4(c). This movement propagates to the other joints affecting their compensations torques as can be seen on Figure 6.4(a) and Figure 6.4(b), those perturbations are later attenuated because the swinging leg shows a small damping factor calculated in the previous chapter. Although the controller has zero derivative gain, therefore no damping is present, this attenuation happens because no compensation was applied at the knee and the ankle joint of the

swinging leg. Because of their low mass when compared against the whole robot, they were given higher gains to reject the perturbations produced by swinging action. Although, this approach accomplishes its objective, it has the drawback that injects some damping because of the relative movement between the links. The torques of the PD controllers of the other joints shown in figures 6.4(a) and 6.4(b) show no change and they keep their natural frequency as expected.

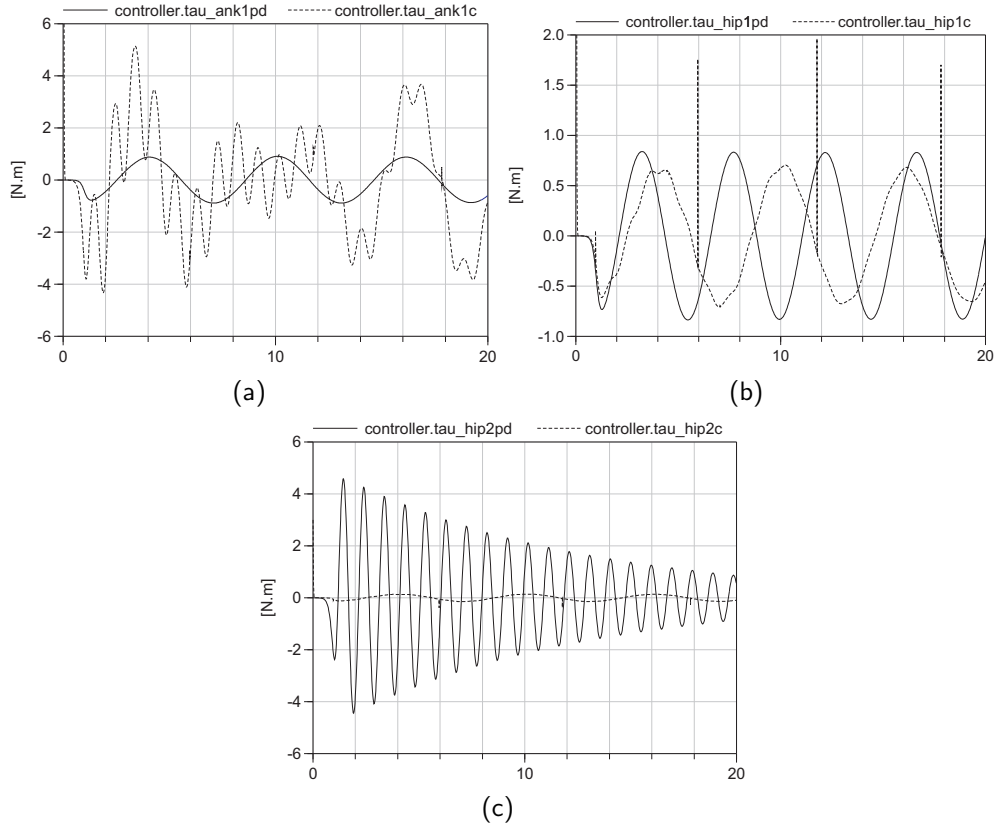

Figure 6.4: Experiments using 40N·m/rad gain at the hip joint of the swinging leg. (a) PD torque (solid line) and Compensation torque (dashed line) at the ankle joint of the stance leg. (b) PD torque (solid line) and Compensation torque (dashed line) at the hip joint of the stance leg. (c) PD torque (solid line) and Compensation torque (dashed line) at the hip joint of the swinging leg. The horizontal axis units are seconds.

Varying the gain of the ankle joint of stance leg

Finally, the gain of the ankle joint is set to 30·m/rad while the other gains are kept to the values shown in Table 6.1. The ankle joint of the stance leg supports all the

robot, therefore any change on the gains of its controller will affect all the system. Figure 6.5 shows the plots of all the joints using the gains described here. Because the dynamics is decoupled, the plots of torques of the PD controllers in figures 6.5(b) and 6.5(c) do not show changes in their natural frequency. By the other hand, the compensation torques of all figures are affected and incremented because the additional compensation action required to reject the perturbations induced by the ankle joint. Because of those perturbations the compensation torques also show glitches in their plots, and nonlinearities are shown at the end of all of them. The nonlinearities are the product of the impossibility of the stance leg to maintain contact against the floor. but, despite this problem the robot is able to recover from those perturbations.

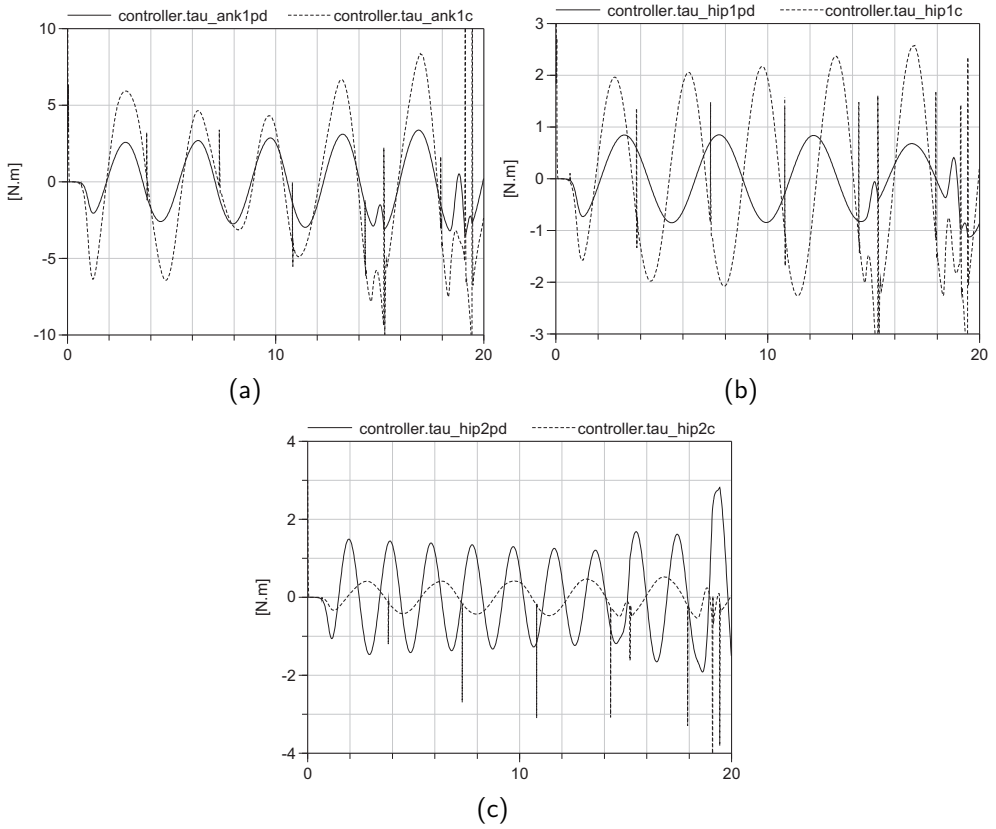

Figure 6.5: Experiments with 40N·m/rad gain at the ankle joint of the stance leg. (a) PD torque (solid line) and Compensation torque (dashed line) at the ankle joint of the stance leg. (b) PD torque (solid line) and Compensation torque (dashed line) at the hip joint of the stance leg. (c) PD torque (solid line) and Compensation torque (dashed line) at the hip joint of the swinging leg. The horizontal axis units are seconds.

6.2 Analysis of the equivalent inverted pendulum

In this section the analysis of a system composed by an inverted pendulum connected to a base that provides information about the center of pressure us performed. The idea is to provide a simple system that can be analyzed to relate the reaction forces of the original system with those of the equivalent inverted pendulum. It is a similar exercise to that already presented in Section 3.1.3 and detailed in Appendix B with the difference that both point masses of the equivalent pendulum are free to move. The objective of this section is to extend the results of the method exposed in Chapter 4, studying additional properties of the equivalent pendulum proposed in that section.

The experiments are performed by applying a step input to the pendulum system, the data about the reaction forces and the applied torque are registered. Using the information of the center of pressure and the center of percussion of the whole system the equivalent pendulum is made and its states are measured. The states of the inverted pendulum are used to calculate its reaction forces and then those forces are compared against those of the original system.

Finally, the term "pendulum system" will be used to name the system composed by the base, the revolute joint and the inverted pendulum; while the term "equivalent pendulum" will be used when the system composed by the two equivalent masses of the real system is being analyzed. Remember that there are two similar systems, one is the system being analyzed, and the idealized system that is calculated from the original one.

6.2.1 The inverted pendulum system

The inverted pendulum system used in this section pretends to emulate the movement of a group of links rotating around the hip joint, in this case can be considered as the HAT group, although the results can be extended without problem. The pendulum can be seen in Figure 6.6. The pendulum is supported by a base with a center of pressure sensor, and it is connected by a revolute joint that can apply a torque input. The torque input has two parts, a gravitational compensation part and a PD control part. Assuming that the base and the floor are always in contact without slipping, the control law can be written as:

$$\tau = -k_p(\theta_d - \theta) - k_d\dot{\theta} - l_2 m_2 g \sin\theta \tag{6.4}$$

τ is the input torque, k_p and k_d are the proportional and derivative gains respectively, θ_d is the desired final position and θ is the position of the revolute joint. The first and second term of equation 6.4 are the PD control action, while the last term is the gravity compensation action, earlier mentioned in this section.

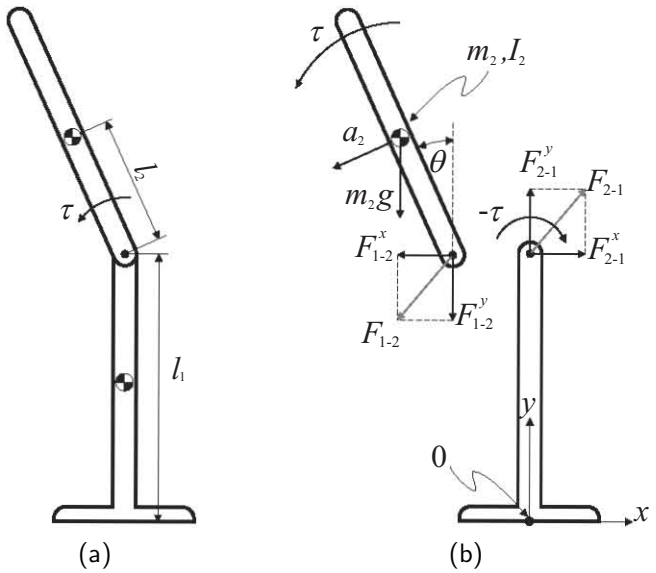

Figure 6.6: Pendulum system used in the analysis. (a) Schematic figure of the pendulum system. (b) Free-body diagram of the pendulum system.

Although the reaction forces will be obtained from the simulations, the reaction moments cannot be computed in the same way because the base of the pendulum is not attached to the floor but only a simple contact interaction, as described in Section 3.2.3 and Appendix C, where the model used for ground-foot interactions is explained. The reaction moments will be calculated with reference to the point 0 shown in Figure 6.6(b), using the free-body diagram of this figure the reaction moment τ_0 is:

$$\tau_0 = -\tau + F^x_{2-1} l_1 \tag{6.5}$$

$F^x_{2-1} l_1$ is the internal reaction at the revolute joint. Following the same approach taken on Chapter 5, where it was demonstrated that other forces different from inertial ones can be dismissed, as for example centrifugal accelerations. Therefore F^x_{2-1} is written as:

$$F^x_{2-1} = -m_2 a_2 l_1 \cos\theta \tag{6.6}$$

a_2 is the module of the acceleration and is found using the angular momentum of the pendulum and the geometric constrictions as follows:

$$\tau = (I_2 + m_2 l_2^2)\ddot{\theta} \tag{6.7}$$

$$l_2\ddot{\theta} = -a_2 \tag{6.8}$$

replacing equations 6.6, 6.7 and 6.8 into equation 6.5, the result is:

$$\tau_0 = \tau\left(\frac{m_2 l_1 l_2}{I_2 + m_2 l_2^2}\cos\theta - 1\right) \tag{6.9}$$

6.2.2 Description of the experiments

In this section a description and an explanation of the relevant measurements of the experiments are exposed. As was said before, the main idea is to compare the reaction forces of both systems in order to find a link between the equations of motion of the original system and the equivalent one. In simple words, the experiments were performed as follows:

1. The system starts at $\theta = 0$ from rest.
2. A step input, approximated with the logistic function[1], is applied to set $\theta = 0.4$.
3. The reaction forces at the base and the states of the inverted pendulum are recorded.

Figure 6.7 shows an schematic of the information gathered in the simulations. The reaction vector force between the base and the floor is calculated, the input torque is used to calculate τ_0 using equation 6.9. The equivalent pendulum is composed by two point masses, one at the center of pressure and another one at the center of percussion. The values of the masses and the location of the center of percussion is calculated with the method exposed 3.1.1 using the center of pressure as reference. The accelerations of the point masses multiplied by their mass values provide the forces to be compared to the reaction forces, while the static moment of the equivalent pendulum respect to the center of pressure[2], marked as τ_{pen} on Figure 6.6(b), is compared against τ_0. Because

[1] The logistic function is preferred over a perfect step, because the last can introduce singularities into the simulation.

[2] i.e., the cross product of the weight of the point mass located at the center of percussion and its position vector with respect to the center of pressure.

Table 6.2: Parameters used in the experiments.

	m (kg)	I (kg·m^2)	l_i (m)	k_p (N·m/rad)	k_c (N·m·s/rad)
Pendulum	16	0.7	0.4	-	-
Base	9	0.1	0.5	-	-
Controller	-	-	-	20	7

of the reference to calculate the inverted pendulum is moving, the analysis cannot be performed in an analytical way as it is done in Appendix B, but breaking the restriction of only one point mass moving generalize the results of this model.

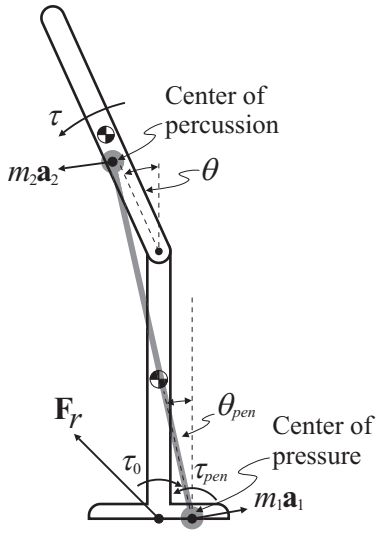

Figure 6.7: Schematic of information gathered on the simulations. The reaction forces of the pendulum system are registered, also the states of the equivalent pendulum are calculated and its reaction forces are compared with the reactions of the pendulum system.

6.2.3 Results of the experiments

The simulations were performed using the parameters shown in Table 6.2. They were selected to be representative with human standards, therefore the proportions of the base and the pendulum are similar to a leg and a HAT group of a human. The results of the experiments are shown in Figure 6.8, the plots show components of the reaction forces, and the torque τ_0 applied at the base of the pendulum system. It should be noticed that only the PD controller term of equation 6.4 is considered to calculate τ_0. The

equivalent pendulum calculates its static torque with respect to the center of pressure, therefore in the absence of any PD action the estimated torque is zero. In other words, when measuring the static moment of the equivalent pendulum the result is a direct measurement of the control action.

Figures 6.8(a) and 6.8(b) show that the inertial forces of the equivalent inverted pendulum are similar to the reaction forces at the base of the pendulum system. About Figure 6.8(c) the similarity is established between τ_0 and τ_{pen}. With the help of Figure 6.7 both conditions are written as:

$$\mathbf{F}_r = m_1\mathbf{a}_1 + m_2\mathbf{a}_2 \tag{6.10}$$

$$\tau_0 = \tau_{pen} = m_2 g l_{pen} \cos\theta_{pen} \tag{6.11}$$

The results, as they can be appreciated in Figure 6.8 show a closed relation to the equation just written. The horizontal component of $\mathbf{F}_r$ and the reaction torque τ_0 are closely followed by their counterparts calculated out of the equivalent pendulum, as appreciated on Figure 6.8(a) and Figure 6.8(c). By the other hand the vertical component of $\mathbf{F}_r$ plotted in Figure 6.8(d) shows more difference with the one obtained from the inverted pendulum system. But the overall observation is that the equivalent inverted pendulum provide excellent approximations of the reaction forces of the original system. The discrepancies between both system happen because there are some internal effects of the equivalent pendulum that are not being considered. Those effects are the variation of the equivalent masses, and the variation of the length of the equivalent pendulum. Remember that those parameters are configuration dependent. Although they were calculated in every step of the simulation, their derivatives were not considered, but the results shown in this section demonstrate that their contribution to the total dynamics of the system is not significant.

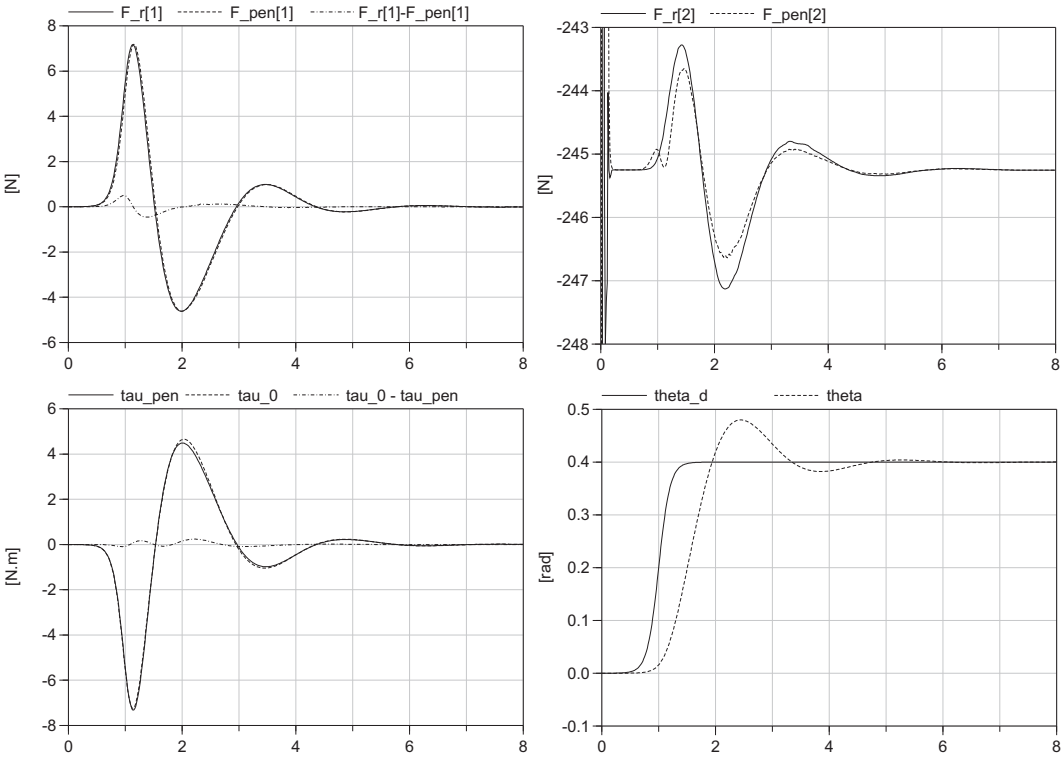

Figure 6.8: Plots of the experiments. (a) Horizontal component of the reaction force, the continuous line is the reaction force measured by the base. The dashed line is calculated using the equivalent pendulum and the dot-dashed line is the difference.(b) Vertical component of the reaction force. The continuous line is the reaction force measured by the base, the dashed line is calculated using the equivalent pendulum. (c) Comparison of τ_0 shown with continuous line, and τ_{pen} plotted with dashed line. (d) Step input applied to θ_d (continuous line), and output of the system θ (dashed line).

7 Conclusions and future work

In Chapter 2 different mathematical models used in biped robots were exposed. They range from very basic but intuitive models to very detailed mathematical models based on rigid body dynamics. Although, the analysis of robots at first sight seems like a solved problem because the required tools are mature, the involved complexity is often the major obstacle when deeper analyses are required. The general solution adopted to this problem is to simplify the system by dismissing effects considered less important according to necessities. The objective of this thesis is to provide a method to apply simplifications to a system and keep most of the dynamics of the original system in the equivalent simplified one. The result of the analysis is the proposition of the center of percussion to construct those simplified systems.

In this chapter the conclusions of the methods developed are exposed. Although some conclusion were already provided at the end of some chapters, here they are put together and summarized from the point of view of the objectives of this work. Also suggestions about future developments are exposed in this chapter. Because most of the efforts in this thesis have been focused on demonstrating the accuracy of the models, refinements and additional applications are the majority of the suggestions proposed as improvements.

7.1 Conclusions

In this thesis the concept of dynamic equivalence has been used to propose a methodology to generate alternative models using idealizations of point masses with massless links. The simplification is done to maintain all the rigid body properties with the same values,

that is the total mass, the first moment of mass[1] and the second moment of mass[2] are the same between both systems. The method is very flexible, because there are infinite possibilities to define equivalent systems according to the point of reference used to construct the equivalent system. In this thesis two references have been used, the first one is the center of pressure and the second one is the hip of the robot. In the following lines, additional details will be exposed.

7.1.1 Equivalent system of a kinematic chain

In Section 3.1.3 the reduction of a kinematic chain to two point masses was performed. Because the reference to construct the system was selected as a fixed point of the kinematic chain, the equivalent system contained only one moving point mass. The reaction forces of the kinematic chain and the equivalent system were calculated analytically, the result was that both systems share exactly the same result. This first approach demonstrated that the center of percussion can be extended to a kinematic chain, and that exact results can be obtained if the right reference is selected. It should be noticed that the geometry of the system produced equivalent point masses with values independent of the geometry. Although, this is not the general case, the existence of a reference point with such characteristics encourages further developments to characterize those points.

7.1.2 Equivalent inverted pendulum

Following the method exposed in Chapter 3 the reduction of a system to two point masses was performed for a bipedal system with a flywheel as a body. This system was selected because it reduces the state variables required to control the body of the robot. With that simplification and using point feet the system was fully controllable. The point feet allowed to fix the center of pressure without additional efforts. The equivalent inverted pendulum was composed by two point masses, one at the center of percussion, and other mass at the center of pressure of the robot. The pendulum was later used to design the control algorithm. The control algorithm was done using a PD strategy, compensating part of the dynamics and gravitational effects the gait was successfully synthesized.

In chapter 6 the results were extended to a system where the center of pressure was not fixed at one point. Instead a continuous ground interaction was provided by means of a base with a center of pressure sensor. Here the reaction forces of both system were compared with excellent results. The conclusion was that the equivalent inverted

[1] i.e., the center of mass.
[2] Also known as the moment of inertia.

pendulum was able to reproduce the dynamic behavior of the original system. Although the result was not perfect, the small error is attributed to non modeled dynamics of the equivalent system. It should be noticed that the derivatives of the parameters of the equivalent system were not included[1]. As expected, the dismissed derivatives did not affect the results in a significant way. The last happens because the variation of the equivalent mass is small in the considered movements of the system.

Proposing an inverted pendulum composed by point masses allows to recycle the knowledge gathered by other researches using inverted pendulums to propose their solutions. The rimless wheel [7], capture points [86] or even Raibert [87] algorithms can be benefited with this model. Because the proposed model is a pendulum it can be inserted directly into the methodology proposed in those publications.

7.1.3 Four point masses model

The inverted pendulum model, although widely used because of its flexibility does not reflect the topology of the system it represents. In some situations a simplification that reflects the parts of the robot are required. Some examples are found in [9] and [26], where links or group of links have been replaced by point masses at their center of mass. A refinement of these simplifications is provided in this thesis with the proposed four point masses model. This model divide the robot in three groups: Two legs and the head-arms-torso group (referred as HAT group). Because all the groups intersect at the hip joint, this point was selected as reference to obtain the centers of percussion of the groups. The final model is composed by four point masses, three masses coming from the centers of percussion and other mass at the hip composed by the combination of the masses of the equivalent model of each group.

The model was validated by using the information of the local centers of percussion to compensate the reaction torques. With this approach the dynamics of the robot was decoupled and each joint was able to move independently. The undamped step response of the controllers of the joints was performed to compare their real natural frequency against the experimental one. The theoretical prediction of the natural frequency of the controllers matched the values found experimentally in the simulations, confirming the four point masses model.

Additionally, different gains of the controllers were tested in order to asses the torque components of the control action of each controller. The result was that most of the power is used to support the own weight of the robot because the major control action was

[1]Those parameters are the values of both point masses and the length of the inverted pendulum.

used for gravity compensation as appreciated in Figure 6.2. Minor energy was required to generate the compensation and the PD torques of each controller. With this in mind, the mechanical design of the links and the joints, as well as the selection of the actuators can be performed using the decoupling presented in Chapter 5 because each term of the torque action can be studied independently.

7.1.4 Summary

The major contribution of this thesis is a methodology to generate dynamically equivalent models. Those models are composed by two point masses that share all the dynamic properties of the original system. The methodology produced two models to simplify biped robots: The equivalent inverted pendulum, and the four point masses model. Both models are not substitutes of the previously used approaches by other researchers, but improvements that can be used in their algorithms without major modifications. To summarize the accomplished objectives the following list is provided:

- The center of percussion, as proposed in this thesis, can successfully be used to construct dynamically equivalent systems.
- Therefore, a technique to provide justified simplifications of models of biped robots has been developed.
- Because the center of percussion is reference dependent there are an infinite number of equivalent systems.
- The selection of the reference to construct the equivalent system, and therefore determine the center, or centers of percussion, is what determines the usefulness of an equivalent model.
- The angular momentum of a system can be included without adding complexity to the equations of motion.
- Linear control strategies can be designed to generate gait, although their stability margins need to be determined.
- The experiments performed in this thesis did not require to include the derivatives of the parameters of the equivalent system.
- The subsystems can be grouped according to the requirements of the application to produce equivalent systems with closer topologies, just as it was done with the four point mass modeling, where local centers of percussion were used.

- Total decoupling of a biped was performed successfully, although very useful to study a system it can stress fragile articulations like the ankle.
- Because only the inertial forces were used to perform the decoupling, the conclusion is that other acceleration like Coriolis or centrifugal acceleration have minor importance to the dynamics of the whole system.
- Thanks to the decoupling of the dynamics, each term composing the total solicitation of a joint or a link can be studied. The last can be used to perform a guided mechanical design, and a wise gait design to reduce the demands of a particular system, without sacrificing performance.
- Supporting the own weight of a biped uses most of the energy of the system, control actions are only a fraction of the required power.

7.2 Observations and remarks

In this thesis particular cases of bipeds have been exposed and analyzed, in this way the application of the technique developed in this work was explained by example. Application to other cases can be done by following the steps provided, according to which model is being implemented. Modifications of the technique can be also applied to propose new alternatives as long as the concept of dynamic equivalence is used.

It should be noticed that the experiments performed in this thesis have been performed using rigid body models. Therefore, in order to use this technique on real robots it is very important that the mechanical construction will be stiff in order to comply the rigid body assumption done when developing this work. In small robots the last will be hard to achieve, but in medium to big walkers this should not be a problem.

Backlash has not been included in the analysis. This will produce impulsive forces that will deviate the expected results, and therefore should be avoided when using the models proposed in this work. Also, it should be noticed that a good control system, or special hardware is good solution. Hence, the limitation introduced by this phenomenon are not determinant when using the techniques proposed in this work.

7.3 Future work

Biped locomotion is a research field with lots of unanswered questions, how humans synthesize gait is an unsolved matter. Although impressive achievements have been done in the field, new tools to design or to analyze these systems are always welcomed. The concept of dynamic equivalence in this thesis has been restricted for the 2D case only. Although valid for most of the cases, because walking can be always decoupled as two tasks[1], 3D improvements can be necessary when studying complex situations. Naming some of them could be recovering from large perturbations, or a dancing robot performing some pirouettes. But it should be noticed that even in complex situations the legs can be still be modeled using 2D models because they are slender elements if they are not completely folded.

Implementation of gait using the four point masses model is a task to be completed. The possibility to have a very simple system to work with, opens the possibilities to obtain full analytical solutions of the internal dynamics. In this way optimization of every stage of the gait cycle can be performed. Also, the model can be combined with the equivalent inverted pendulum proposed in this thesis. The study of foot ground interactions, and the weight transfer from one foot to the other can be greatly simplified by using the combination of those models.

Implementation of this work into other compatible robotic researches is also very encouraging. For example, the widely adaption of the inverted pendulum and its variations opens the possibility to slightly modify the original algorithms and introduce a model that shares the same dynamic properties of the original system. For example calculate capture points out of the equivalent inverted pendulum can be an option to discover the possibilities of this model. Also modification of the linear inverted pendulum is compatible with the equivalent inverted pendulum developed here. In general, any system based on the center of pressure and using an inverted pendulum to estimate its dynamics, it is adaptable to this work.

Several efforts have been made to characterize human locomotion with dimensionless parameters. One of the best known example is the Froude number that separates running from walking in any locomotion system. Similar quantities can be designed by using the fact that an equivalent model can be done to any locomotion system following the guidelines presented in this thesis. Therefore, the possibility to characterize any walking

[1] One focused on walking on the sagittal plane, and the other on keeping lateral equilibrium on the frontal plane

machine with few parameters is open, therefore the similarity can be established by comparing the dimensionless numbers obtained with the simplified equivalent models. Finally, the study of human locomotion with the models proposed in this work is an interesting subject to be developed. The complexity found in the human body produces dynamics with a great degree of complexity. This quality makes this problem very hard to manage with traditional techniques. The guided simplifications produced here, can help to unveil information that in other ways will be hidden by the sophistication of its own properties.

Bibliography

[1] Muhammad Abdallah and Ambarish Goswami. A biomechanically motivated two-phase strategy for biped upright balance control. In *Proceedings of the IEEE International Conference on Robots and Automation*, pages 1996 – 2001, 2005.

[2] Mauricio Alba, Juan Carlos García Prada, and Cristina Castejon. Object oriented modeling for walking machines. In *International Symposium on Multibody Systems and Mechatronics*, pages 371–384. IFToMM, 2011.

[3] Mauricio Alba, Juan Carlos Garcia Prada, Jesus Meneses, and Higinio Rubio. Center of percussion and gait design of biped robots. *Mechanism and Machine Theory*, 45(11):1681–1693, November 2010.

[4] Shinya Aoi, Naomichi Ogihara, Tetsuro Funato, Yasuhiro Sugimoto, and Kazuo Tsuchiya. Evaluating functional roles of phase resetting in generation of adaptive human bipedal walking with a physiologically based model of the spinal pattern generator. *Biological cybernetics*, 102(5):373–387, May 2010.

[5] Haruhiko Asada and Jean-Jacques Slotine. *Robot Analysis and Control*. John Willey and Sons, 1st edition, 1986.

[6] Fumihiko Asano, Takeshi Hayashi, Zhi-Wei Luo, Shinya Hirano, and Atsuo Kato. Parametric excitation approaches to efficient dynamic bipedal walking. In *Intelligent Robots and Systems, 2007. IROS 2007. IEEE/RSJ International Conference on*, pages 2210 –2216, 29 2007-nov. 2 2007.

[7] Fumihiko Asano and Zhi-Wei Luo. Asymptotically stable biped gait generation based on stability principle of rimless wheel. *Robotica*, 27(06):949, March 2009.

[8] Fumihiko Asano, Zhi-Wei. Luo, and Sang Hyon. Parametric excitation mechanisms for dynamic bipedal walking. In *Robotics and Automation, 2005. ICRA 2005. Proceedings of the 2005 IEEE International Conference on*, pages 609–615, 2005.

[9] Fumihiko Asano and Masaki Yamakita. Virtual gravity and coupling control for robotic gait synthesis. *IEEE Transactions on Systems, Man, and Cybernetics*, 31(6):737–745, 2001.

[10] Modelica Association. Language specification v2.2, February 2002.

[11] Wolfgang Borutzky. Bond graph modeling from an object oriented modeling point of view. *Simulation and Practice Theory*, 7(5-6):439–461, 1999.

[12] Wolfgang Borutzky. Bond graphs and object-oriented modelling- a comparison. *Proceedings of the Institution of Mechanical Engineers, Part I: Journal of Systems and Control Engineering*, 216(1):21–33, 2002.

[13] Wolfgang Borutzky. *Bond Graph Metodoloy: Development and Analysis of Multidisciplinary Dynamic System Models*. Springer, 2010.

[14] Jan Broenink. Bond-graph modeling in modelica. In *Simulation in Industry, 9th European Simulation Symposium*, pages 137–141. The European Council for Modelling and Simulation, 1997.

[15] Jan Broenink. Object-oriented modeling with bond graphs and modelica. In *Proceedings of the Western MultiConference*, pages 163–168. The Society for Modeling and Simulation International, 1999.

[16] Michael Clifford and Bishop Steven. Inverted oscillations of a driven pendulum. In *Proceedings: Mathematical, Physical and Engineering Science*, pages 2811–2817. The Royal Society, 1998.

[17] Michael Coleman. *A stability study of a three-dimensional passive-dynamic model of human gait*. PhD thesis, Cornell University, 1998.

[18] Michael Coleman. Dynamics and stability of a rimless spoked wheel: a simple 2d system with impacts. *Dynamical Systems*, 25(2):215–238, 2010.

[19] Michael Coleman, Chatterjee Anindya, and Andy Ruina. Motions of a rimless spoked wheel: a simple 3d system with impacts. *Dynamics and Stability of Systems*, 12(3):139, 1997.

[20] SH Collins and Andy Ruina. A bipedal walking robot with efficient and human-like gait. In *Robotics and Automation, 2005. ICRA 2005. Proceedings of the 2005 IEEE International Conference on*, pages 1983–1988, 2005.

[21] Luca Consolini and Mario Tosques. On the exact tracking of the spherical inverted pendulum via an homotopy method. *Systems & Control Letters*, 58(1):1–6, January 2009.

[22] Jeff Crandall, Laurent Portier, Philippe Petit, Gregory Hall, Cameron Bass, Gregory Klopp, Shepard Hurwitz, Walter Pilkey, Xavier Trosseille, Calude Tarriere, and JeanPierre Lassau. Biomechanical response and physical propeties of the leg, foot, and ankle. In *Stapp Car Crash Conference Proceedings*, pages 173–192, 1996.

[23] Peter Daemen. Zmp based control in 3d passive dynamic walking, February 2008.

[24] Tomas de Boer, Martin Wisse, and Frans van der Helm. Mechanical analysis of the preferred strategy selection in human stumble recovery. *Journal of biomechanical engineering*, 132(7):071012, July 2010.

[25] Alessandro De Luca, Alin Albu-Schäffer, Sami Haddalin, and Gerd Hirzinger. Collision detection and safe reaction with the dlr-iii lightweight manipulator arm. In *Proceedings of the International Conference on Intelligent Robots and Systems*, pages 1623–1630. IEEE/RSJ, 2006.

[26] Shuai Feng and Zengqi Sun. Biped Robot Walking Using Three-Mass Linear. In *International Conference on Intelligent Robotics and Applications: Part I*, pages 371–380. Springer Berlin / Heidelberg, 2008.

[27] Gianni Ferreti, Stefano Filippi, Claudio Maffezzoni, Gianantonio Magnani, and Paolo Rocco. Modular dynamic virtual-reality modeling of robotics systems. *IEEE Robotics and Automation Magazine*, 6(4):13–23, December 1999.

[28] Gianni Ferreti, Gianantonio Magnani, and Paolo Rocco. Modular dynamic modeling and simulation of grasping. In *Proceedings of the International Conference on Advanced Intelligent Mechatronics*, pages 428–433, 1999.

[29] Gianni Ferreti, Gianantonio Magnani, Paolo Rocco, and Luca Vigano. Modelling and simulation of a gripper with Dymola. *Mathematical and Computer Modelling of Dynamical Systems*, 12(1):89–102, February 2006.

[30] Louis Flynn, Rouhollah Jafari, and Ranjan Mukherjee. Active Synthetic-Wheel Biped With Torso. *Robotics, IEEE Transactions on*, 26(99):1–11, 2010.

[31] Josep Font-Llagunes and Jozef Kovecses. Dynamics and energetics of a class of bipedal walking systems. *Mechanism and Machine Theory*, 44(11):1999–2019, 2009.

[32] Josep Font-Llagunes and Jozsef Kovecses. Efficient dynamic walking: Design strategies to reduce energetic losses of a compass walker at heel strike. *Mechanics based design of structures and machines*, 37(3):259–282, 2009.

[33] Alexander M. Formal'skii. Ballistic Walking Design via Impulsive Control. *Journal of Aerospace Engineering*, 23(2):129, 2010.

[34] Nico Galoppo, Miguel Otaduy, Paul Mecklenburg, Markus Gross, and Ming Lin. Fast simulation of deformable models in contact using dynamic deformation textures. In M. Cani and J. O'Brien, editors, *Proceedings of ACM SIGGRAPH Symposium on Computer Animation*, pages 73–82, 2006.

[35] Mariano Garcia, Anindya Chatterjee, Andy Ruina, and Michael Coleman. The simplest walking model: stability, complexity, and scaling. *Journal of biomechanical engineering*, 120(2):281–8, April 1998.

[36] Tao Geng and John Q. Gan. Planar Biped Walking With an Equilibrium Point Controller and State Machines. *IEEE Transactions on Mechatronics*, 15(2):253–260, 2010.

[37] A.R. Ghiasi, G. Alizadeh, and M. Mirzaei. Simultaneous design of optimal gait pattern and controller for a bipedal robot. *Multibody System Dynamics*, pages 1–29, 2010.

[38] Pablo Gonzales de Santos, Elena Garcia, and Estremera Joaquin. *Quadrupedal Locomotion: An introduction to the Control of four legged robots*. Springer, 1 edition, 2006.

[39] Ambarish Goswami. Foot rotation indicator (fri) point: A new gait planning tool to evaluate postural stability of biped robots. In *IEEE International Conference on Robotics and Automation*, pages 47–52, 1999.

[40] Eran Guendelman, Robert Bridson, and Ronald Fedkiw. Nonconvex rigid bodies with stacking. *ACM Transactions on Graphics.*, 22(3):871–878, July 2003.

[41] Yuji Harata, Fumihiko. Asano, Zhi-Wei. Luo, Kouichi Taji, and Yoji Uno. Biped gait generation based on parametric excitation by knee-joint actuation. *Robotica*, 27(07):1063–1073, 2009.

[42] Shoichi Hasegawa and M. Sato. Real-time rigid body simulation for haptics interactions based on contact volume of polygonal objects. *Computer Graphics Forum*, 23(3):529–538, 2004.

[43] Andreas Heckmann, Martin Otter, Stefan Dietz, and Jose Diaz Lopez. The dlr flexiblebodies library to model large motions of beams and of flexible bodies exported from finite element programs. In *Proceedings of the International Modelica Conference*, pages 85–95, March 2006.

[44] Jochen Heinzmann and Alex Zelinsky. A safe-control paradigm for human-robot interaction. *Journal of Intelligent and Robotic systems*, 25(4):295, 310 1999.

[45] Gerhard Hippmann. An algorithm for compliant contact between complexly shaped bodies. *Multibody system dynamics*, 12(4):345–362, 2004.

[46] Kazuo Hirai, Masato Hirose, Yuji Haikawa, and Toru Takenaka. The development of honda humanoid robot. In *Proceedings of the IEEE/RAS International Conference on Robotics and Automation (ICRA)*, pages 1321–1326, 1998.

[47] Daan Hobbelen and Martijn Wisse. Limit cycle walking. In Matthias Hackel, editor, *Humanoid Robots: Human-like Machines*, pages 278–294. InTech, 2007.

[48] Dann Hobbelen, Thomas Boer, and Martijn Wisse. System overview of bipedal robots flame and tulip: tailor-made for limit cycle walking. In *Int. Conf. Intelligent Robots and Systems*, pages 2486–2491. IEEE/RSJ, September 2008.

[49] At L. Hof. The 'extrapolated center of mass' concept suggests a simple control of balance in walking. *Human movement science*, 27(1):112–25, February 2008.

[50] Toyoyuki Honjo, Z.W. Luo, and Akinori Nagano. Parametric excitation of a biped robot as an inverted pendulum. In *IEEE/RSJ International Conference on Intelligent Robots and Systems, 2008. IROS 2008*, pages 3408–3413, 2008.

[51] Fumiya Iida and Russ Tedrake. Minimalistic control of a compass gait robot in rough terrain. In *Proceedings of the IEEE/RAS International Conference on Robotics and Automation (ICRA)*, 2009.

[52] Doug James and Dinesh Pai. A unified treatment of elastostatic contact simulation for real time haptics. *Haptics-e*, 2(1):1–13, 2001.

[53] Shuuji Kajita, Fumio Kanehiro, Kenji Kaneko, Kazuhito Yokoi, and Hiruka Hirukawa. The 3D linear inverted pendulum mode: a simple modeling for a biped walking pattern generation. In *Proceedings of the IEEE/RSJ International Conference on Intelligent Robots and Systems*, pages 239–246. IEEE, 2001.

[54] Shuuji Kajita and Kazuo Tan. Study of Dynamic Biped Locomotion on Rugged Terrain - Derivation and application of the linear inverted pendulum model. In *Proceedings of the IEEE International conference on Robotics and Automation*, volume 2, pages 1405–1411, Sacramento, 1991.

[55] Shuuji Kajita and Kazuo Tani. Study of dynamic biped locomotion on rugged terrain-theory and basic experiment. In *Proceedings of the International Conference on Advanced Robotics*, pages 741–746. IEEE, 2002.

[56] Kenji Kaneko, Fumio Kanehiro, Shuuji Kajita, Hirohisa Hirukawa, TToshikazu Kawasaki, Masaru Hirata, Kazuhiko Akachi, and Takakatsu Isozumi. Humanoid robot hrp-2. In *Proceedings of the IEEE International Conference on Robotics and Automation*, volume 2, pages 1083 – 1090 Vol.2, 2004.

[57] Pei-Chun Kao, Cara L Lewis, and Daniel P Ferris. Joint kinetic response during unexpectedly reduced plantar flexor torque provided by a robotic ankle exoskeleton during walking. *Journal of biomechanics*, 43(7):1401–7, May 2010.

[58] Karthik Kappaganthu and C. Nataraj. a Biped With a Moving Torso. *International Journal of Humanoid Robotics*, 06(04):657, 2009.

[59] Taku Komura, Akinori Nagano, Howard Leung, and Yoshihisa Shinagawa. Simulating pathological gait using the enhanced linear inverted pendulum model. *IEEE Transactions on biomedical engineering*, 52(9):1502–1513, 2005.

[60] Dimitrios Kotiadis, Hermie Hermens, and Peter Veltink. Inertial Gait Phase Detection for control of a drop foot stimulator Inertial sensing for gait phase detection. *Medical engineering & physics*, 32(4):287–97, May 2010.

[61] Paul Kry and Pai Denish. Continuous contact simulation for smooth surfaces. *ACM Transactions on Graphics*, 22(1):106–129, January 2003.

[62] Prasanth Kumar, Jungwon Yoon, and Gabsoon Kim. The simplest passive dynamic walking model with toed feet: a parametric study. *Robotica*, 2008.

[63] Arthur D. Kuo, J. Maxwell Donelan, and Andy Ruina. Energetic consequences of walking like an inverted pendulum: step-to-step transitions. *Exercise and sport sciences reviews*, 33(2):88–97, April 2005.

[64] E. K. Lavrovskii and Alexander M. Formal'skii. Optimal control of the pumping and damping of a swing. *Journal of Applied Mathematics and Mechanics*, 57(2):311–320, 1993.

[65] Sung-Hee Lee and Ambarish Goswami. Reaction Mass Pendulum (RMP): An explicit model for centroidal angular momentum of humanoid robots. In *Proceedings of the IEEE International Conference on Robotics and Automation*, pages 4667–4672. Ieee, 2007.

[66] Oumnia Licer, Noureddine El Alami, and Mostafa Mrabti. Lyapunov Stability of Hybrid System Limit Cycle Application to the Compass Gait Biped. *Journal of Intelligent and Robotic Systems*, 53(2):853–856, 2008.

[67] Li Liu, Andrew Wright, and Gray Anderson. Trajectory planning and control for a huma-like robot leg with coupled neural oscillators. In Martin Ruck, editor, *Proceedings of the 7th Mechatronics Forum: International Conference and Mechatronics Education Workshop*. Elsevier, 2000.

[68] Mohsen Mahvash and Vincent Hayward. Haptic simulation of a tool in contact with a nonlinear deformable body. In N. Ayache and H. Delingette, editors, *Proceedings of the International Symposium on Surgery Simulation and Soft Tissue Modelling*, pages 311–320. Springer Verlag, 2003.

[69] Tad McGeer. Passive Dynamic Walking. *The International Journal of Robotics Research*, 9(2):62–82, April 1990.

[70] Tad McGeer. Passive walking with knees. In *Proceedings of the IEEE International Conference on Robotics and Automation*, pages 1640–1645. IEEE Comput. Soc. Press, 1990.

[71] Ali Meghdari, Saeed Sohrabpour, Davood Naderi, Sayed Tamaddoni, Farid Jafari, and H. Salarieh. A Novel Method of Gait Synthesis for Bipedal Fast Locomotion. *Journal of Intelligent and Robotic Systems*, 53(2):101–118, April 2008.

[72] Jesus Meneses, Cristina Castejon, Eduardo Corral, Higino Rubio, and Juan Carlos Garcia-Prada. Kinematics and dynamics of the quasi-passive biped pasibot. *Strojniski vestnik - Journal of Mechanical Engineering*, Accepted for publication.

[73] Matthew Millard, Derek Wight, John McPhee, Eric Kubica, and David Wang. Human foot placement and balance in the sagittal plane. *Journal of biomechanical engineering*, 131(12):121001, December 2009.

[74] Brian Mirtich. *Impulse-based dynamic simulation of rigid body systems*. PhD thesis, University of California, Berkeley, December 1996.

[75] Charles a Moffatt, Edward Harris, and Edward Haslam. An experimental and analytic study of the dynamic properties of the human leg. *Journal of biomechanics*, 2(4):373–387, October 1969.

[76] Naoki Motoi, Tomoyuki Suzuki, and Kouhei Ohnishi. A Bipedal Locomotion Planning Based on Virtual Linear Inverted Pendulum Mode. *IEEE Transactions on Industrial Electronics*, 56(1):54–61, 2009.

[77] Saeed Niku. *Introduction to Robotics*. John Wiley and Sons, 2nd edition, 2010.

[78] Katsuhiko Ogata. *Modern Control Engineering*. Prentice Hall PTR, Upper Saddle River, NJ, USA, 4th edition, 2001.

[79] Martin Otter, Hilding Elmqvist, and Jose Diaz Lopez. Collision handling for the modelica multibody library. In *Proceedings of the International Modelica Conference*, pages 45–53, March 2005.

[80] Martin Otter, Hilding Elmqvist, and Sven Mattson. The new modelica multibody library. In *Proceedings of the International Modelica Conference*, pages 311–330, November 2003.

[81] Roberto Ponticelli and Pablo Gonzalez de Santos. Obtaining terrain maps and obstacle contours for terrain recognition tasks. *Mechatronics*, 28(2):236–250, 2010.

[82] Marko Popovic, Ambarish Goswami, and Hugg Herr. Ground Reference Points in Legged Locomotion: Definitions, Biological Trajectories and Control Implications. *The International Journal of Robotics Research*, 24(12):1013–1032, December 2005.

[83] Marko Popovic, Andreas Hofmann, and Hugh Herr. Angular momentum regulation during human walking: biomechanics and control. In *Proceedings of the IEEE International Conference on Robotics and Automation*, pages 2405–2411, 2004.

[84] Jerry Pratt. *Exploiting inherent robustness and natural dynamics in the control of bipedal walking robots*. PhD thesis, Massachusetts Institute of Technology, 2000.

[85] Jerry Pratt, John Carff, Sergey Drakunov, and Ambarish Goswami. Capture point: A step toward humanoid push recovery. In *Humanoid Robots, 2006 6th IEEE-RAS International Conference on*, pages 200–207, 2006.

[86] Jerry Pratt and Russ Tedrake. Velocity-based stability margins for fast bipedal walking. *Lecture notes in control and information sciences*, 340:299–324, 2006.

[87] Marc H. Raibert. *Legged robots that balance*. Massachusetts Institute of Technology, Cambridge, MA, USA, 1986.

[88] John Rebula, Fabian Canas, and Jerry Pratt. Learning capture points for humanoid push recovery. *Humanoid Robots, 2007*, pages 65–72, November 2009.

[89] Lei Ren, David Howard, Luquan Ren, Chris Nester, and Limei Tian. A generic analytical foot rollover model for predicting translational ankle kinematics in gait simulation studies. *Journal of biomechanics*, 43(2):194–202, January 2010.

[90] Philippe Sardain and Guy Bessonnet. Forces acting on a biped robot. center of pressure-zero moment point. *IEEE Transactions on Systems, Man, and Cybernetics, Part A: Systems and Humans*, 34(5):630–637, 2004.

[91] Hirotake Sasaki and Masaki Yamakita. Efficient walking control of robot with torso based on passive dynamic walking. In *Proceedings of International Conference on Mechatronics*, pages 1–5, 2007.

[92] Rud Selles, Sabine Korteland, A.J. Van Soest, Johannes Bussman, and Henk Stam. Lower-leg inertial properties in transtivial amputees and control subject and their influence on the swing phase during gait. *Archives of Physical Medicine and Rehabilitation*, 84(4):569–577, 2003.

[93] Hayssam Serhan, Chaiban Nasr, Patrick Henaff, and Fathi Ouezdou. A new control strategy for ROBIAN biped robot inspired from human walking. In *IEEE/RSJ International Conference on Intelligent Robots and Systems, 2008. IROS 2008*, pages 2479–2485, 2008.

[94] David Sudor and Steben Bishop. Inverted dynamics of a tilted parametric pendulum. *European Journal of Mechanics*, 18(3):517–526, 1999.

[95] Tomomichi Sugihara and Yoshihiko Nakamura. Variable Impedant Inverted Pendulum Model Control for a Seamless Contact Phase Transition on Humanoid Robot. In *IEEE International Conference on Humaniod Robots*, 2003.

[96] Satoshi Suzuki, Katsuhisa Furuta, Yaodong Pan, and Shoushirou Hatakeyama. Biped walking robot control with passive walker model by new VSC servo. In *Proceedings of the American Control Conference*, volume 1, pages 107–112, 2001.

[97] Russ Tedrake, Teresa .W. Zhang, Ming-fai Fong, and Sebastian Seung. Actuating a simple 3D passive dynamic walker. In *IEEE International Conference on Robotics and Automation*, volume 5, pages 4656–4661. Citeseer, 2004.

[98] Luigi Tesio, Viviana Rota, Cecilia Chessa, and Laura Perucca. The 3D path of body centre of mass during adult human walking on force treadmill. *Journal of biomechanics*, 43(5):938–44, March 2010.

[99] David Tlalolini, Yannick Aoustin, and Christine Chevallereau. Modeling and optimal trajectory planning of a biped robot using Newton-Euler formulation. In *Proceedings of the International conference of informatics in control, automation and robotics*, pages 76–83, 2007.

[100] John Uicker, Pennock Gordon, and Joseph Shigley. *Theory of Machines and Mechanisms*. Oxford University Press, 2003.

[101] Fabian van Beek and J. Rooda. Index reduction and discontinuity handling using substitute equations. *Mathematical and Computer Modelling of Dynamical Systems*, 7(2):173–187, 2001.

[102] Christopher Vaughan and Mark O'Malley. Froude and the contribution of naval architecture to our understanding of bipedal locomotion. *Gait & posture*, 21(3):350–362, April 2005.

[103] Miomir Vukobratovic and Branislav Borovac. Zero-moment point - thirty five years of its life. *International Journal of Humanoid Robotics*, 1(1):157–173, 2004.

[104] Pandu Vundavilli and Dilip Pratihar. Dynamically balanced optimal gaits of a ditch-crossing biped robot. *Robotics and Autonomous Systems*, 58(4):349–361, 2009.

[105] David A. Winter. *Biomechanics and Motor Control of Human Movement*. Wiley, 4th edition, 2004.

[106] Martijn Wisse. *Essentials of dynamic walking; Analysis and design of two-legged robots*. PhD thesis, Delft University, 2004.

[107] Terence Wong and Yeung Sam Hung. Stabilization of biped dynamic walking using gyroscopic couple. In *IEEE International Joint Symposia on Intelligence and Systems*, pages 102 –108, November 1996.

[108] Qiong Wu and Joon Chen. Effects of ramp angle and mass distribution on passive dynamic gait-an experimental study. *International Journal of humanoid robotics*, 7(1):55–72, 2010.

[109] Yujiang Xiang, Hyun-Joon Chung, Joo H. Kim, Rajankumar Bhatt, Salam Rahmatalla, Jingzhou Yang, Timothy Marler, Jasbir S. Arora, and Karim Abdel-Malek. Predictive dynamics: an optimization-based novel approach for human motion simulation. *Structural and Multidisciplinary Optimization*, 41(3):465–479, August 2009.

[110] Takashi Yamaguchi and Masaaki Shibata. Walking planning based on artificial vector field with prediction simulation for biped robot. *Electric engineering in Japan*, 159(4):54–61, 2007.

[111] Gabriel Zachmann. Rapid collision detection by dynamically aligned dop-trees. In *In Proc. of IEEE Virtual Reality Annual International Symposium*, pages 90–97, 1998.

[112] Maria Zakynthinaki, James Stirling, Carlos Cordente, Alfonso Lopez, Manuel Sillero, Gabriel Rodriguez, and Javier Sampedro. Modeling the basin of attraction as a two-dimensional manifold from experimental data: Applications to balance in humans. *Chaos: An Interdisciplinary Journal of Nonlinear Science*, 20(May):013119, 2010.

A

Dynamic equivalence of a rigid body in 2D

A rigid body can be represented by not less than two point masses, this is the simplest dynamically equivalent system in 2D. Two system are said to be equivalent, when the following conditions occur:

- Both systems share the same mass value.
- The center of mass of both systems have the same location.
- The mass moment of inertia is also the same.

Considering the rigid body in Figure A.1 the previous mentioned conditions produce the following equations:

$$m_1 + m_2 = m \tag{A.1}$$

$$m_1(r_{x_1}^2 + r_{y_1}^2)^{\frac{1}{2}} = m_2(r_{x_2}^2 + r_{y_2}^2)^{\frac{1}{2}} \tag{A.2}$$

$$m_1(r_{x_1}^2 + r_{y_1}^2) + m_2(r_{x_2}^2 + r_{y_2}^2) = I_{zz} \tag{A.3}$$

The system of equations can be solved by arbitrarily fixing the position of m_1, then from A.2 the following equations are obtained:

$$m_1 = m_2 \frac{(r_{x_2}^2 + r_{y_2}^2)^{\frac{1}{2}}}{(r_{x_1}^2 + r_{y_1}^2)^{\frac{1}{2}}} \tag{A.4}$$

$$m_2 = m_1 \frac{(r_{x_1}^2 + r_{y_1}^2)^{\frac{1}{2}}}{(r_{x_2}^2 + r_{y_2}^2)^{\frac{1}{2}}} \tag{A.5}$$

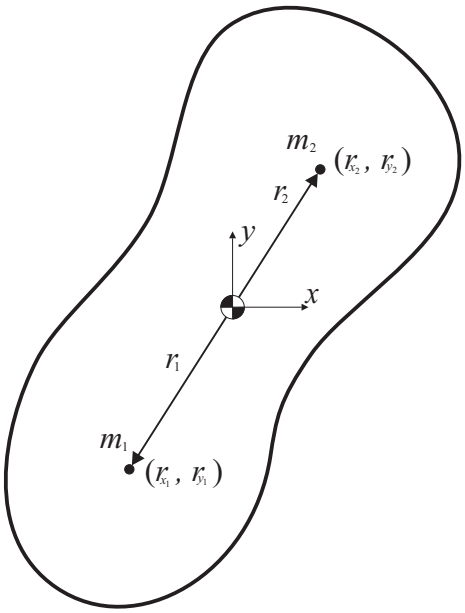

Figure A.1: Rigid body with two point masses. The value of the masses and its location can be selected to maintain dynamic equivalence. The position of the second mass is on the center of percussion respect to the other one.

Replacing A.1, A.4 and A.5 in A.3 and rearranging terms:

$$(r_{x_2}^2 + r_{y_2}^2)^{\frac{1}{2}} = \frac{I}{m(r_{x_1}^2 + r_{y_1}^2)^{\frac{1}{2}}} \tag{A.6}$$

The terms $(r_{x_1}^2 + r_{y_1}^2)^{\frac{1}{2}}$ and $(r_{x_2}^2 + r_{y_2}^2)^{\frac{1}{2}}$ represent the magnitudes r_1 and r_2 respectively. Theses magnitudes are used to find r_{x_2} and r_{y_2}, cross-multiplying the variables:

$$r_{x_2} = \frac{r_2 r_{x_1}}{r_1} = \frac{I r_{x_1}}{m r_1^2} \tag{A.7}$$

$$r_{y_2} = \frac{r_2 r_{y_1}}{r_1} = \frac{I r_{y_1}}{m r_1^2} \tag{A.8}$$

The magnitude r_2 is found with Pythagoras theorem, and equations A.7 and A.8. The result is:

$$(r_{x_2}^2 + r_{y_2}^2)^2 = \frac{I^2}{m^2 r_1^4}(r_{x_1}^2 + r_{y_2}^2) \tag{A.9}$$

$$r_2 = \frac{I}{m r_1} \tag{A.10}$$

Now that r_2 is known, equations A.1 and A.2 are used to find m_1 and m_2:

$$m_1 = \frac{m r_2}{r_1 + r_2} \tag{A.11}$$

$$m_2 = \frac{m r_1}{r_1 + r_2} \tag{A.12}$$

It should be noted that equations A.7 and A.8 does not include the signs of the components r_{x_2} and r_{y_2}. They are obtained considering that center of mass should be always between m_1 and m_2. Finally the point where m_2 is located corresponds to the center of percussion when the body is rotating around m_1. The opposite is also true.

B

Equations of motion of a mechanism

In this appendix the equations of motion of a mechanism and its equivalent system, depicted in Figure B.1, are calculated. The mechanism is composed by two thin bars with distributed mass, and there is no friction in the joints. After both system have their respective equations of motion, the reactions are compared. The result is that both system have the same reactions, therefore both systems are dynamically equivalent.

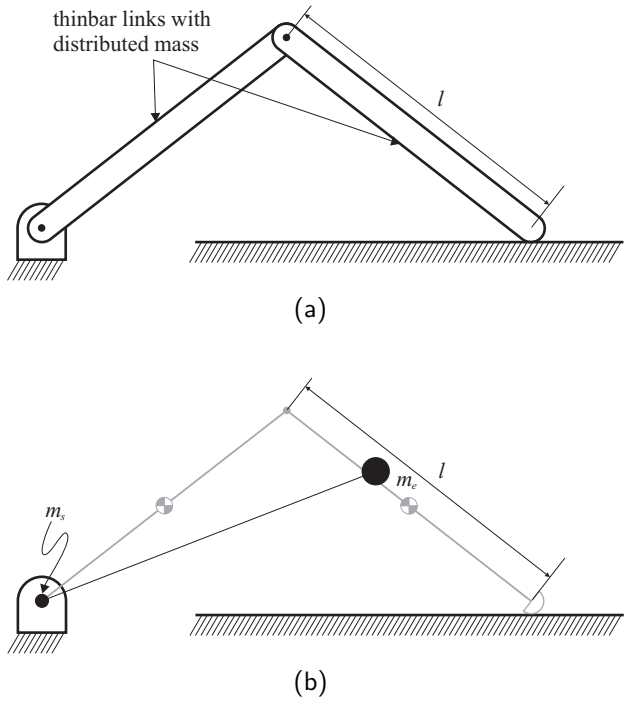

Figure B.1: Center of percussion of a mechanism. (a) real mechanism composed by thin bars, (b) idealized equivalent mechanism.

B.1 Equations of motion of the mechanism

In order to compare the equivalence of the systems shown in Figure B.1, the equations of motions of each system will be found. Because the topologies of the systems are different direct comparison of generalized coordinates cannot be done, instead the reaction forces will be calculated in each case and then compared to see the similarities.

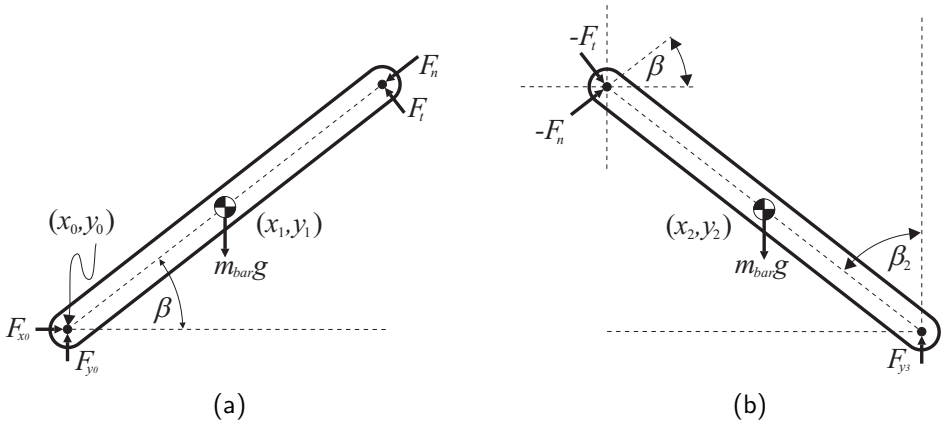

Figure B.2: Free body diagrams of the bars. (a) left bar of the mechanism, (b) right bar of the mechanism. The origin of coordinates is located in the lower pin joint of the left bar. (x_1, y_1) and (x_2, y_2) represent the centers of mass of each bar.

To derive the equations of motion consider the free body diagrams shown in Figure B.2. The origin of coordinates (x_0, y_0) is located in the lower pin joint of the bar in Figure B.2(a). The centers of mass are also marked and its coordinates are represented by (x_1, y_1) and (x_2, y_2). Therefore the kinematic equation for the left bar are:

$$x_1 = \frac{l}{2}\cos\beta \tag{B.1}$$

$$\dot{x}_1 = -\dot{\beta}\frac{l}{2}\sin\beta \tag{B.2}$$

$$\ddot{x}_1 = -\frac{l}{2}(\dot{\beta}^2\cos\beta + \ddot{\beta}\sin\beta) \tag{B.3}$$

$$y_1 = \frac{l}{2}\sin\beta \tag{B.4}$$

$$\dot{y}_1 = \frac{l}{2}\dot{\beta}\cos\beta \tag{B.5}$$

$$\ddot{y}_1 = \frac{l}{2}(-\dot{\beta}^2\sin\beta + \ddot{\beta}\cos\beta) \tag{B.6}$$

In the same way, similar results are found for the second bar:

$$x_2 = \frac{3}{2} l \cos\beta \tag{B.7}$$

$$\dot{x}_2 = -\frac{3}{2} l \dot{\beta} \sin\beta \tag{B.8}$$

$$\ddot{x}_2 = -\frac{3}{2} l (\dot{\beta}^2 \cos\beta + \ddot{\beta} \sin\beta) \tag{B.9}$$

$$y_2 = \frac{l}{2} \sin\beta \tag{B.10}$$

$$\dot{y}_2 = \dot{\beta} \frac{l}{2} \cos\beta \tag{B.11}$$

$$\ddot{y}_2 = \frac{l}{2} (-\dot{\beta}^2 \sin\beta + \ddot{\beta} \cos\beta) \tag{B.12}$$

Before applying Newton's second law, the rotation of the bar in Figure B.2(b) is considered respect to β_2, the relation with the β angle is:

$$\beta_2 = \frac{\pi}{2} - \beta \tag{B.13}$$

$$\dot{\beta}_2 = -\dot{\beta} \tag{B.14}$$

$$\ddot{\beta}_2 = -\ddot{\beta} \tag{B.15}$$

Finally, applying D'Alembert's principle the following equations are obtained:

$$m_{bar} \ddot{x}_1 = F_{x_0} - F_n \cos\beta - F_t \sin\beta \tag{B.16}$$

$$m_{bar} \ddot{y}_1 = F_{y_0} - F_n \sin\beta - F_t \cos\beta - m_{bar} g \tag{B.17}$$

$$I_{bar} \ddot{\beta} = F_{x_0} \frac{l}{2} \sin\beta - F_{y_0} \frac{l}{2} \cos\beta + F_t \frac{l}{2} \tag{B.18}$$

$$m_{bar} \ddot{x}_2 = F_n \cos\beta + F_T \sin\beta \tag{B.19}$$

$$m_{bar} \ddot{y}_2 = F_n \sin\beta - F_t \cos\beta - m_{bar} g + F_{y_3} \tag{B.20}$$

$$I_{bar} \ddot{\beta}_2 = -\frac{l}{2} F_n \sin 2\beta + F_t \frac{l}{2} \cos 2\beta + \frac{l}{2} F_{y_3} \cos\beta \tag{B.21}$$

This 21 equations form a system used to find the values of the reaction forces. The equations of the reaction forces are:

$$F_{x_0} = -2m_{bar}l(\dot{\beta}^2 \cos\beta + \ddot{\beta}\sin\beta) \tag{B.22}$$

$$F_{y_0} = m_{bar}g - m_{bar}l\ddot{\beta}^2 \sin\beta + m_{bar}l\ddot{\beta}\left(\cos\beta - \frac{2}{3\cos\beta}\right) \tag{B.23}$$

$$F_{y_3} = m_{bar}g + \frac{2ml\ddot{\beta}}{3\cos\beta} \tag{B.24}$$

B.2 Equations of motion of the equivalent mechanism

As stated in Chapter 3 a kinematic chain can be reduced to two point masses. If one of them is selected in a fixed position the analysis is reduced to the analysis of one point mass. In Figure B.3 the equivalent system of the one shown in Figure B.1(a) is detailed. The equivalent system is composed by the two point masses that are found when the center of percussion of the whole mechanism is found with respect to the pivot 0. Therefore the masses are located one over the center of percussion called m_e and other over point 0 marked as m_s.

The modulus r_{CM} is found in the next expression:

$$r_{CM}^2 = l^2\cos^2\beta + \frac{l^2}{4}\sin^2\beta \tag{B.25}$$

and after some mathematics the result is:

$$r_{CM}^2 = \frac{1}{4}l^2(3\cos^2\beta + 1) \tag{B.26}$$

The moment of inertia of the mechanism is the sum of the moment of inertia of both thin bars calculated with respect to the center of mass of the system, therefore using the Huynes-Steiner's Theorem:

$$I_{CM} = 2\left(I_{bar} + m_{bar}\left(\frac{l\cos\beta}{2}\right)^2\right) \tag{B.27}$$

$$I_{CM} = 2I_{CM} + \frac{m_{bar}}{2}l^2\cos^2\beta \tag{B.28}$$

where I_{CM} is the moment of inertia of the system around the center of mass, I_{bar} and m_{bar} are the moment of inertia and the mass of the thin bars respectively, and l and β are described in figure B.3.

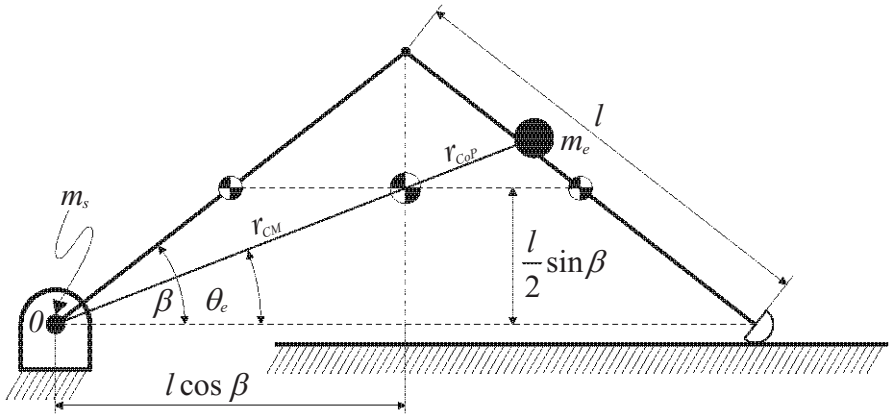

Figure B.3: Schematic of the equivalent mechanism. The equivalent system is composed by a point mass located at the center of percussion.

The center of percussion of the system is written as:

$$r_{CoP} = \frac{I_{CM}}{2m_{bar}r_{CM}} \tag{B.29}$$

$$r_{CoP} = \frac{2I_{bar} + \frac{m_{bar}}{2}l^2\cos^2\beta}{2m\left(\frac{1}{4}l^2(3\cos^2\beta + 1)\right)^{\frac{1}{2}}} \tag{B.30}$$

after some simplifications, and considering that $I_{bar} = ml^2/12$ the result is:

$$r_{CoP} = \frac{l}{6}\sqrt{3\cos^2\beta + 1} \tag{B.31}$$

Now the only unknowns left are the point masses m_s and m_e. The point mass at the center of percussion is calculated with:

$$m_e = 2m_{bar}\frac{r_{CM}}{r_{CM} + r_{CoP}} \tag{B.32}$$

$$m_e = 2m_{bar}\left(1 + \frac{r_{CoP}}{r_{CM}}\right)^{-1} \tag{B.33}$$

$$m_e = \frac{3}{2}m_{bar} \tag{B.34}$$

Although the same approach could be use to find the value of m_s, it also can be calculated by remembering that the original system and the equivalent one shares the same mass, therefore:

$$2m_{bar} = m_e + m_s \tag{B.35}$$

$$m_s = \frac{1}{2}m_{bar} \tag{B.36}$$

At this point the system has been reduced to one moving point mass m_e with unknown restrictions. Such restrictions will be found using the similar triangles formed by the center of mass and center of percussion position vectors and its individual x and y coordinates. Therefore, to find x_e we can write:

$$\frac{x_e}{r_{CM} + r_{CoP}} = \frac{x_{CM}}{r_{CM}} \tag{B.37}$$

$$\frac{x_e}{\frac{2}{3}l^2\sqrt{3\cos^2\beta + 1}} = \frac{l\cos\beta}{\frac{1}{2}l^2\sqrt{3\cos^2\beta + 1}} \tag{B.38}$$

$$x_e = \frac{4}{3}l\cos\beta \tag{B.39}$$

The same process can be repeated to find y_e:

$$\frac{y_e}{r_{CM} + r_{CoP}} = \frac{y_{CM}}{r_{CM}} \tag{B.40}$$

$$\frac{y_e}{\frac{2}{3}l^2\sqrt{3\cos^2\beta + 1}} = \frac{\frac{1}{2}l\sin\beta}{\frac{1}{2}l^2\sqrt{3\cos^2\beta + 1}} \tag{B.41}$$

$$y_e = \frac{2}{3}l\sin\beta \tag{B.42}$$

Now, all the conditions required to derive the equations of motions have been defined. The velocity and acceleration is found with the derivatives of equation B.39 and equation B.42:

$$\dot{x}_e = -\frac{4}{3} l\dot{\beta}\sin\beta \tag{B.43}$$

$$\ddot{x}_e = -\frac{4}{3} l(\dot{\beta}^2\cos\beta + \ddot{\beta}\sin\beta) \tag{B.44}$$

$$\dot{y}_e = \frac{2}{3} l\dot{\beta}\cos\beta \tag{B.45}$$

$$\ddot{y}_e = \frac{2}{3} l(-\dot{\beta}^2\sin\beta + \cos\beta) \tag{B.46}$$

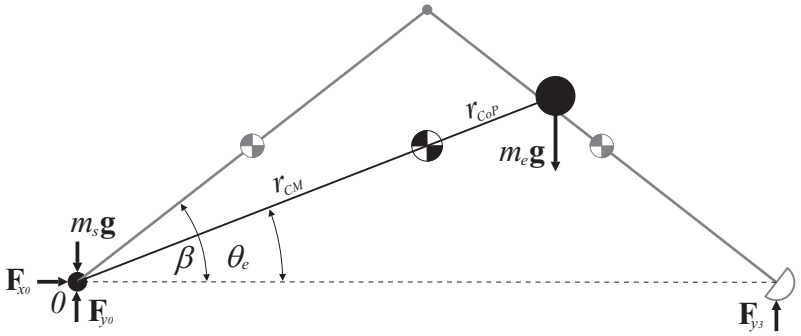

Figure B.4: Free body diagram of the equivalent mechanism. The original mechanism is shown in gray to illustrate where the reaction forces are applied.

Then only force acting over the system is the attraction of gravity in the point masses, but only the force due to m_e the point mass can make work over the system. Considering the reaction forces shown in figure B.4 and applying Newton's laws of motion:

$$m_e\ddot{x}_e = F_{x_0} \tag{B.47}$$

$$m_e\ddot{y}_e = F_{y_0} + F_{y_3} + (m_e + m_s)g \tag{B.48}$$

$$I_e\ddot{\theta}_e = -m_e g x_e + 2F_{y_3} l\cos\beta \tag{B.49}$$

Equation B.39, equation B.42 and equations from B.43 until B.49 describe the motion of the equivalent system. From this system of equations the reactions are found F_{x_0},F_{y_0} and F_{x_3}, once the system is solved the results are:

$$F_{x_0} = -2m_{bar}l(\dot{\beta}^2 \cos\beta + \ddot{\beta}\sin\beta) \tag{B.50}$$

$$F_{y_0} = m_{bar}g - m_{bar}l\ddot{\beta}^2 \sin\beta + m_{bar}l\ddot{\beta}\left(\cos\beta - \frac{2}{3\cos\beta}\right) \tag{B.51}$$

$$F_{y_3} = m_{bar}g + \frac{2m_{bar}l\ddot{\beta}}{3\cos\beta} \tag{B.52}$$

These equations are exactly the result already obtained in section B.1, this is the probe that both systems are equivalent. In this particular case the values of the point masses were constant, this is not always true. Fortunately the variations of such quantities are low and their derivatives smooth, therefore the equivalence is still maintained in other cases.

C

Modelica code for point contact objects

In this appendix the code implemented in the simulations of contact used in this thesis is shown. The implemented contact is "soft" contact instead of the impulsive methods often used in other applications. The reason for this is to avoid chattering problems encountered in momentum methods based on the reinitialization of the velocity vector.

C.1 Contact with viscous friction

The model simulates contact on the x-z plane. It has three parameters to control the stiffness, damping and viscosity. The contact is defined by following equation:

$$F_y = \begin{cases} ky - \nu\dot{y} & \text{for } y < 0, \\ 0 & \text{otherwise} \end{cases} \tag{C.1}$$

The friction in x and z direction is defined by:

$$F_x = \begin{cases} -\eta\dot{x} & \text{for } y < 0, \\ 0 & \text{otherwise} \end{cases} \tag{C.2}$$

$$F_z = \begin{cases} -\eta\dot{z} & \text{for } y < 0, \\ 0 & \text{otherwise} \end{cases} \tag{C.3}$$

The stiffness is regulated by `k` and determines the resistance of the x-z plane to be penetrated, in the same way the damping also in y direction is controlled by `v`. In x and z direction the friction is velocity dependent and is controlled by the parameter `eta`. The code implemented in Dymola® is detailed in the rest of the section.

```
model one_point2
  "One point contact over the x-z plane, viscous friction"

  import SI = Modelica.SIunits;

parameter Real k(final unit="N/m", final min=0) =
1000000 "Spring constant";
parameter Real v(final unit="N.s/m", final min=0)=
120000 "Damping constant";
parameter Real eta = 1200 "Viscosity constant";

SI.Force f_n;
SI.Force f_r[3];
SI.Position x_td[3];

protected
SI.Velocity v_0[3];

public
  Modelica.Mechanics.MultiBody.Interfaces.Frame_b frame_b

equation
//to record touch down event
when frame_b.r_0[2]<0 then
x_td=frame_b.r_0;
end when;

v_0=der(frame_b.r_0);

f_n=if frame_b.r_0[2]<0 then -k*(frame_b.r_0[2])-v*v_0[2] else 0;

f_r[1]= v_0[1]*eta;
f_r[2]=-f_n;
f_r[3]=v_0[3]*eta;

frame_b.f=Modelica.Mechanics.MultiBody.Frames.resolve2(
                                    frame_b.R,f_r);
frame_b.t = zeros(3);

end one_point2;
```

C.2 Contact with sticky friction

The tangential forces in the previous model depends on the relative velocity of the contact point with respect to the $x-z$ plane, therefore slippage is always present in the contact interface. To solve this problem the contact point is detected and store in `x_td` variable by the following code:

```
when frame_b.r_0[2]<0 then
x_td=frame_b.r_0;
end when;
```

As long as the contact is happening `x_td` is used as reference to calculate the tangential forces with the following expression:

$$F_x = \begin{cases} k(x - x_{td}) - \nu\dot{x} & \text{for } y < 0, \\ 0 & \text{otherwise} \end{cases} \tag{C.4}$$

In this model only two parameters are required `k` and `v`, they control stiffness and damping respectively. The contact detection is done with event generation when $y < 0$ in the same way of the previous model. Finally, the detailed code is specified in the next lines.

```
model one_point2
  "One point contact over the x-z plane, viscous friction"

  import SI = Modelica.SIunits;

parameter Real k(final unit="N/m", final min=0) =
1000000 "Spring constant";
parameter Real v(final unit="N.s/m", final min=0)=
120000 "Damping constant";

SI.Force f_n;
SI.Force f_r[3];
SI.Position x_td[3];

protected
SI.Velocity v_0[3];

public
```

```
  Modelica.Mechanics.MultiBody.Interfaces.Frame_b frame_b;

equation
//to record touch down event
when frame_b.r_0[2]<0 then
x_td=frame_b.r_0;
end when;

v_0=der(frame_b.r_0);

f_n=if frame_b.r_0[2]<0 then -k*(frame_b.r_0[2])-v*v_0[2] else 0;

f_r[1]=0;
f_r[2]=-f_n;
f_r[3]=0;

frame_b.f=Modelica.Mechanics.MultiBody.Frames.resolve2(
                                    frame_b.R,f_r);
frame_b.t = zeros(3);

end one_point2;
```

C.3 Contact with continuous functions

Contact based on event generation using conditional statements can compromise the computational efficiency. To avoid this problem continuous approximations of the step function can be used, as for example the logistic function $1/(1+e^{tx})$. In this case t is used to control the gradient of the step, and x is the independent variable. Other problem with soft contact is that in real life when the reaction forces become large they do not behave linearly and a hardening effect can be observed. This two phenomena are combined and the normal reaction of the contact is written as:

$$F_y = \frac{1}{1+e^{5000y}}(e^{-ky} - 1 + F_v) \tag{C.5}$$

Here k is the stiffness constant and F_v is the damping force. This last formulation of contact avoids deep penetration when high forces are present. Another problem present in the previous model was how damping was modeled. When the condition of contact $y < 0$ was active, the damping force in the form of a viscous force was acting over the

system. This produces a sticky effect when pulling away from the $x-z$ plane. To solve this problem F_v is defined as follows:

$$F_v = \begin{cases} -\nu\dot{y} & \text{for } \dot{y} < 0 \\ 0 & \text{for } \dot{y} \geq 0 \\ 0 & \text{otherwise} \end{cases} \tag{C.6}$$

The model was implemented using four parameters. `k` and `v` are used to control stiffness and damping normal to $x-z$ plane, while `k_t` and `v_t` are used to control the same values but in tangent direction. The rest of this section is dedicated to show the code implemented in this thesis.

```
model one_point3
  "One point contact over the x-z plane, sticky friction. using
continous functions"

  import SI = Modelica.SIunits;

parameter Real k(final unit="N/m", final min=0) =
1000 "Spring constant";
parameter Real v(final unit="N.s/m", final min=0) =
10000 "Damping constant";
parameter Real k_t(final unit="N/m", final min=0) =
30000 "Tangential constant";
parameter Real v_t(final unit="N/m", final min=0) =
10000 "Tangential dampting";

SI.Force f_n( min=0) "normal reaction force";
SI.Force f_v;
SI.Force f_r[3];
SI.Position x_td[3];

protected
SI.Velocity v_0[3];

public
  Modelica.Mechanics.MultiBody.Interfaces.Frame_b frame_b

equation
//to record touch down event
when frame_b.r_0[2]<=0.001 then
```

```
x_td=frame_b.r_0;
end when;


f_n =  1/(1+exp(5000*frame_b.r_0[2]))*(exp(-k*frame_b.r_0[2])-1+
f_v);

if noEvent( v_0[2]<0) then
f_v =  -v*v_0[2];
elseif noEvent( v_0[2]>0) then
f_v = 0;
else
f_v = 0;
end if;

v_0=der(frame_b.r_0);

f_r[1]= 1/(1+exp(5000*frame_b.r_0[2]))*(k_t*(frame_b.r_0[1]-
x_td[1])+v_t*v_0[1]);
f_r[2]=-f_n;
f_r[3]= 1/(1+exp(5000*frame_b.r_0[2]))*(k_t*(frame_b.r_0[3]-
x_td[3])+v_t*v_0[3]);

frame_b.f=Modelica.Mechanics.MultiBody.Frames.
resolve2(frame_b.R,f_r);
frame_b.t = zeros(3);

end one_point3;
```

D

Modelica code for rotational joints with mechanical stops

The rotational joints included in the standard library of Modelica® does not support locks or similar stops. This is required to simulate knee or ankles joints, where the movement is limited. In fact, one of the most important parts in the design of passive walkers are the knee locks [69]. In this appendix the implementation of this elements is explained, besides it is an excellent example of the power of object oriented modeling.

D.1 Rotational joint with mechanical stops based on events

The model is implemented by extending the class `Mechanics.MultiBody.Joints.Revolute` to inherit the properties of the standard rotational joint. Also a connector is added to provide input and output controls. The code for the connector is:

```
connector connector_M
  "Motor connector, carrying an input for control and an output
   for the position"

output Real angle;
input Real torque;
output Real w;

end connector_M;
```

The mechanical stops are simulated with conditional statements. Therefore, events are generated during the simulation in order to calculate the reaction forces of the stops. Their mathematical formulation is as follows:

$$\tau_r = \begin{cases} 0 & \text{for } \theta \leq \theta_s \\ 0 & \text{for } \theta \geq \theta_i \\ k_r\theta - \nu_r\dot{\theta} & \text{otherwise} \end{cases} \tag{D.1}$$

The stiffness and damping are shown by k_r and ν_r, and θ_s and θ_i are the position of the stops. The model has four parameters to adjust the behavior of the joint. `k_lock` and `nu_lock` control the stiffness and damping respectively, while `phi_lock1` and `phi_lock2` are used to determine the position of the locks. The rest of the section is dedicated to show the implemented code.

```
model Revolute1 "Revolute joint with locks"

  import Cv = Modelica.SIunits.Conversions;
  import SI = Modelica.SIunits;

parameter Real k(final unit="N*m/rad",  final min=0)=
0.01 "Spring constant";
parameter Real nu(final unit="N*m*s/rad")=
0 "Damping Coefficient";
parameter Cv.NonSIunits.Angle_deg delta_load=
0 "Spring preload";

parameter Cv.NonSIunits.Angle_deg phi_lock1=-90
    "Position of the mechanical lock 1"
annotation(Dialog(group= "Knee lock parameters"));
parameter Cv.NonSIunits.Angle_deg phi_lock2=90
    "Position of the mechanical lock 2"
annotation(Dialog(group = "Knee lock parameters"));
parameter Real k_lock = 500000 "Spring constant"
parameter Real nu_lock = 50000 "Damping constant"

SI.Torque tau_lock1; //Reaction at lock 1
SI.Torque tau_lock2; //Reaction at lock 2
SI.Torque tau_spring; //Spring reaction
SI.Torque tau_motor; //Motor torque
SI.Torque tau_damping; //Damping torque

extends Modelica.Mechanics.MultiBody.Joints.Revolute(final
tau=tau_spring+tau_lock1+tau_lock2+tau_motor+tau_damping);

  Interfaces.connector_M conM
```

```
equation

tau_lock1=if (phi>Cv.from_deg(phi_lock1)) then 0 else
-(phi-Cv.from_deg(phi_lock1))*k_lock - w*nu_lock;
tau_lock2=if (phi<Cv.from_deg(phi_lock2)) then 0 else
-(phi-Cv.from_deg(phi_lock2))*k_lock - w*nu_lock;
tau_spring=-k*(phi-Cv.from_deg(delta_load));
tau_motor=conM.torque;
tau_damping=-nu*w;

conM.angle=phi;
conM.w  = w;

end Revolute1;
```

D.2 Joint with mechanical stops and no events

To improve computational efficiency the conditional statements are replaced by the logistic function in a similar way as done in Section C.3. Therefore the reactions for the first lock are written as:

$$\tau_{r_1} = \frac{1}{1+e^{-b(\theta-\theta_s)}}(-k_r(\theta-\theta_s)+\tau_{\nu_1}) \tag{D.2}$$

$$\tau_{\nu_1} = \begin{cases} 0 & \text{for } \dot{\theta} < 0 \\ -\dot{\theta}\nu & \text{otherwise} \end{cases} \tag{D.3}$$

In the case of the second lock the conditions are slightly modified as follows:

$$\tau_{r_2} = \frac{1}{1+e^{-b(\theta-\theta_i)}}(-k_r(\theta-\theta_i)+\tau_{\nu_2}) \tag{D.4}$$

$$\tau_{\nu_2} = \begin{cases} 0 & \text{for } \dot{\theta} > 0 \\ -\dot{\theta}\nu & \text{otherwise} \end{cases} \tag{D.5}$$

In the same way as in Section C.3 a conditional viscous force is introduced in order to avoid the sticky behavior observed in some of the one point contact models. The model is controlled by the same parameters shown in Section D.1 with the same functions. Finally the complete code of this model is listed down in this section.

```
model Revolute4 "Revolute joint with locks, continous contact"

  import Cv = Modelica.SIunits.Conversions;
  import SI = Modelica.SIunits;
  import Walking_robots2.Functions.*;

parameter Cv.NonSIunits.Angle_deg phi_lock1=-90
    "Position of the mechanical lock 1"
parameter Cv.NonSIunits.Angle_deg phi_lock2=90
    "Position of the mechanical lock 2";
parameter Real k_lock = 30000 "Spring constant";
parameter Real nu_lock = 5000 "Damping constant";

SI.Torque tau_lock1; //Reaction at lock 1
SI.Torque tau_lock2; //Reaction at lock 2
SI.Torque tau_motor; //Motor torque

extends Modelica.Mechanics.MultiBody.Joints.Revolute(final tau =
 tau_motor+tau_lock1+tau_lock2);

Real tau_nu1 "Dummy to desactivate damping";
Real tau_nu2 "Dummy to desactivate damping";

  Interfaces.connector_M conM
equation

if noEvent( w<0) then
tau_nu1 = w*nu_lock;
tau_nu2 = 0;
elseif noEvent( w>0) then
tau_nu1 = 0;
tau_nu2 = w*nu_lock;
else
tau_nu1 = 0;
tau_nu2 = 0;
end if;

tau_lock1 = logistic(-phi,-Cv.from_deg(phi_lock1),12000)*
(-(phi-Cv.from_deg(phi_lock1))*k_lock - tau_nu1);
tau_lock2 = logistic( phi, Cv.from_deg(phi_lock2),12000)*
(-(phi-Cv.from_deg(phi_lock2))*k_lock - tau_nu2);
tau_motor=conM.torque;

conM.angle=phi;
```

```
conM.w = w;
```

The function `logistic()` is defined as:

```
function logistic "Logistic function. (variable,offset,decay)"

input Real x;
input Real offset;
input Real decay;
output Real y;

algorithm
 y :=1/(1 + exp(-decay*(x - offset)));

end logistic;
```